IN THE UNITED STATES PATENT AND TRADEMARKS OFFICE

In re Application of:

Masato HORIE

Serial No.: 10/781,841 Art Unit: 1635

Filed: February 20, 2004 Examiner: WHITEMAN, BRIAN A

For: HUMAN SKELETAL MUSCLE-SPECIFIC UBIQUITIN-CONJUGATING ENZYME

Declaration

Honorable Commissioner of Patents and Trademarks

Washington, D.C. 20231

SIR:

I, Masato HORIE declare that:

1) I am one of the inventors of the above-identified application, and am familiar with the subject matter of said application.
2) In order to demonstrate the utility of the present invention, the following experiments were carried out under my direction and supervision.

Experimental Data

Experiment 1. Test of the influence of recombinant NRP1 protein on cranial nerve growth activity

Since the mRNA and protein of NRP1 were observed to be highly expressed in the hippocampal region of the brain, this test examined the influence of recombinant rat NELL1 protein on survival of primary cultured neurons of rat hippocampus.

The reasons for using rat cells in this experiment are as follows:

(1) use of human cells raises many ethical problems, but rat cells are free from such problems and are readily available;
(2) although fresh primary cultured cells are most suitable as cells used for observing the development and extension of neurites, primary cultured human neurons cannot be easily prepared or obtained; and

(3) rat NRP1 has a high sequence homology with human NRP1, and therefore it can be presumed that the results obtained by using rat cells can be adequately extended to humans.

The DNA sequence of rat NRP1 mRNA is deposited in GenBank under accession number U48246, and its CDS (product="protein kinase C-binding protein NELL1") has about 93% homology with that of humans (Kang T et al., J. Bone and Mineral Research, Vol. 14, No. 1, pp. 80-89 (1999).

Kang et al., discloses that rat NELL1 has about 93 % homology with human NELL1. The "human NELL1" disclosed in Kang et al., means a polypeptide having amino acid sequence that is identical with the amino acid sequence of SEQ ID NO: 34 of the present invention.

Accordingly, as shown in Fig.4 of Kang T et al., the amino acid sequence of rat NELL1 is highly homologous, i.e., not less than 93%, to SEQ ID NO. 34 of the present invention. SEQ ID NO: 34 is encoded by the nucleotide sequence of SEQ ID NO: 35.

1) Reagents etc. used in the test

- The anti-microtubule-associated protein-2 (MAP-2) mouse monoclonal antibody used as a neuron marker was purchased from Sternberger Monoclonals Inc.
- The anti-glial fibrillary acid protein (GFAP) antibody used as an astrocyte (nerve glial cells) marker was purchased from Sigma-Aldrich.
- The basic fibroblast growth factor (bFGF) was purchased from Upstate Biotechnology.
- The water-soluble tetrazolium salt was purchased from Dojindo Laboratories.
- Cell Counting Kit-8 for WST-8 assay, which contains WST-8 [2-(2-methoxy-4-nitrophenyl)-3-(4-nitropheyl)-5-(2,4-disulfophenyl)-2H-tetrazolium, monosodium salt], was purchased from Dojindo Laboratories.

2) Production of recombinant rat NRP1 protein (NELL1)

For production of the C-terminally FLAG-tagged NELL1 protein, a

pIZT-mel-NELL-FLC plasmid was constructed by inserting the rat *NELL1* cDNA linked N-terminally to a mellitin signal peptide sequence and C-terminally to a FLAG epitope sequence into baculoviral vector pIZT/V5-His (Invitrogen).

High Five cells (BTI-TN-5B1-4, Trichoplusa nr.) were purchased from Invitrogen, and were cultured in High Five Serum-Free Medium (Invitrogen).

High Five cells were transfected with the pIZT-mel-Nell1-FLC plasmid using Cellfection (Invitrogen) according to the manufacturer's protocol. Forty-eight hours after transfection, cells were selected with 400 μg/mL of Zeocin (Invitrogen). The recombinant rat NELL1 protein was purified from the culture medium of Zeocin-resistant High Five cells by anion exchange chromatography using a UNO Q-6 column (Bio-Rad).

3) Test method

3-1) The influence of NRP1 protein on survival of hippocampal cells (WST-8 assay)

Primary culturing of rat neurons was performed as follows, according to a method described in the literature (K. Abe, et al., "Effect of recombinant human basic fibroblast growth factor and its modified protein CS23 on survival of primary cultured neurons from various regions of fetal rat brain" Jpn. J. Pharmacol., 53, (1990), 221-227): the hippocampus was excised from the 18-day-old fetal Sprague-Dawley rat brain, and enzymatically digested with 0.25% trypsin and 0.002% DNaseI at 37°C for 15 minutes to obtain hippocampal cells. The obtained hippocampal cells were suspended in 10% FBS-containing DMEM medium, and inoculated into a poly-L-lysine-coated 96-well plate at a density of $3x10^5$ cells/cm^2. On the next day, the medium was replaced with non-serum DMEM medium containing 1% N-2 supplements (Invitrogen), and culturing was performed for 3 days.

Neurons cannot survive in non-serum media, and gradually decrease in number as the number of days of culturing increases.

Predetermined amounts (1, 10, 100 or 1000 ng/mL) of NRP1 protein (the above purified NELL1) were added to the non-serum medium to continue culturing the hippocampal cells, and the survival of the cells after four-day culturing was determined by WST-8 assay.

3-2) The influence of NRP1 protein on survival of hippocampal cells (immunostaining)

Subsequently, the hippocampal cells after four-day culturing (cells cultured in the presence of 1000 ng/mL of NRP1 protein), and hippocampal cells cultured in a system without NELL1 for comparison (control) were fixed with 4% paraformaldehyde for immunohistological staining, permeabilized with 0.1% TritonX-100, blocked with 10% goat serum, and then washed with phosphate buffer.

Neurons and nerve glial cells (astrocytes) were identified with anti-MAP2 antibody and anti-GFAP antibody, respectively, and counterstained with hematoxylin. The staining was visualized using Envision-labeled polymer reagent (DAKO) in combination with 3,3'-diaminobenzidine·tetrahydrochloride reagent.

4) Results

4-1) Results of WST-8 assay

Attached Fig. A is a graph showing survival (A450/650 nm) of the hippocampal cells after four-day culturing at each concentration of NELL1 used.

The results shown in Fig. A reveal that addition of NELL1 protein (purified NELL1) at a concentration of 10 ng/mL or more significantly enhances survival of hippocampal cells, compared to survival in the no-addition control ($p<0.05$ vs control for 10ng/ml; $p<0.01$ vs control for 100ng/ml and 1000ng/ml).

4-2) Results of immunostaining

Attached Fig. B is a set of stained images (photographs) of cells stained using anti-MAP-2 antibody, which is a neuron marker, and anti-GFAP antibody, which is an astrocyte marker. In Fig. B, the photograph on the upper left shows control hippocampal cells that were cultured in the absence of NELL1 and stained using anti-MAP-2 antibody (indicated as "Control (MAP-2)" in the figure); the photograph on the lower left shows control hippocampal cells that were cultured in the absence of NELL1 and stained using anti-GFAP antibody (indicated as "Control (GFAP)"); the photograph on the upper right shows

hippocampal cells that were cultured in the presence of 1000 ng/mL of NELL1 and stained using anti-MAP-2 antibody (indicated as "NELL1 (MAP-2)"); and the photograph on the lower right shows hippocampal cells that were cultured in the presence of 1000 ng/mL of NELL1 and stained using anti-GFAP antibody (indicated as "NELL1 (GFAP)"). The bar (—) in each photograph is 100 μm long.

Fig. B shows that, in the stained images obtained using anti-MAP-2 antibody, a greater number of stained cells and greater degree of development and extension of neurites are observed in the system containing NRP1 protein than in the control system containing no NRP1 protein.

In the stained images obtained using anti-GFAP antibody, there is no difference between the system containing NRP1 protein and the system containing no NRP1 protein.

5) Conclusions

The above experimental results demonstrate that NRP1 protein selectively enhances survival of neurons.

It was also demonstrated that NRP1 protein not only increases the survival of neurons, but also develops and extends the length of neurites.

As is evident from these results, NRP1 protein has nerve growth activity.

Fig. A

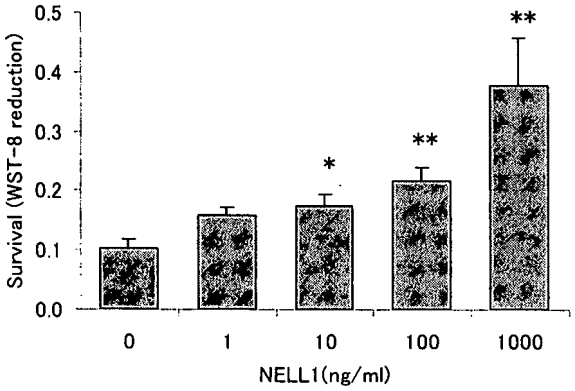
Survival (WST-8 reduction)
0.5
0.4
0.3
0.2
0.1
0.0
*
**
**
0
1
10
100
1000
NELL1(ng/ml)

Fig. B

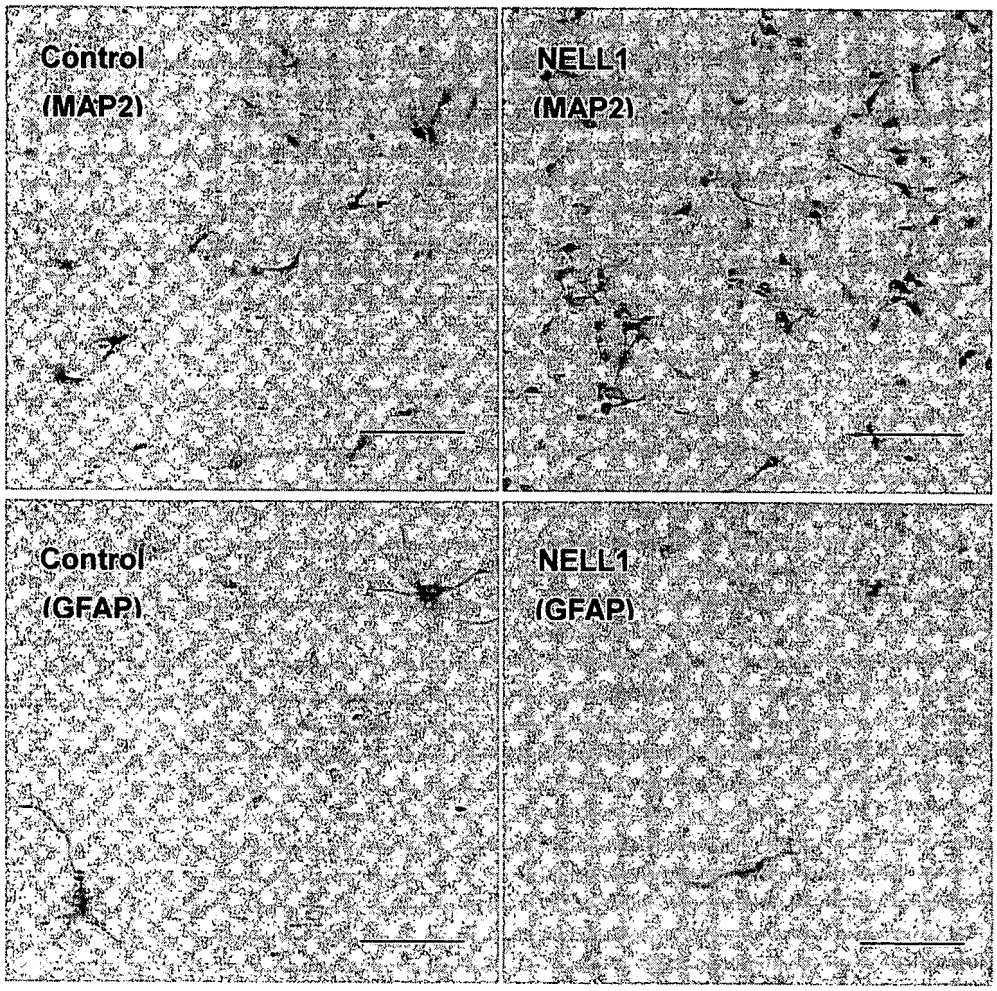

Photomicrographs of hippocampal cells survived in the presence of NELL1

E18 rat hippocampal cells were cultured in the presence of 1000 ng/mL of NELL1 for 3 days. The cells were stained for MAP2 (neurons) and GFAP(astrocytes). Bar, 100 μm.

I, the undersigned, declare that all statements made herein of my own knowledge are true and that all statements made on information and belief are believed to be true; and further that these statements were made with the knowledge that willful false statements and the like so made are punishable by fine or imprisonment, or both, under section 1001 of Title 18 of the United States Code and that such willful false statements may jeopardize the validity of the application or any patent issuing thereon.

Date: 3/5/2007

Masato Horie

Masato HORIE

JOURNAL OF BONE AND MINERAL RESEARCH
Volume 14, Number 1, 1999
Blackwell Science, Inc.

Human *NELL-1* Expressed in Unilateral Coronal Synostosis

KANG TING,[1] HELENI VASTARDIS,[2] JOHN B. MULLIKEN,[3] CHIA SOO,[4] ANDY TIEU,[1] HUY DO,[1] EMILY KWONG,[1] CHARLES N. BERTOLAMI,[5] HENRY KAWAMOTO,[4] SHUN'ICHI KURODA,[6,7] and MICHAEL T. LONGAKER[7,8]

ABSTRACT

Surgical correction of unilateral coronal synostosis offers a unique opportunity to examine the molecular differences between an abnormal and a normal cranial suture. We isolated and identified a cDNA fragment whose expression was up-regulated in the premature fusing and fused coronal sutures, as compared with normal coronal sutures. The nucleotide sequence of the full-length cDNA of this gene, human *NELL-1*, has ~61% homology with the chicken *Nel* gene. Both chicken Nel and human NELL-1 are comprised of six epidermal growth factor–like repeats. The human *NELL-1* messages were localized primarily in the mesenchymal cells and osteoblasts at the osteogenic front, along the parasutural bone margins, and within the condensing mesenchymal cells of newly formed bone in sites of premature sutural fusion. Human multiorgan tissue mRNA blot showed that *NELL-1* was specifically expressed in fetal brain but not in fetal kidney, liver, or lung. We also showed that *Nell-1* was expressed in rat calvarial osteoprogenitor cells and was largely absent in rat tibiae and fibroblast cell cultures. In conclusion, our data suggest that the *NELL-1* gene is preferentially expressed in cranial intramembranous bone and neural tissue (both of neural crest cell origin) and is up-regulated during unilateral premature closure of the coronal suture. The precise role of this gene is unknown. (J Bone Miner Res 1999;14:80–89)

INTRODUCTION

HUMAN CRANIAL SUTURES fuse slowly after brain growth ceases. The metopic suture closes first at around 2 years of age. The sagittal, coronal, and lambdoid sutures do not fuse until between 20 and 30 years of age.[1]

Craniosynostosis (CS) is the abnormal development and premature obliteration of cranial sutures, resulting in cranial dysmorphism. This abnormally accelerated sutural fusion can be secondary to extrinsic fetal factors, e.g., intrauterine constraint, maternal hematologic, metabolic disorders, or specific intrinsic fetal anomalies, either familial or sporadic.[1]

Molecular genetics has revealed the specific defects in several autosomal dominant syndromes whose common feature is CS. Via linkage analysis,[2] a point mutation in the homeobox gene *MSX2* that maps to 5qter was found in a single large family with autosomal dominant Boston-type CS.[3] *MSX2* is expressed along the osteogenic fronts of developing cranial sutures. Being involved in the differentiation of cranial membranous bone and in cartilage and mandibular development, *MSX2* is believed to be important in regulating craniofacial growth.[4] Liu and colleagues[5] (1995) engineered the same *Msx2* Pro7 His mutation as found in the Boston-type synostosis in transgenic mice; this mutation caused premature sutural closure and ectopic cranial bone formation. For the more common forms of syndromic and familial CS, the candidate gene approach has successfully identified mutations in the fibroblast growth factor receptor (*FGFR*) family. Mutations in

[1]Dental Research Institute, University of California, Los Angeles, California, U.S.A.
[2]Department of Genetics, Harvard Medical School, Boston, Massachusetts, U.S.A.
[3]Children's Hospital, Division of Plastic Surgery, Harvard Medical School, Boston, Massachusetts, U.S.A.
[4]Department of Surgery, University of California, Los Angeles, California, U.S.A.
[5]University of California, San Francisco, California, U.S.A.
[6]Biosignal Research Center, Kobe University, Japan.
[7]Both Dr. Kuroda and Dr. Longaker serve as cosenior authors.
[8]Institute of Reconstructive Plastic Surgery, New York University, New York, U.S.A.

the *FGFR2* gene on chromosome 10 cause the autosomal dominant craniosynostotic syndromes of Apert, Crouzon, Jackson-Weiss, and Pfeiffer.[6–11] A second variant of Pfeiffer syndrome results from a single mutation of the *FGFR1* gene on chromosome 8.[12] A variant of Crouzon syndrome, in association with *acanthosis nigricans*, is caused by a specific mutation of *FGFR3* on chromosome 4.[13] Another mutation in *FGFR3* has been found in familial coronal synostosis, previously undesignated by an eponym.[14]

FGFRs are members of the tyrosine kinase receptor family, known to play critical roles in signal transduction during growth and development.[15] Collectively, these results suggest that homeobox genes, growth factors, and growth factor receptors are important in both craniofacial and limb development. While genetic linkage analysis and the candidate gene approach are powerful tools to investigate familial cases of CS, the majority of patients with CS are nonfamilial.

Unilateral coronal synostosis (UCS; or synostotic frontal plagiocephaly) is a relatively common nonfamilial (sporadic) form of CS, estimated to occur once in every 10,000 births.[16] It is usually not associated with other extracraniofacial congenital abnormalities and is presumed to only involve early closure of one side of the coronal ring. UCS infrequently occurs in association with the FGFR3 Pro250Arg mutations.[14] UCS can also be expressed in Salthre–Chatzen syndrome, which is caused by mutations of the *TWIST* gene on chromosome 7.[7,17]

UCS first appears in a small zone in the inferior portion of the frontoparietal suture and extends superiorly.[1] Surgical correction involves a bifrontal craniotomy. This procedure offers the opportunity to obtain tissue from both the presumably normal patent (unaffected) coronal suture for comparison with biopsies from the prematurely fused (inferior) and fusing (superior) coronal suture on the affected side. Histomorphometric analysis of such specimens shows increases of bony remodeling at the prematurely fused suture sites as compared with contralateral normal patent sutures. The parasutural bone of the prematurely fused sutures is thicker and is populated with more osteoclast-like cells. We hypothesized that the pathogenesis of UCS involves alterations in time- and region-specific gene expression. Identification of differential gene expression between a prematurely fused/fusing coronal suture and the contralateral normal patent coronal site should enhance our understanding of mechanisms controlling sutural closure. There is a well-studied animal model of UCS: naturally occurring and autosomal dominant synostostotic in a rabbit colony.[18] However, gene expression analysis is very difficult due to the limited availability of gene sequences in the rabbit.

In this study, we applied a differential display polymerase chain reaction (DD-PCR) protocol to screen and identify differences in genetic expression in specimens of prematurely fusing, prematurely fused, and normal patent suture sites in humans. We report the identification of a gene, human *NELL-1*, that is up-regulated in the prematurely fusing and fused sutural sites of four different UCS patients. The human NELL-1 contains six epidermal growth factor (EGF)-like repeats and is homologous to the chicken *nel* gene that is strongly expressed in the neural tissue of early stage chick embryos.[19] The well-conserved structure of EGF-like repeats and Ca^{2+} binding sequences suggest that NELL may mediate specific ligand–receptor interactions.[20]

MATERIALS AND METHODS

DD-PCR analysis

Sample collection: Four specimens of sutures were obtained from an infant with nonfamilial UCS (UCS #1) during craniofacial repair and served as tissue for the initial DD-PCR. The biopsies comprised the following: patent coronal suture on the normal side (control) (Fig. 1A); prematurely fusing coronal suture on the affected side (Fig. 1B); prematurely completely fused coronal suture (Fig. 1C); normal patent metopic suture (control); and normal patent anterior sagittal suture (control). The completely fused coronal suture sample was solid bone; all the other sutural specimens had a margin of surrounding bone (Fig. 2). Specimens were frozen in liquid nitrogen and stored at −70°C. Suture samples were obtained from three additional UCS infants during operative correction (UCS #2–4).

Extraction of cellular RNA: Each of the samples was homogenized separately and total RNA was extracted by the guanidinium isothiocyanade method (RNA isolation kit; Invitrogen, San Diego, CA, U.S.A.). A modified protocol previously described for homogenizing calcified tissue was used to generate high-quality RNA from calcified bone.[21]

Differential display: DD-PCR was performed, as previously described,[22,23] using arbitrary primer sequence sets from the RNAimage Kit (GenHunter Corp., Nashville, TN, U.S.A.). Reverse transcription (RT) reactions were performed for each RNA sample. Each tube contained one of the four different $T_{12}MN$ anchored primers, and 0.2 $\mu g/\mu l$ total RNA was used for each reaction. Mouse murine leukemia virus (MMLV) reverse transcriptase was added and the reaction was carried out at the following temperatures and times: 65°C for 5 minutes for denaturing; 37°C for 30 minutes for RT; and 95°C for 5 minutes and chilled on ice for quenching. 5′ random primers designed by Genhunter, taq polymerase, ^{35}S-dATP, and dNTP were added. A short elongation time of 30 s at 40°C for 40 cycles was used. The PCR products were separated on a 6% sequencing gel.

Isolation of PCR products: Differentially up- or down-regulated gene fragments were extracted from the gel and reamplified using the same set of DD-PCR primers and cloned into the pCR™ 2.1 vector using the TA Cloning Kit (Invitrogen). Plasmids from positive colonies were purified and sequenced. The cDNA sequences were analyzed using the Basic Local Alignment Search Tool at the National Center for Biotechnology Information. cDNA sequences with homology to known growth factors and receptors or known cell/tissue differentiation regulatory sequences were investigated.

5′ rapid amplification of 5′-cDNA ends of NELL-1

One microgram of total RNA was converted to first strand cDNA using cDNA synthesis primer oligo dT at

FIG. 1. Cross-section of bilateral coronal suture sites from a UCS patient. (A) Partially fused coronal suture. The tissue near the fusion site is relatively acellular and well organized. Further away from the fusion, the sutural tissue is more cellular and less organized, as indicated by arrows. (B) Normal patent coronal suture. The patent suture site is similar histologically to the cellular suture site further away from the fusion in (A). (C) Abnormal fused suture. The suture is completely obliterated. Hematoxylin and eiosin staining was used. Original magnification. ×10. Sutures arrowed.

70°C for 2 minutes and 42°C for 1 h (Clontech, Palo Alto, CA, U.S.A.). Second strand synthesis was performed with RNAse H, *Escherichia coli* DNA ligase, and *E. coli* DNA polymerase at 16°C for 1.5 h. T4 DNA polymerase was added and incubated at 16°C for 45 minutes. Thereafter, 5 μl of ds-cDNA was ligated to the 5′ cDNA adapter: 5′-CTAATACGACTCACTATAGGGCTCGAGC-GGCCGCCCGGGCAGGT-3′ with T4 ligase. The product was used for PCR reaction. The 5′ primer, AP1, is a 27-mer taken from the cDNA adapter. The 3′ sequence specific antisense primer was: 5′-CCCGCGTTGTAAATCATG-3′. The PCR amplification reactions were performed at 94°C for 1 minute for a single cycle, followed by 30 cycles at 94°C for 30 s, 60°C for 30 s, and 68°C for 4 minutes

Nested PCR was performed using 0.1 ml of the PCR product for 20 cycles at 94°C for 30 s and 68°C for 4 minutes. The primers used were AP2 primers, a 23-mer from the 3′ end of the cDNA adapter, and a 3′ specific primer 50 base pairs (bp) closer to the 5′ end. The PCR products were analyzed on 1% agarose gels and confirmed by Southern blotting using the labeled cDNA clone as a probe. One hundred microliters of each PCR product was run on preparative gels, and appropriate size fragments were extracted. The purified products were cloned by the TA cloning method (Invitrogen). Plasmids were purified and sent to the DNA Sequencing Facility at UCLA for complete analysis.

Verification of the NELL-1 gene on four sets of unrelated nonfamalial UCS samples by sequence-specific PCR

The normal coronal sutures served as controls for the prematurely fusing coronal sutures. To verify that the human *NELL-1* gene identified by DD-PCR on UCS #1 was present in the other UCS patients (#2, #3, and #4), two *NELL-1* sequence-specific primers for RT-PCR were designed: 5′ primer, GCTACTTGTGAGTGCAAGAGTGG and 3′ primer, GGACAGTGTTGGTGCAGATGGC. Total RNA, 0.4 μg, was used with 4 μM oligo(dT) (16–20

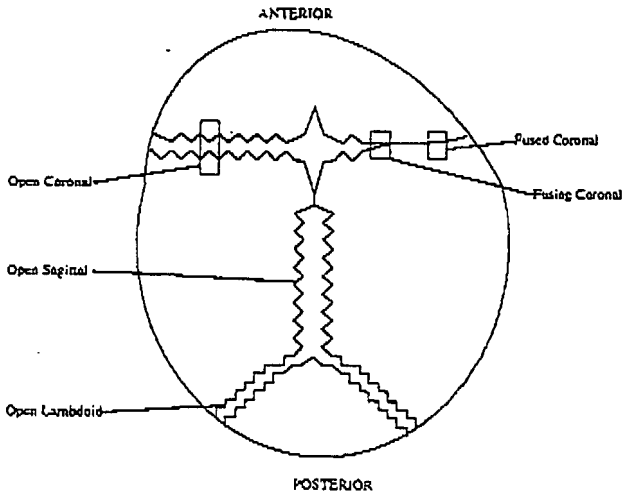

FIG. 2. Vertex cranial view: sites of biopsies.

mers) and MMLV RT.[21] Semiquantitative PCRs were performed at 20, 25, and 30 cycles of amplification at 94°C for 30 s, 70°C for 2 minutes, and 72°C for 30 s to approximate PCR on the linear amplication range. To compare general trends in *NELL-1* mRNA expression, autoradiograms were scanned and analyzed on a Macintosh computer using the public domain National Institutes of Health Image program. For each specimen, the densitometry value was divided by the glyceraldehyde-3-phosphate dehydrogenase (*GAPDH*) value (performed at 20 cycles) and normalized by setting the *NELL-1* value of the normal patent suture to one. Thirty-cycle RT-PCR was repeated three times. Means and SDs were calculated.

Identification of cells expressing NELL-1 within the suture site using in situ hybridization

In situ hybridization was performed on paraffin-embedded UCS specimens, according to the method of Haya-

shi[24] et al. (1986) with several modifications. Block sections of the specimens, measuring 10 mm along the suture by 5 mm perpendicular to the suture without dura, were immediately fixed in 4% paraformaldehyde in phosphate-buffered saline at pH 7.4 for 2 days at 4°C. The specimens were transferred to a decalcifying solution (Fisher, Pittsburgh, PA, U.S.A.) containing 0.7 g/l of EDTA, 8 mg/l of sodium potassium tartrate, 99.2 ml/l of HCl, and 0.14 g/l of sodium tartrate. The specimens remained in the decalcifying solution for 3–5 days at 4°C; the solution was changed every 24 h. After dehydration, the specimens were embedded in paraffin. Eight-micrometer sagittal sections were prepared and mounted on subbed slides. Twenty-five to 50 ng of the [^{33}P]dATP radiolabeled cDNA probe was applied after thermal denaturation. Sections were dried and coated with Ilford K.5 nuclear emulsion (Kodak, Eastman, NY, U.S.A.). Slides were exposed in a tightly sealed slide box at 4°C for 10 days. Slides were developed with D19 (Kodak) for 4 minutes and fixed with hypofixer for 4 minutes at 18°C. After counterstaining with Harri's alum-hematoxylin, sections were examined with a light microscope.[21]

Osteogenic cell isolation from newborn rat calvariae

Isolation of osteogenic cells from newborn rat calvariae was performed as previously described.[10] The crania were dissected from newborn Sprague Dawley rats and digested in 25 mM HEPES, 10 mM $NaHCO_3$, 100 mM NaCl, 60 mM mannitol, 3 mM K_2HPO_4, 1 mM $CaCl_2$, 1 mg/ml of bovine serum albumin (fraction V; Sigma Chemical Co., St. Louis, MO, U.S.A.), 5 mg/ml of glucose, and 2 mg/ml of collagenase B (Boehringer Mannheim, Indianapolis, IN, U.S.A.) at 37°C for 120 minutes. Every 20 minutes, the incubation medium was collected and the cells centrifuged at 100*g* for 5 minutes. The cells collected from digestions 4, 5, and 6 were pooled and plated at 2.5×10^4/cm^2. Minimum essential medium with nonessential amino acids, Earle's salts, 10% fetal bovine serum (FBS), and penicillin and streptomycin (100 U and 10 μg/ml, respectively) was used to maintain the cells at 37°C, 5% CO_2 for 1 day. On the following day, the medium was changed for a fresh culture medium containing 150 μg/ml of ascorbic acid. After 3, 6, and 9 days, the cells were harvested and poly(A)$^+$ RNA was isolated (Fast Track Kit; Invitrogen, Austin, TX, U.S.A.). Ribonucleic acid from adult rat tibiae and rat fibroblast cell cultures were extracted as controls.

Adult rat dorsal dermis tissues were harvested, washed with Hank's buffer, and cut into small pieces. The tissues were minced and digested with collagenase (500 U/m; Sigma) with gentle shaking for 3 h at 37°C. An equal amount of 0.01% Trypsin was added for 30 minutes. Dissociation was stopped by adding basal Eagle medium (GIBCO Labs, Long Island, NY, U.S.A.) supplemented with 10% FBS. After passage through a 15 υ nylon mesh (Nitex; Tetko, Inc., Elmsford, NY, U.S.A.), cells were counted and seeded at a density of 5×10^5/75 cm^2 tissue flask (Corning Glass Works, Corning, NY, U.S.A.) in basal Eagle medium supplemented with 25 mM HEPES buffers, penicillin (100 μg/ml), streptomycin (100 μg/ml), and 10% FBS. Cells were utilized for the experiment after the third passage.

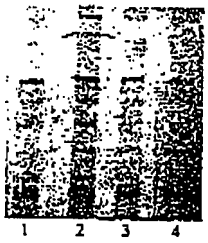

FIG. 3. Differential display of UCS (arrows in lane 2 indicate the specific band expressed only in the fusing site). Lane 1, left normal patent coronal suture (superior); lane 2, right prematurely fusing coronal suture; lane 3, normal patent metopic suture; lane 4, normal patent sagittal suture.

RT-PCR was performed with 0.2 μg of poly(A)$^+$ RNA with rat *Nell-1*–specific primers: 5′ sense primer 5′-CTGTGTGGCTCCTAACAAGTGTG-3′ and 3′ antisense primer 5′-GGATTCTGGCAATCACAAGCTGTC-3′ at an annealing temperature of 70°C for 30 cycles. The sequence of rat *Nell-1* homolog was obtained from GenBank (accession #U48246). ^{32}P-labeled rat *Nell-1* homolog oligo probe was used. Ribonucleic acid extracted from adult rat tibiae was the control (Trizol; GIBCO BRL, Gaithersburg, MD, U.S.A.).

Human fetal multitissue mRNA transfer blot analysis

Human fetal mRNA transfer blot was obtained from Clontech. mRNA from human fetal brain, kidney, liver, and lung was extracted and purified by several passages through an oligo(dT) column. Two micrograms of poly(A)$^+$ RNA from these specific tissues was run on a denaturing formaldehyde 1.2% agarose gel and blotted onto a positively charged membrane (Clontech). A ^{32}P *NELL-1* cDNA probe was used for hybridization.

RESULTS

Differential display of gene expression at different suture sites

The patterns of gene expression in the patent coronal sutures (from the normal side) and the patent sagittal and metopic suture sites (lanes 1, 4, 3, respectively) were very similar with minor variation in intensity (Fig. 3). This observation suggests that gene expression patterns were essentially identical in all the normal open suture sites. A direct comparison between the abnormal fusing coronal suture site (Fig. 3, lane 2) and normal patent coronal suture site (Fig. 3, lane 1) showed similar expression patterns, except for one 360-nucleotide (nt) band (indicated by arrows in lane 2). This band was expressed only in the prematurely fusing suture site and was absent from all the normal patent suture sites. The experiment was repeated with a consistent expression pattern. Thus, this finding suggests a differen-

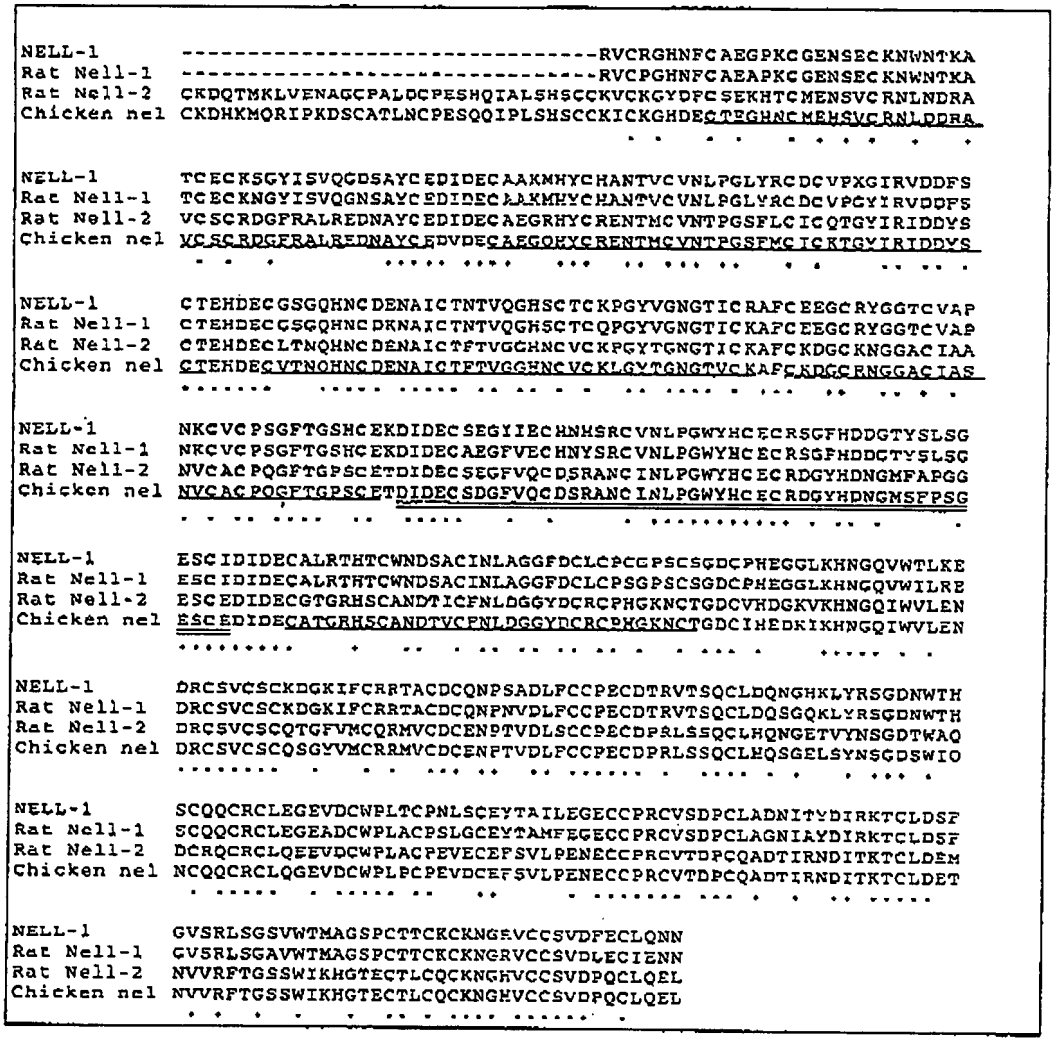

FIG. 4. CLUSTAL translation of human *NELL-1* to rodent (*Rattus norvegicus*) *Nell-1, Nell-2* genes, and chicken *nel* gene. Six conserved cysteines in each EGF-like repeat shown in bold. EGF-like repeats designated by underlined regions. Double-underlined region represents the deleted EGF repeat in the splicing variant. (·) Conserved amino acids between four sequences. Human NELL-1 versus rat Nell-1, rat Nell-2, and chicken nel has 93, 61, and 60% homology in amino acids, respectively. Rat Nell-1 versus rat Nell-2 has 59% homology.

tially expressed genetic fragment may be associated with premature sutural closure.

The Basic Local Alignment Search Tool analysis of the overexpressed 360-nt gene fragment from the fusing coronal suture showed high homology to rat *Nel* homolog and to molecules with EGF-like repeats, such as transforming growth factor-β nucleotide sequence at the 3′ untranslated region and the *notch* gene in Drosophila.[25]

Cloning the human NELL-1 from differential display

The human *NEL* homolog partial cDNA, of 1800 bp, was isolated by 5′ Rapid Amplification of cDNA Ends (RACE) (Marathon cDNA Amplification Kit, Clontech, Palo Alto, CA, U.S.A.). The sequence was deposited into the GenBank database with accession #U57523. This gene was also simultaneously identified by Watanabe et al.[26] and was named human *NELL-1*.

Other *NEL*-related molecules have been identified by studies in mouse (accession #U59230), rat (accession #U48246), and human.[26] NELL-1 contains six EGF-like repeats, as in the rat, mouse, and chicken *Nel* homolog nucleotide sequence, and shares high homology in the translated amino acids (59–93%). At the 3′ end of the transcript, a polyadenylation consensual sequence AAUAAA was found in our human sequence.[27] The *NELL*-related molecules are highly conserved in cysteine-rich domains (von Willebrand factor-like repeats with 6 Cys) (Fig. 4).

In addition to the six EGF-like repeats at the carboxy end of the gene, NELL-1 contains a highly hydrophobic

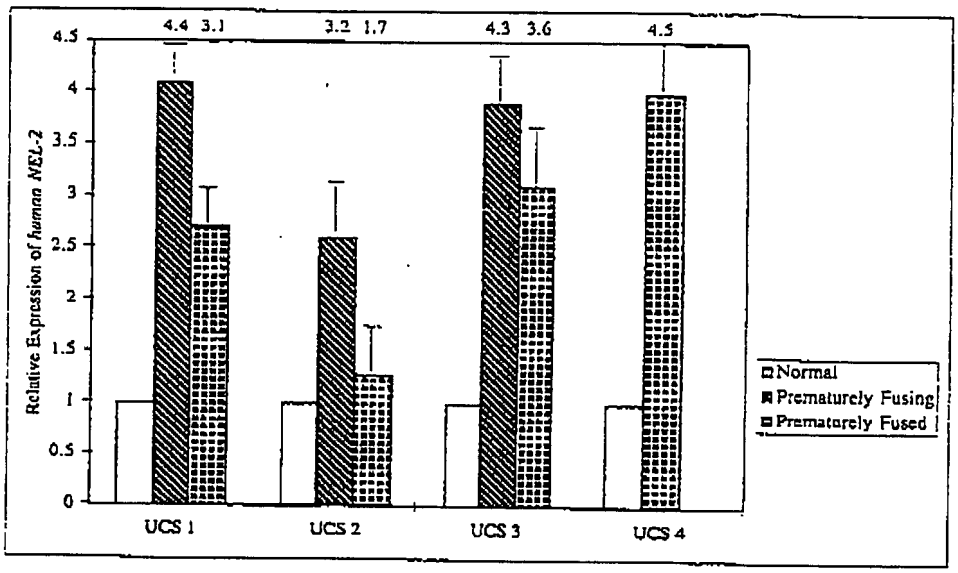

FIG. 5. Histogram of relative intensity of human *NELL-1* in nonsyndromic UCS samples. For each specimen, RT-PCR quantitations normalized with GAPDH values and divided by intensity of contralateral normal coronal suture.

region at the amino terminus that could represent a signal peptide sequence.

Expression of human NELL-1 in three additional sets of prematurely fusing/fused coronal samples

Human *NELL-1*–specific PCR products began to appear radiographically after a 24 h exposure with 30 cycles but not with 20 and 25 cycles. Therefore, 30 cycles was most likely to be within the linear amplication range.[28] For *GAPDH*, hybridization was observed starting with 20 cycles. Therefore, 20 cycles was likely to be within the linear range of amplification. Thirty *NELL-1* PCR cycles were divided by 20 GAPDH PCR cycles. Approximately a 4-fold increase of *NELL-1* expression was estimated in most of the fusing and/or fused coronal sutures, in comparison with the contralateral normal patent coronal sutures (Fig. 5). This quantitative difference in *NELL-1* expression suggests that *NELL-1* manifests in cranial sutures undergoing active suture fusion, and, furthermore, that the expression of *NELL-1* expression is temporally accelerated in the prematurely fusing/fused coronal suture sites.

In situ hybridization

In situ hybridization of *NELL-1* in prematurely fused coronal sutures showed expression of *NELL-1* in suture fusion and bony remodeling. In the prematurely fusing UCS specimens, *NELL-1* was mainly expressed in the cells around the newly formed osteoid tissue undergoing active bone formation (Fig. 6). *NELL-1* was also expressed in those osteoprogenitor cells located closely along the margins of calvarial bone undergoing active bone formation (suture fusion). The predominant cellular type, as seen in Fig. 6, appeared to be condensing mesenchymal cells and osteoblast-like cells.

Osteoprogenitor cell culture

The expected sequence-specific PCR product of 444 bp was present in the osteogenic cells of newborn rat calvariae and absent from tibiae and fibroblast cell culture (Fig. 7). Therefore, it is highly probable that the osteoblast in newborn rat calvariae (neural crest origin) is the major source of the *Nell-1* molecules and not fibroblasts. A second band of ~350 bp size was observed in the day 3 cell culture. This lower size product was cloned, sequenced, and confirmed to be a rat *Nell-1* variant. The nucleotide sequence was exactly the same as rat Nell-1, except that amino acids 550–596, which represent the fifth EGF repeat with the amino acid sequence, DIDE Ca^{2+} binding site, was completely deleted in comparison with rat Nell-1. It may represent a splicing variant.

Human fetal multitissue mRNA transfer blot analysis

A *NELL-1* probe was hybridized to 3.4–3.6 kb transcripts in brain, but not to mRNA from, kidney, liver, or lung (Fig. 8). Multiple bands were observed. This could represent cross hybridization to the human *NELL-1* gene.

DISCUSSION

Linkage analysis has served to identify the primary germline mutations in most of the well-known autosomal dominant CS. It is possible that a somatic mutation may be the cause for nonsyndromic UCS. Using DD-PCR, we identi-

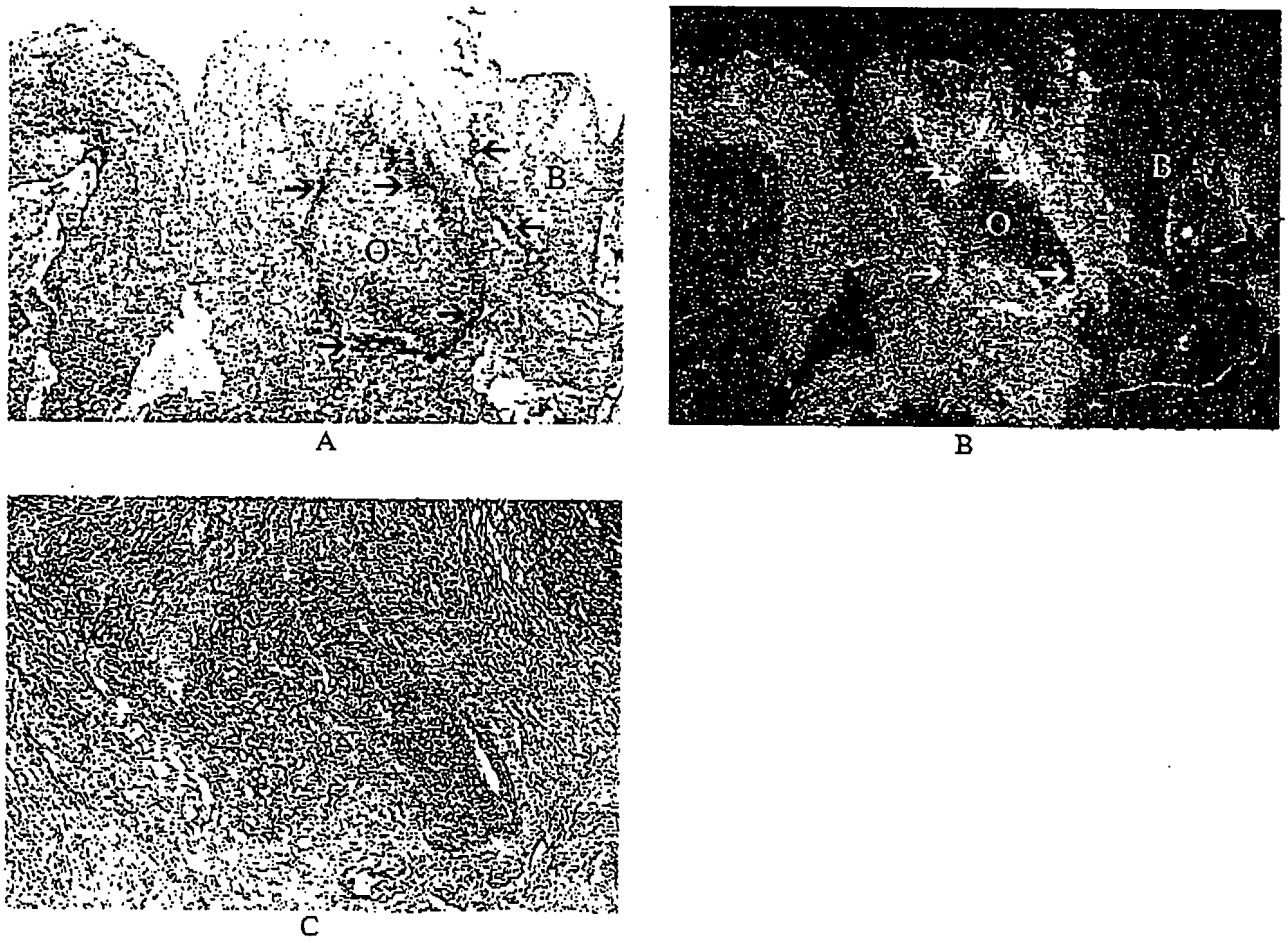

FIG. 6. In situ hybridization of human *NELL-1* in prematurely fusing/fused suture sites of nonsyndromic UCS. Letter "B" indicates cranial bone edge of fusing site. Letter "O" indicates newly formed osteoid. (A) Signals present newly formed osteoid (black arrows). Magnification, ×200. (B) Dark field of (A). Bright white rim around osteoid represents signals (white arrows). Signals also present near margins of actively fusing area (red arrows). (C) Hematoxylin stained. Magnification, ×400.

fied and isolated the human *NELL-1* gene and found it to be preferentially expressed at premature fusing and fused coronal suture sites in human UCS. We demonstrated that DD-PCR can be applied to identify genes up or down-regulated in this common type of unilateral human CS. The identification of these components may contribute to understanding the molecular cascades that produce the UCS phenotype. Because there are no extracraniofacial anomalies, the molecular genetic alterations observed in nonsyndromic UCS are likely to be due to local effectors of suture closure rather than a molecule with broad expression in other tissues such as *MSX2* or *FGFR*. In this report, we identified the *NELL-1* gene, which seems to be expressed in a tissue- and time-specific fashion.

The *Nel* molecule to be identified was found in fowl, from a 9-day-old chick embryo cDNA library.[19,29] Chicken Nel is 4.5 kb and encodes for a 816 amino acid 91 kDa protein. There is a distinct temporal and spatial sequence in the expression of *nel* in the developing chick embryo, as it first appears in neural tissues such as brain, spinal cord, and dorsal root ganglia. In tissues of the developing chick limb, *Nel* appears later and diminishes after gestation.

We identified the partial sequence (1800 nt) of human *NELL-1* encoding for 421 amino acid from the carboxy-terminal end of the gene. The full length of the human *NELL-1* molecule was simultaneously isolated, as well as another full-length cDNA sequence with high homology to the *NELL-1* molecule, from human fetal brain, termed *NELL-2* by Watanabe.[26] NELL-2 and NELL-1 are 816 amino acids and 810 amino acids, respectively.[26]

In addition to the six EGF-like repeats at the carboxyl end of the gene, NELL-1 contains a highly hydrophobic region at the amino terminus that may represent a signal peptide sequence deduced from computer analysis (Patscan; Pedro's Tool, Iowa State University). Actual experimental protein analysis by Dr. Kuroda (unpublished data) of NELL-1 and NELL-2 showed that NELL/Nel-related proteins have a cleavable signal peptide on the N-terminal and N-linked carbohydrate moiety (about 50 kDa each). Furthermore, Nell-1 protein is secreted and forms

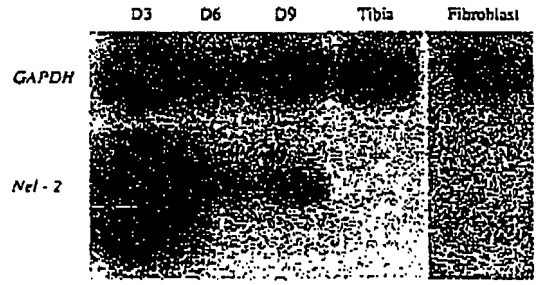

FIG. 7. RT-PCR of rat calvarial osteogenic cell culture (3-, 6-, and 9-day cultures), rat tibia, and fibroblast cell culture.

high molecular weight structures (MW > 400 kDa; monomer size is 130 kDa). The secreted proteins, Nell-1 and Nell-2, do not effectively bind to the known EGF receptors (EGFR, HeregullinR, BetacellulinR, and HB-EGFR), suggesting that other receptors probably exist (unpublished data).

Important roles for EGF-like molecules, such as *Delta,*[30] *Notch,*[25,31] and *Reeler,*[32] in growth and development are well documented. Underexpression of *Reeler* molecules causes Reeler syndrome, which is characterized by tremors, dystonia, and ataxia. In addition, other EGF-like molecules, such as tenascin and fibrillin, serve as extracellular matrix and cell adhesion molecules. Mutations in fibrillin cause Marfan syndrome manifested as ocular, cardiovascular, and musculoskeletal anomalies.[33,34]

The highly conserved nature of Nel-related molecules (Fig. 4) and the identification of Nel family members within species imply the existence of a unique type of ligand-signaling molecules. Even though the specific biological effects of the Nel-related molecules are currently unknown, their well-conserved structure, and the temporally and spatially localized expression patterns during development, suggest important roles during embryogenesis. We believe this is the first report to associate Nel-related molecules with a human developmental anomaly.

NELL-1 PCR product was not detected in normal site in the DD-PCR experiment, while in the primer-specific RT-PCR experiment, the *NELL-1* PCR product was detected in the normal site with approximately one quarter intensity as compared with the fusing site. It may be because that DD-PCR uses arbitrarily 13 oligonucleotides as primers to randomly amplify cDNA fragments. Therefore, the sensitivity to detect *NELL-1* is not as specific and sensitive as primer-specific PCR. Primer-specific PCR is a more accurate way to semiquantitate cDNAs. From our primer-specific RT-PCR result, the *NELL-1* expression pattern was consistently low in all patent sutures, as compared with that in fusing and fused coronal sites. It was markedly up-regulated in prematurely fusing and fused unilateral coronal sutures and down-regulated or absent in patent normal coronal sutures sampled from UCS infants. In addition, *NELL-1* was specifically expressed by osteoblasts and mesenchymal cells around the newly formed osteoid and within the abnormally fusing and recently fused sutures. Thus, the expression of *NELL-1* corresponded, both temporally and spatially, to sites of abnormal sutural fusion in UCS. This suggests an important role for NELL-1 during sutural closure and intramembranous bone formation. Additional specimens of cranial sutures from patients with sagittal synostosis and pansynostosis were investigated with RT-PCR for *NELL-1* expression. *NELL-1* was overexpressed in most of the abnormally fusing sutures and the recently fused human sutures. However, *NELL-1* expression levels were significantly lower in the quiescent normal patent sutures sampled from all other craniosynostotic patients (unpublished data). This quantitative difference in *NELL-1* expression suggests that a cranial suture, undergoing active or recently active bone formation/remodeling, is not unique to UCS. Furthermore, it is likely that there are more upstream regulatory molecules than NELL-1 in the molecular pathogenesis of UCS.

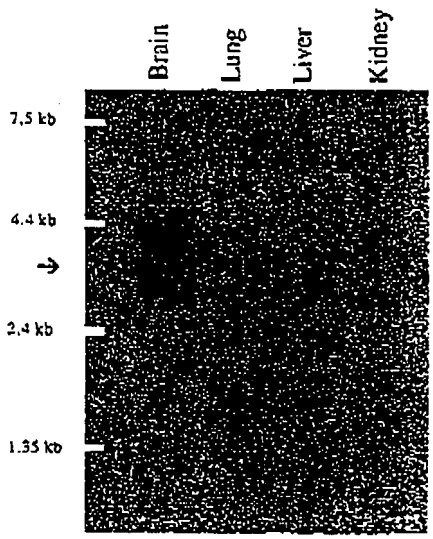

FIG. 8. Fetal multiple organs mRNA analysis. Human *NELL-1* expressed mainly in the fetal brain tissue as indicated by arrow.

The sutures at the edge of the calvarial plates have an osteogenic front comprised of actively dividing cells. In general, the cell population is believed to be mainly osteoblastic in origin and responsible for bone growth.[35] The localization of *NELL-1* to human CS suture mesenchymal cells, the presence of osteoblastoid cells at the osteogenic front, and localization of rat *Nell-1* ortholog to rat osteoprogenitor cells suggests that *NELL-1* and the rodent ortholog are important during intramembranous bone formation. There is additional evidence in the observation that rat *Nell-1* ortholog expression was absent in rat tibia, which is primarily composed of endochondral bone and cartilage. Thus, *Nell-1* may be a molecule that is differentially expressed in craniofacial intramembranous bone but not in endochondral bone.

Last, a multiorgan tissue mRNA blot showed that *NELL-1* is preferentially expressed in specific tissues, i.e., human fetal brain and not in fetal, kidney, liver, or lung. *Nell-1* was absent from rat fibroblast cell culture. Because *NELL-1* is preferentially expressed in neural structures and

in developing/remodeling intramembranous bone, it may play a role in the development of neural and skeletal structures during craniofacial growth. Interestingly, both CNS cells and craniofacial membranous bone cells arise from neural crest. In addition, it is known that dura mater and suture interactions can directly determine suture fusion, presumably through a signaling ligand.[34,35] Perhaps there is an expanded signal pathway consisting of brain, dura mater, and sutures with Nel-related molecules playing a role in this cascade.

In conclusion, NELL-1 and its related molecules may represent a new class of proteins involved in growth and development. The presence of EGF-like repeats and its secretory nature, suggests that NELL-1 is a ligand-type molecule with potential cell membrane receptors. This study documented increased expressions of *NELL-1* in intramembranous bone formation and in the pathological entity of premature UCS. To the best of our knowledge, this is the first report using differential display of human tissue specimens to isolate a gene associated with a pathologic process.

ACKNOWLEDGMENTS

We thank Dr. Ichiro Nishimura for his innovative ideas and continuous support. This work was supported by the American Association of Orthodontists Foundation grant number 012874, the Academic Senate Research Grant of the University of California at Los Angeles, the Research Endowment Fund from the Department of Surgery at UCLA, and a generous donation from Synthes Maxillofacial Biotechnology Corporation.

REFERENCES

1. Cohen MM Jr 1993 Sutural biology and the correlates of craniosynostosis. Am J Med Genet 47:581–615.
2. Jabs EW, Li X, Scott AF, Meyers G, Chen W, Eccles M, Mao JI, Charnas LR, Jackson CE, Jaye M 1994 Jackson-Weiss and Crouzon syndromes are allelic with mutations in fibroblast growth factor receptor 2. Nat Genet 8:275–279.
3. Müller U, Warman ML, Mulliken JB, Weber JL 1993 Assignment of a gene locus involved in craniosynostosis to chromosome 5*qter*. Hum Mol Genet 2:119–122.
4. Takahashi Y, Bontoux M, Le Douarin N 1991 Epithelio-mesenchymal interactions are critical for Qoux 7 expression and membrane bone differentiation in the neural derived mandibular mesenchyme. EMBO J 10:2387–2393.
5. Liu YH, Kundu R, Wu L, Luo W, Ignelzi MA Jr, Snead ML, Maxson RE Jr 1995 Premature suture and closure and ectopic cranial bone in mice expressing Msx2 transgenes in the developing skull. Proc Natl Acad Sci USA 92:6137–6141.
6. Reardon W, Winter RM, Rutland P, Pulleyn LJ, Jones BM, Malcolm S 1994 Mutations in the fibroblast growth factor receptor 2 gene cause Crouzon syndrome. Nat Genet 8:98–103.
7. Howard TD, Paznekas WA, Green ED, Chiang LC, Ma N, Ortiz de Luna RI, Garcia Delgado C, Gonzalez-Ramos M, Kline AD, Jabs EW 1997 Mutations in TWIST, a basic helix-loop-helix transcription factor in Saethre–Chotzen syndrome. Nat Genet 15:36–41.
8. Rutland P, Pulleyn LJ, Reardon W, Baraister M, Hayward R, Jones B, Malcolm S, Winter RM, Olridge M, Slaney SF, Poole MD, Wilkie AOM 1995 Identical mutations in the FGFR2 gene cause both Pfeiffer and Crouzon syndrome phenotypes. Nat Genet 9:173–176.
9. Lajeunie E, Ma HW, Bonaventure J, Munnich A, LeMerrer M, Renier D 1995 FGFR2 mutations in Pfeiffer sundrome. Nat Genet 9:108.
10. Wong GL, Cohn DV 1975 Target cells in bone for parathormone and calcitonin are different: Enrichment for each cell type by sequential digestion of mouse calvaria and selective adhesion to polymeric surfaces. Proc Natl Acad Sci USA 72:3167–3171.
11. Steinberger D, Mulliken JB, Müller U 1996 Crouzon syndrome: Previously unrecognized deletion, duplication and point mutation within FGFR2 gene. Hum Mutat 8:386–390.
12. Muenke M, Schell U, Hehr A, Robin NH, Losken HW, Schinzel A, Pulleyn LJ, Rutland P, Reardon W, Malcolm S, et al. 1994 A common mutation in the fibroblast growth factor receptor-1 gene in Pfeiffer syndrome. Nat Genet 8:269–274.
13. Meyers GA, Orlow SJ, Munro IR, Przylepa KA, Jabs EW 1995 Fibroblast growth factor receptor 3 (FGFR3) transmembrane mutation in Crouzon syndrome with acanthosis nigricans. Nat Genet 11:462–464.
14. Muenke M, Gripp KW, McDonald-McGinn DM, Gaudenz K, Whitaker LA, Bartlett SP, et al. 1997 A unique point mutation in the fibroblast growth factor receptor 3 gene (FGFR3) defines a new craniosynostosis syndrome. Am J Hum Genet 60:555–564.
15. Givol D, Yayon A 1994 Complexity of FGF receptors: Genetic basis for structural diversity and functional specificity. FASEB J 6:3362–3369.
16. Bruneteau RJ, Mulliken JB 1992 Frontal plagiocephaly: Synostotic composational or deformational. Plast Reconstr Surg 89:21–31.
17. El Ghouzzi V, LeMerrer M, Perrin-Schimdt F, Lajeunie E, Benit P, Renier D, Bourgeois P, Bolcato-Bellemin AL, Munnich A, Bonaventure J 1997 Mutations of the *Twist* gene on the Saethre–Chatzensyndrome. Nat Genet 15:42–46.
18. Mooney MP, Losken HW, Siegel MI, Lalikos JF, Losken A, Smith TD, Burrows AM 1994 Development of a strain of rabbits with congenital simple nonsyndromic coronal suture synostosis. Part I: Breeding demographics, inheritance pattern, and craniofacial anomalies. Cleft Palate Craniofac J 31:1–7.
19. Matsuhashi S, Noji S, Koyama E, Myokai F, Ohuchi H, Taniguchi S, Hori K 1995 New gene, nel, encoding a M (r) 93 K protein with EGF-like repeats is strongly expressed in neural tissue of early stage chick embryos. Dev Dyn 203:212–222.
20. Campbell ID, Baron M 1991 The structure and function of protein molecules. Philos Trans R Soc Lond [Biol] 332:165–170.
21. Ting K, Petropoulos LA, Iwatsuki M, Nishimura I 1993 Altered cartilage phenotype expressed during intramembranous bone formation. J Bone Miner Res 8:1377–1387.
22. Liang L, Arthur BP 1992 Differential display of Eukaryotic messenger RNA by means of the polymerase chain reaction. Science 257:967–971.
23. Liang L, Lidia A, Arthur BP 1992 Distribution and cloning of eukaryotic mRNAs by means of differential display: Refinements and optimization. Nucleic Acids Res 21:3269–3275.
24. Hayashi M, Ninomiya YY, Parsons J, Hayashi K, Olsen BR, Trelstad RL 1986 Differential localization of mRNAs of collagens type I and II in chick fibroblast, chondrocytes and corneal cells by in situ hybridization using cDNA probes. J Cell Biol 102:2302–2309.
25. Ellisen LW, Bird J, West DC, Soreng AL, Reynolds TC, Smith SD, Sklar J 1991TAN-1, The human homolog of the Drosophila Notch gene, is broken by chromosomal translocations in T lymphoblastic neoplasms. Cell 66:649–661.
26. Watanabe TK, Katagiri T, Suzuki M, Shimizu F, Fujiwara T, Kanemoto N, Nakamura Y, Hirai Y, Maekawa H, Takahashi E 1996 Cloning and characterization of two novel human cDNAs (NELL1 and NELL2) encoding proteins with six EGF-like repeats. Genomics 38:273–276.
27. Proudfoot NJ, Brownlee GG 1976 3′ Non-coding region sequences in eukaryotic mRNA. Nature 263:211–214.

28. Diaco R 1995 Practical considerations for the design of quantitative PCR assays. In: Innis MA, Gelfand DH, Sninsky JJ (eds.) PCR Strategies. Academic Press, San Diego, CA, U.S.A., pp. 84–108.
29. Matsuhashi S, Noji S, Koyama E, Myokai F, Ohuchi H, Taniguchi S, Hori K 1996 New gene, nel, encoding a M (r) 91 K protein with EGF-like repeats is strongly expressed in neural tissue of early stage chick embryos. Dev Dyn 207:233–234.
30. Fehon RG, Kooh PJ, Rebay I, Regan CL, Xu T, Muskavitch MA, Artavanis-Tsakonas S 1990 Molecular interactions between the protein products of the neurogenic loci Notch and Delta, two EGF-homologous genes in Drosophila. Cell 61:523–534.
31. Wharton KA, Johansen KM, Xu T, Artavanis-Tsakonas S 1985 Nucleotide sequence from the neurogenic locus notch implies a gene product that shares homology with proteins containing EGF-like repeats. Cell 43:567–581.
32. Hirotsune S, Takahara T, Sasaki N, Hirose K, Yoshiki A, Ohashi T, Kusakabe M 1995 The reeler gene encodes a protein with an EGF-like motif expressed by pioneer neurons. Nat Genet 10:77–83.
33. Dietz HC, Cutting GR, Pyeritz RE, Maslen CL, Sakai LY, Corson GM 1991 Marfan syndrome caused by a recurrent *de novo* missense mutation in the fibrillin gene. Nature 352:337–339.
34. Sood S, Eldadah ZA, Krause WL, McIntosh I, Dietz HC 1996 Mutation in fibrillin-1 and the Marfanoid–craniosynostosis (Shprintzen-Goldrung) syndrome. Nat Genet 12:209–211.
35. Pritchard JJ, Scott JH, Girgis FG 1956 The structure and development of cranial and facial sutures. J Anat 90:73–86.
36. Bradley JP, Levine JP, Roth DA, McCarthy JG, Longaker MT 1996 Studies in cranial suture biology: IV. Temporal sequence of posterior frontal cranial suture fusion in the mouse. Plast Reconstr Surg 98:1039–1045.
37. Roth DA, Gold LI, Han VK, McCarthy JG, Sung JJ, Wisoff JH, Longaker MT 1997 Immunolocalization of transforming growth factor beta 1, beta 2, and beta 3 and insulin-like growth factor I in premature cranial suture fusion. Plast Reconstr Surg 99:300–309.

Address reprint requests to:
Dr. Kang Ting
UCLA School of Dentistry
10833 Le Conte Avenue
CHS 30-113
Los Angeles, CA 90095 U.S.A.

Received in original form February 10, 1998; in revised form July 24, 1998; accepted August 18, 1998.

GENOMICS 38, 273–276 (1996)
ARTICLE NO. 0628

Cloning and Characterization of Two Novel Human cDNAs (NELL1 and NELL2) Encoding Proteins with Six EGF-like Repeats

TAKESHI K. WATANABE,*,[1] TOYOMASA KATAGIRI,*,†,[1] MIKIO SUZUKI,*,‡ FUMIO SHIMIZU,* TSUTOMU FUJIWARA,* NAOHIDE KANEMOTO,* YUSUKE NAKAMURA,§ YOSHIKATSU HIRAI,* HIROUMI MAEKAWA,* AND EI-ICHI TAKAHASHI*,[2]

*Otsuka GEN Research Institute, Otsuka Pharmaceutical Co., Ltd., 463-10 Kagasuno, Kawauchi-cho, Tokushima 771-01, Japan; †Division of Human Genome Analysis, Cancer Chemotherapy Center, Japanese Foundation for Cancer Research, 1-37-1, Kami-ikebukuro, Toshima-ku, Tokyo 170, Japan; ‡Department of Molecular and Cell Genetics, School of Life Sciences, Faculty of Medicine, Tottori University, Nishi-machi 86, Yonago 683, Japan; and §Laboratory of Molecular Medicine, Institute of Medical Science, The University of Tokyo, 4-6-1, Shirokanedai Minato-ku, Tokyo 108, Japan

Received April 10, 1996; accepted October 10, 1996

From a human fetal-brain cDNA library we isolated two novel genes encoding peptides containing six EGF-like repeats. Both showed significant homologies with nel, a gene strongly expressed in neural tissues of chicken. The cDNAs, designated NELL1 (nel-like, type 1) and NELL2 (nel-like, type 2), contained open reading frames encoding 810 and 816 amino acids, respectively. NELL2 is strongly expressed in brain of adult and fetus but only weakly in fetal kidney. NELL1 and NELL2 were mapped by FISH to chromosomal bands 11p15.1–p15.2 and 12q13.11–q13.12, respectively.

INTRODUCTION

EGF-like repeats have been found in many membrane proteins and in secreted proteins related to growth regulation and differentiation. Recently the gene encoding nel, a novel protein containing five EGF-like repeats, was cloned from a chick embryonic cDNA library (Matsuhashi *et al.*, 1995); the product appeared to be a transmembrane molecule, with its EGF-like repeats in the extracellular domain. The 4.5-kb transcript was expressed in various tissues at the embryonic stage and exclusively in brain and retina after hatching. Although the function of nel was unknown, its discoverers speculated that it might function as a receptor or a ligand in a neuron-specific signaling-pathway.

In this paper we report primary structures, expression patterns and chromosomal localizations of two novel human genes, both of them homologous with nel, which encode peptides containing six EGF-like repeats.

Sequence data from this article have been deposited with the GenBank/EMBL Data Libraries under Accession Nos. D83017 and D83018.

[1] These two authors contributed equally to this work.

[2] To whom correspondence and reprint requests should be addressed. Telephone: +81-886-65-2888. Fax: +81-886-37-1035.

MATERIALS AND METHODS

Cloning and DNA sequencing. As a part of the Human Genome Project, we have been determining the nucleotide sequences of cDNA clones randomly selected from a human fetal brain, aorta, and placenta cDNA library. The analyses are routinely performed in the manner described elsewhere (Watanabe *et al.*, 1996a).

5′ RACE (5′ Rapid Amplification of cDNA Ends). 5′ RACE has been applied in the experiments reported here according to the manufacturer's protocol (5′-AmpliFinder RACE kit; Clontech) with slight modifications that we have described elsewhere (Watanabe *et al.*, 1996a).

Northern blot analysis. Northern blot analysis was carried out with human multiple tissue Northern blots (Clontech) according to the manufacturer's instructions. The entire sequences of the cloned cDNAs were labeled and used as probes. The blots were prehybridized, hybridized, and washed in the manner described elsewhere (Watanabe *et al.*, 1996a). The blot of NELL1 was exposed at −80°C for 3 days. The filter of NELL2 was exposed for 18 h.

Cosmid cloning and chromosomal localization by direct R-banding FISH. The precise methods for cosmid cloning have been described elsewhere (Watanabe *et al.*, 1996a). The pairs of primers to screen cosmids of NELL1 were C3 (5′-CCCGTGTTGTAAATCATGTT) and C4 (5′-AAAAGTCACAACAGGCAACTT). The primers for NELL2 were C1 (5′-TTAAATTGGGTGATTTGTGG-3′) and C2 (5′-CCATTCTTCTACATGGTGAT-3′). Independent clones obtained in this way were used for mapping by direct R-banding fluorescence *in situ* hybridization (FISH), a technique based on FISH combined with replicated prometaphase R-bands (Takahashi *et al.*, 1990, 1991). Provia 100 film (Fuji ISO100) was used for the microphotography (filter combinations, Nikon B-2A and B-2E).

RESULTS

Cloning and DNA Sequencing of NELL1 and NELL2

By examining databases, we found that two human cDNA clones, GEN-073E07 (NELL1) and GEN-093E05 (NELL2), revealed significant homologies with nel.

0888-7543/96 $18.00

Since these clones seemed to lack their 5′ portions compared to the chick cDNA, we applied the technique of 5′ RACE (Frohman *et al.*, 1988) to isolate the missing segments. By performing several 5′ RACE experiments, we were able to obtain the entire coding sequences of these genes. In each step several independent clones were sequenced to exclude misincorporations by the *Taq* polymerase. Total lengths of the NELL1 and NELL2 cDNAs appeared to be 2977 and 3198 bp, respectively (data not shown). To exclude the possibility that either of these composite sequences was chimeric, we performed RT-PCR analyses. The entire coding sequences were amplified and proved to be identical with the sequences we had established. The nucleotide sequences of both genes will appear in the GSDB, DDBJ, EMBL and NCBI nucleotide sequence databases under Accession Nos. D83017 (NELL1) and D83018 (NELL2).

Characterization of Putative Peptides of NELL1 and NELL2

The deduced NELL1 and NELL2 gene products both exhibited highly hydrophobic N-termini that could function as signal peptides for membrane insertion. In contrast to nel, neither seemed to possess a hydrophobic transmembrane domain. To evaluate the conserved domains precisely, we performed multiple alignments among the NELL1, NELL2, and nel peptides (Fig. 1). NELL2 was more closely related to nel (80% identity at the amino acid level) than NELL1 (50% identity). Cysteine residues within Cys-rich domains and EGF-like repeats were completely conserved. The most striking difference between the NELLs and the chick protein was that the human homologues lacked nel's putative transmembrane domain, although even in this region the nucleotide sequences of NELLs and nel were very similar (see Discussion). Both NELLs possessed six EGF-like repeats, whereas nel has only five. Other unique motifs of nel reported by Matsuhashi *et al.* (1995) were also found in the NELLs, at equivalent positions (Fig. 1).

Expression of NELLs in Human Tissues

The expression patterns of the two NELLs in eight adult and four fetal human tissues were assessed by Northern blotting (Fig. 2). A single 3.5-kb transcript of NELL1 seemed to be very weakly expressed in brain and kidney of fetus and adult (data not shown). A 3.6-kb transcript of NELL2 was expressed strongly only in brain from fetus and adult, although weak expression could be detected in fetal kidney.

Cosmid Cloning and Mapping of NELLs by FISH

We obtained cosmids corresponding to NELL1 and NELL2. By amplifying and sequencing fragments corresponding to the 3′ noncoding regions of each

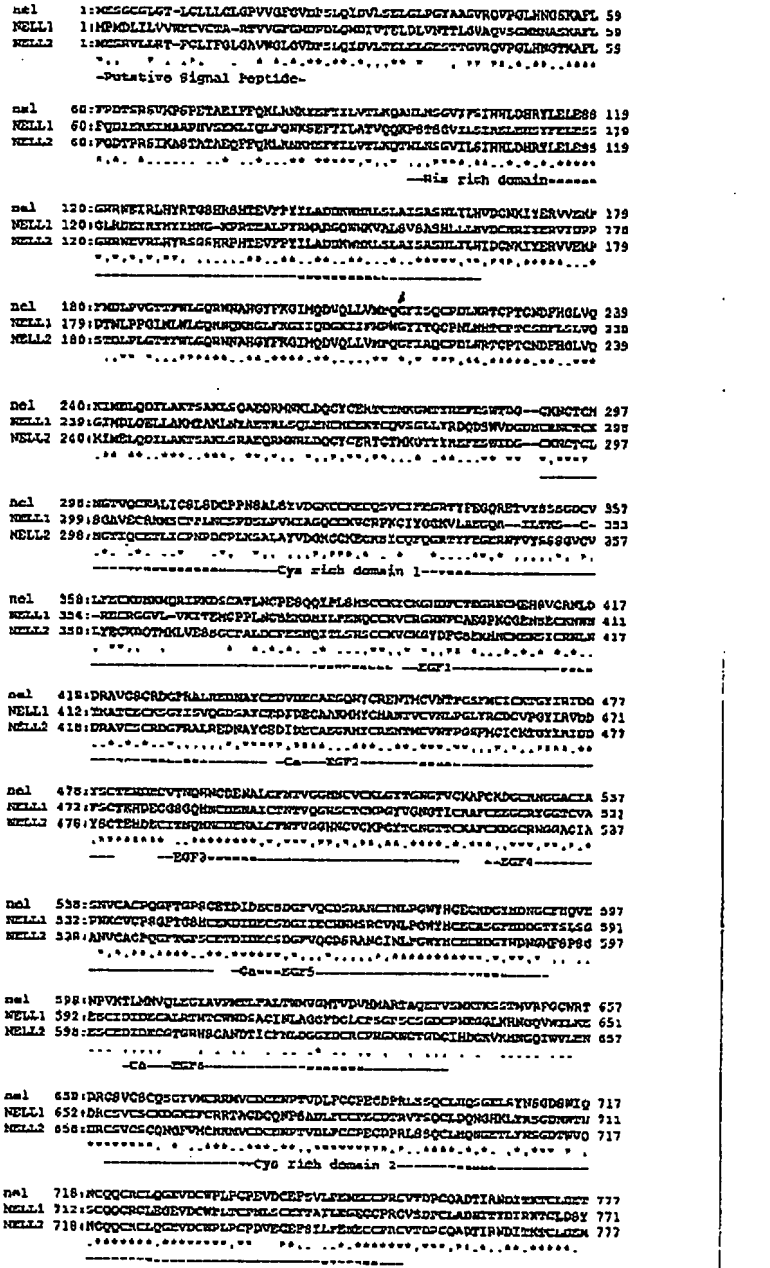

FIG. 1. Multiple alignments among NELL1, NELL2, and nel. Asterisks indicate residues conserved among all three proteins. Dots denote the residues conserved between two of the three proteins (most of these are conserved between nel and NELL2). Ca, calcium binding domains.

NELL, we confirmed that the cosmids were genomic clones corresponding to the respective NELL cDNAs. We performed direct R-banding FISH with these cosmids in two independent experiments; the signals localized NELL1 to chromosome 11p15.1–p15.2 and NELL2 to 12q13.11–q13.12 (Fig. 3). Specific labeling was observed on two chromatids (20 metaphases for NELL1 and 25 for NELL2), three chromatids (25 and

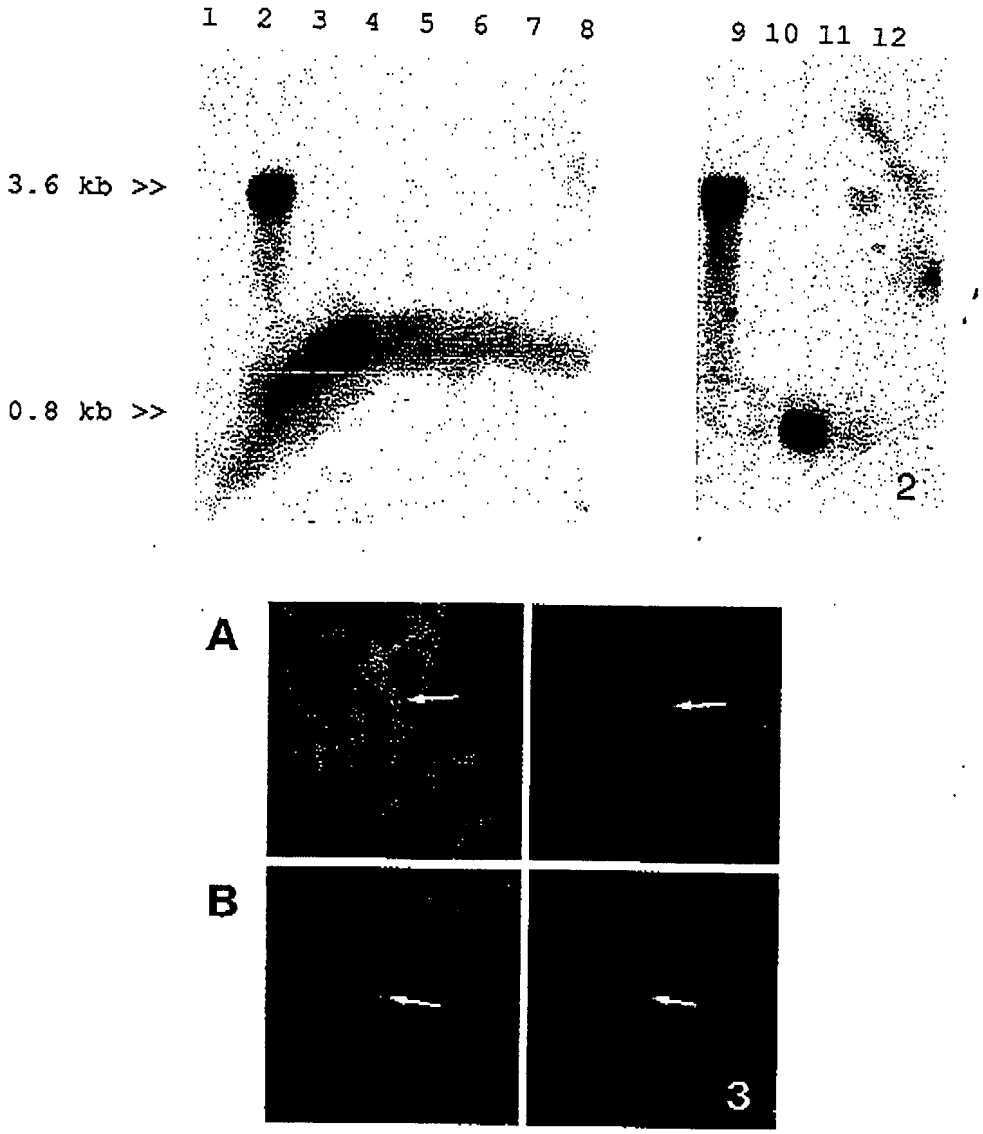

FIG. 2. Northern blot analyses of NELL2 in eight adult and four fetal tissues. Each lane contained approximately 2 μg of poly(A)$^+$ RNA. Lanes 1–8 contain, in order from left to right, RNA from adult heart, brain, placenta, lung, liver, skeletal muscle, kidney, and pancreas. Lanes 9–12 contain RNA from fetal brain, lung, liver, and kidney.

FIG. 3. Partial R-banded metaphase plates after FISH with the NELL1 (A) and NELL2 (B) cosmids. Left panels were examined with filter B-2A, and right panels were examined with filter B-2E. Arrows point to signals on chromosomes 11p15.1–p15.2 (A) and 12q13.11–q13.12 (B).

19 metaphases), or four chromatids (39 and 35 metaphases) among 100 metaphase spreads examined. No signal was observed at any other site.

DISCUSSION

Our large-scale sequencing and mapping approach identified two novel human genes (NELL1 and NELL2) closely related to the nel gene of chick embryo. At the nucleotide level overall identities with nel were about 57 and 75%, respectively. In cross species hybridization experiments using chicken nel as the probe, Matsuhashi *et al.* (1995) had failed to detect any bands in lanes containing human or *Xenopus* DNA. However, we ourselves tried cross species Southern hybridizations between human and mouse using part of NELL2 as the probe. After a relatively stringent wash, clear bands were detectable (data not shown), which suggested that NELL2 was highly conserved between human and mouse. We failed to detect a clear signal for NELL1 under the same conditions.

The predicted peptides of the two NELLs do not possess structures indicative of integral membrane proteins (since they seem to have no transmembrane domains), but they might be secreted proteins or proteins anchored to membranes by posttranslational modifica-

tion. We speculate that NELLs might function as ligands by stimulating other molecules such as EGF receptors. As to the existence of an apparent transmembrane domain in nel, Matsuhashi *et al.* (pers. comm., August, 1996, Naga, Japan) noticed that the nucleotide sequence they reported at first, which included a potential transmembrane domain, was slightly different from the sequences determined later by independent PCR and sequencing experiments. Moreover, we found that an "extra" EGF-like repeat could occur in nel by frame-shifting in this region (not shown). When aligned, the frame-shifted sequence showed overall similarity between nel and NELL2, which suggested that NELL2 might be nel's human counterpart. In contrast, the relationship between NELL1 and nel was somewhat more distant. At this time we cannot exclude the possibility that two types of nel (membrane-integrated and secreted) might exist.

Expression patterns of the two human genes in several tissues were similar in fetus but distinct in adult. NELL1 seemed to be expressed very weakly in brain and kidney from fetus and adult. This very weak expression, which made it difficult to assess NELL1 expression, might mean that only a small specific population of cells expressed this gene, as was the case with reelin (Hirotsune *et al.*, 1995). NELL2 was expressed strongly in brain and weakly in fetal kidney. As for a smaller band (0.8 kb) observed in fetal liver, we tried to confirm whether it was derived from the same genes as NELL2 or from a closely related, unknown gene. RT-PCR analysis with seven pairs of primers designed to amplify parts of NELL2 cDNA detected PCR products with expected size from human fetal brain, but not from a fetal liver cDNA library (data not shown). This result implies that this smaller transcript might be derived from a gene distinct from but closely related to NELL2. The expression pattern and putative sequence imply that they might function as signaling molecules in brain and other tissues. To study these possibilities functional analyses are in progress.

ACKNOWLEDGMENTS

We thank all the staff of the GEN Research Institute for technical assistance. We appreciate Dr. S. Matsuhashi for providing important information and Dr. Y. Matsuda for a kind gift of mouse Southern blotting membrane. This work was supported in part by a Grant-in-Aid for Creative Basic Research (Human Genome Project) of the Ministry of Education, Culture and Science, Japan (E.T.).

REFERENCES

Frohman, M. A., Dush, M. K., and Martin, G. R. (1988). Rapid production of full-length cDNAs from rare transcripts: Amplification using a single gene-specific oligonucleotide primer. *Proc. Natl. Acad. Sci. USA* **8**: 8998–9002.

Hirotsune, S., Takahara, T., Sasaki, N., Hirose, K., Yoshiki, A., Ohashi, T., Kusakabe, M., Murakami, Y., Muramatsu, M., Watanabe, S., Nakao, K., Katsuki, M., and Hayashizaki, Y. (1995). The reeler gene encodes a protein with an EGF-like motif expressed by pioneer neurons. *Nature Genet.* **10**: 77–83.

Matsuhashi, S., Noji, S., Koyama, E., Myokai, F., Ohuchi, H., Taniguchi, S., and Hori, K. (1995). New gene, nel, encoding a Mr 93K protein with EGF-like repeats is strongly expressed in neural tissues of early stage chick embryo. *Dev. Dyn.* **203**: 212–222.

Takahashi, E., Hori, T., O'Connell, P., Leppert, M., White, R. (1990). R-banding and nonisotopic *in situ* hybridization: Precise localization of the human type II collagen gene (COL2A1). *Hum. Genet.* **86**: 14–16.

Takahashi, E., Yamauchi, M., Tsuji, H., Hitomi, A., Meuth, M., and Hori, T. (1991). Chromosome mapping of the human cytidine-5'-triphosphate (CTPS) gene to band 1p34–1p34.3 by fluorescence *in situ* hybridization. *Hum. Genet.* **88**: 119–121.

Watanabe, T. K., Fujiwara, T., Kawai, A., Shimizu, F., Takami, S., Hirano, H., Okuno, S., Ozaki, K., Takeda, S., Shimada, Y., Nagata, M., Takaichi, A., Ei-ichi, T., Nakamura, Y., Shin, S. (1996a). Cloning, expression, and mapping of UBE2I, a novel gene encoding a human homologue of yeast ubiquitin-conjugating enzymes which are critical for regulating cell cycle. *Cytogenet. Cell Genet.* **72**: 86–89.

Watanabe, T. K., Fujiwara, T., Shimizu, F., Okuno, S., Suzuki, M., Takahashi, E., Nakamura, Y., Hirai, Y. (1996b). Cloning, expression, and mapping of TCTEL1, a putative human homologue of murine *Tctel*, to 6q. *Cytogenet. Cell Genet.* **73**: 153–156.

(12)

Craniosynostosis in transgenic mice overexpressing *Nell-1*

Xinli Zhang,[1] Shun'ichi Kuroda,[2] Dale Carpenter,[3] Ichiro Nishimura,[4] Chia Soo,[5] Rex Moats,[6] Keisuke Iida,[4] Eric Wisner,[7] Fei-Ya Hu,[8] Steve Miao,[1] Steve Beanes,[5] Catherine Dang,[5] Heleni Vastardis,[9] Michael Longaker,[10] Katsuyuki Tanizawa,[2] Norihiro Kanayama,[2] Naoaki Saito,[11] and Kang Ting[1,5]

[1]Dental and Craniofacial Research Institute, University of California, Los Angeles, Los Angeles, California, USA
[2]Institute of Scientific and Industrial Research, Osaka University, Ibaraki, Japan
[3]Department of Neurology, University of California, Irvine, Irvine, California, USA
[4]The Jane and Jerry Weintraub Center for Reconstructive Biotechnology, and
[5]Department of Surgery, University of California, Los Angeles, Los Angeles, California, USA
[6]Department of Radiology, Children's Hospital, Los Angeles, California, USA
[7]Department of Surgical and Radiological Sciences, School of Veterinary Medicine, University of California, Davis, Davis, California, USA
[8]Chang-Gung Memorial Hospital, Taipei, Taiwan
[9]School of Dentistry, Tufts University, Boston, Massachusetts, USA
[10]Department of Surgery, Stanford University, Stanford, California, USA
[11]Biosignal Research Center, Kobe University, Kobe, Japan

Previously, we reported *NELL-1* as a novel molecule overexpressed during premature cranial suture closure in patients with craniosynostosis (CS), one of the most common congenital craniofacial deformities. Here we describe the creation and analysis of transgenic mice overexpressing *Nell-1*. *Nell-1* transgenic animals exhibited CS-like phenotypes that ranged from simple to compound synostoses. Histologically, the osteogenic fronts of abnormally closing/closed sutures in these animals revealed calvarial overgrowth and overlap along with increased osteoblast differentiation and reduced cell proliferation. Furthermore, anomalies were restricted to calvarial bone, despite generalized, non-tissue-specific overexpression of *Nell-1*. In vitro, *Nell-1* overexpression accelerated calvarial osteoblast differentiation and mineralization under normal culture conditions. Moreover, *Nell-1* overexpression in osteoblasts was sufficient to promote alkaline phosphatase expression and micronodule formation. Conversely, downregulation of Nell-1 inhibited osteoblast differentiation in vitro. In summary, *Nell-1* overexpression induced calvarial overgrowth resulting in premature suture closure in a rodent model. *Nell-1*, therefore, has a novel role in CS development, perhaps as part of a complex chain of events resulting in premature suture closure. On a cellular level, *Nell-1* expression may modulate and be both sufficient and required for osteoblast differentiation.

J. Clin. Invest. 110:861–870 (2002). doi:10.1172/JCI200215375.

Introduction

Craniosynostosis (CS), the premature closure of cranial sutures, affects 1 in 3,000 infants and therefore is one of the most common human congenital craniofacial deformities (1). Premature suture closure, which results in cranial dysmorphism, can be either familial or sporadic in origin (1). Neither gender nor ethnicity can be used to predict which infants will be affected. Although genetic linkage analyses of CS-related syndromes have provided a wealth of new information about the molecular control of suture formation, the biology of local suture closure, especially in nonsyndromic, nonfamilial CS, is still largely unknown.

Presently, more than 85 human mutations, which produce various familial CS syndromes, have been localized to the FGF receptor genes *FGFR1*, *FGFR2*, and *FGFR3*. All are "gain-of-function" mutations that result in increased receptor activity (1). No human CS syndromes have been linked to the FGF ligands; however, several animal models of CS have been associated with FGF overexpression (2, 3). The only described *MSX2* mutation associated with CS (4) also results in increased *MSX2* activity (5–7). While these candidate genes are known to play important roles in osteoblast proliferation and differentiation, they also have more generalized roles during embryogenesis. Thus, it is not surprising that transgenic mouse models with mutations in these genes often manifest extracranial abnormalities not observed in the majority of patients with CS (1, 2, 8).

Received for publication March 1, 2002, and accepted in revised form July 16, 2002.

Address correspondence to: Kang Ting, Center for the Health Sciences 30-113, University of California, Los Angeles, 10833 Le Conte Avenue, Los Angeles, California 90095, USA. Phone: (310) 206-6305; Fax: (310) 206-5349; E-mail: kting@ucla.edu.

Conflict of interest: No conflict of interest has been declared.

Nonstandard abbreviations used: craniosynostosis (CS); FGF receptor (FGFR); cytomegalovirus, (CMV); magnetic resonance imaging (MRI); adenovirus (Ad); embryonic day 18 (E18); β-Galactosidase (β-Gal); fetal rat calvarial cell (FRCC); transgenic F_2 (TF_2); normal F_2 (NF_2); posterior-frontal (PF); microcomputerized tomography (MCT).

Premature suture closure in human CS can be divided into two possibly distinct processes: calvarial overgrowth and bony fusion. While calvarial overgrowth may be essential to bringing the two opposing osteogenic fronts into proximity in order to induce bony fusion, it does not necessarily follow that calvarial overgrowth or overlap alone will result in bony fusion. Thus, the study of premature suture closure mechanisms must include study of both abnormal suture overgrowth/overlap and bony fusion (6).

Recently, FGF2 and FGFR1 have been implicated in premature cranial suture fusion via *CBFA1*-mediated pathways (8). Missense mutation of CBFA1 is linked to cleidocranial dysplasia, manifested as delayed suture closure (9). Therefore, examination of *Cbfa1* (*Runx2*), a downstream target of *Fgfr1* that is essential for bone formation, may be key to understanding the signaling cascade in CS. In addition, *Msx2*, a member of the highly conserved *Msx* homeobox gene family with pleiotropic effects in development, has been implicated in an animal model of CS (5, 6). Specifically, increased osteogenic cell proliferation has been proposed as a mechanism for premature suture closure in *Msx2*-overexpressing transgenic mice, which exhibit suture overgrowth/overlap without suture fusion.

To elucidate the molecular pathway for suture closure, we previously used differential display to identify genes that were specifically upregulated within abnormally fused sutures in patients with nonfamilial, nonsyndromic CS. We isolated and characterized NELL-1, which is a Nel-like, type 1 molecule (a protein strongly expressed in neural tissue, encoding an EGF-like domain) (10–12). Nell-1 is a secreted protein. Structurally, Nell-1 encodes a secretory signal peptide sequence, an NH_2-terminal thrombospondin-1–like module, five von Willebrand factor–like repeats with six cysteine residues, and six EGF-like domains. *Nell-1* is also highly conserved across species. For example, 93% amino acid sequence homology exists between rat Nell-1 and human NELL-1.

Nell-1 encodes a polypeptide with a molecular weight of 90 kDa. When overexpressed in COS cells, the glycosylated form is N-linked to a 50-kDa carbohydrate moiety in eukaryotic cells to generate the 140-kDa form found in the cytoplasm. This 140-kDa protein is further processed to a 130-kDa protein. The Nell-1 protein is secreted as a trimeric form with a high molecular weight (approximately 400 kDa) (13, 14).

Initial studies have suggested that *NELL-1* is preferentially expressed in the craniofacial region of calvarial tissues (12–14). Premature suture closure in CS patients is remarkable for the degree of *NELL-1* overexpression by osteoblast-like cells in osteogenic areas (12). Although *NELL-1* overexpression and premature suture closure may be coincidental findings, our data suggest that *NELL-1* may be a local regulatory factor in cranial suture closure.

In this study, we further verified that *Nell-1* has a role in CS. We created a transgenic mouse model exhibiting generalized *Nell-1* overexpression. *Nell-1* transgenic animals share many of the same features as humans with CS. They demonstrate calvarial overgrowth/overlap and premature suture closure. Infection of osteoblasts with *Nell-1* adenoviral constructs showed that *Nell-1* promotes and accelerates differentiation in osteoblast lineage cells. In addition, Nell-1 downregulation inhibited osteoblast differentiation. *Nell-1*, therefore, represents a candidate gene for producing cranial suture closure and provides new insights in the study of CS and craniofacial development.

Methods

Preparation of transgenic mice overexpressing Nell-1. Rat *Nell-1* cDNA was subcloned from pTM-70 (13, 14) into pCDNA1.1 (Invitrogen, Carlsbad, California, USA), which uses a CMV promoter and an SV40 polyadenylation site. The recombinant plasmid was first transfected into MC3T3 cells (a mouse calvarial cell line) to verify proper protein expression (data not shown). The 4.76-kb DNA fragment containing the CMV promoter, *Nell-1* cDNA, and the SV40 polyadenylation site was then used for microinjection of oocytes. B6C3 mice were used to generate transgenic mice using standard protocols (15). The founders were mated with their nontransgenic littermates to set up transgenic lines.

Analysis of transgene copy number. Transgene copy numbers were estimated by PCR and Southern blot analysis. The PCR protocol of establishing transgene copy number was obtained at http://www.med.umich.edu/tamc/spike.html (16). The mass of transgene DNA per 5 μg genomic DNA was calculated as N bp transgene DNA/3×10^9 genomic DNA, based on the assumption that the haploid content of a mammalian genome is 3×10^9 bp and that it takes 10 μg DNA to spike. The size of the insert is 4.76 kb, and the one-copy standard is 7.933 pg per 10 μg genomic DNA. Thirty cycles of PCR were performed and products were separated on electrophoresis gels with ethidium bromide. The intensities were calculated using Eagle Eye II (Stratagene, La Jolla, California, USA).

Immunohistochemistry. Detailed preparation of Nell-1 antibody has been documented by Kuroda et al. (13, 14). The antibody recognizes the COOH-terminal region of Nell-1 (CSVDLECIENN). The specificity of the antibody was confirmed by Western blot using protein extracted from *Nell-1*–transfected NIH3T3 cells. A standard avidin-biotin complex/immunoperoxidase protocol (Vector Elite Kit; Vector Laboratories Inc., Burlingame, California, USA) was used with 1:100 Nell-1 antibody dilution. Diaminobenzidine peroxidase substrate and 3-amino-9-ethylcarbazole were used for visualization, and sections were counterstained with hematoxylin.

Magnetic resonance imaging. Magnetic resonance imaging (MRI) was performed on formalin-preserved specimens using a Bruker Biospec MR imager (Bruker BioSpin GmbH, Rheinstetten, Germany) with a 7.0-T, 18-cm clear-bore magnet equipped with a microimaging gradient set and a 35-mm internal diameter birdcage radiofrequency coil. Transaxial and sagittal images of the brain and calvarium were obtained using a gradient echo filtered imaging steady-state pulse sequence

with the following parameters: TR/TE, 229.3/64.1 ms; flip angle, 30°; field of view, 2.3 cm; matrix, 256 × 256; slice thickness, 1 mm; and number of excitations, 8. In-plane spatial resolution was approximately 90 μm.

Microcomputerized tomography scan. All the data were collected at 30 kVp and 750 mA. The data was reconstructed using the cone-beam algorithm supplied with the MicroCat scanner (Oak Ridge National Laboratory, Oak Ridge, Tennessee, USA). The matrix was 256 × 256 × 256, yielding an isotropic resolution of 140 μm. The quantitative procedures involve the placement of bone phantoms (long rods in the images) containing 0, 50, 250, and 750 mg/cc hydroxyapatite. Visualization of the data was performed using MetaMorph (two dimensional) (Universal Imaging Corp., West Chester, Pennsylvania, USA) and Amira (three dimensional) (Indeed – Visual Concepts GmbH, Berlin, Germany).

In vivo proliferation analysis. Newborn mice were injected with BrdU at 100 μg/g. Animals were sacrificed 2 hours after injection. The animals were fixed and immunostained with BrdU antibodies (Sigma-Aldrich, St. Louis, Missouri, USA). Calvarial sutures, brain, and tibiae from transgenic animals and their normal littermates were compared.

Recombinant defective adenovirus vectors harboring Nell-1 (AdNell-1) and antisense Nell-1 (AdAntiNell-1). Rat Nell-1 cDNA was inserted bidirectionally between the human CMV IE1 promoter and the SV40 splice/polyadenylation site flanked by nucleotide sequences from 1 to 454 and from 3,334 to 6,231 of the Ad5 virus. The resulting plasmid, pAdCMV-*Nell-1*, transcribes *Nell-1* leftward relative to the standard Ad5 map. The recombinant adenovirus (Ad) (Ad*Nell-1*) were isolated by cotransfecting 293 cells with pAdCMV-*Nell-1* and pJM17 (Microbix Biosystems Inc., Toronto, Canada), resulting in vectors defective in the *E1-A* viral gene. Clones of recombinant virus were plaque purified and confirmed by Southern blot analysis. Both Ad*Nell-1* and Ad*LacZ* were grown to a high titer and purified once through a CsCl cushion and again on a continuous CsCl gradient. The resulting stocks were 5×10^9 pfu/ml as assayed by plaque formation on 293 cells. Northern and Western blots were performed to assure the incorporation and expression of the *Nell-1* gene and its protein product.

Rat calvarial primary cell cultures (FRCCs). The isolation of osteogenic cells from embryonic day 18 (E18) rat calvaria was performed as previously described (12). The cells collected from digestions four, five, and six were pooled and plated at $2.5 \times 10^4/cm^2$. Cells within passage two were used.

Adenoviral infection of osteoblasts. In order to observe the effects of overexpressing Nell-1, osteoblasts from different lineages were grown to 80% confluence in six-well plates. The media was aspirated and an infective dose (20 pfu/cell in 1 ml serum-free medium) was added to the cultures. Five sets of Ad*Nell-1*, Ad*AntiNell-1*, and control Ad carrying β-Galactosidase (Adβ-Gal) were used. On days 12, 15, and 21 after infection, von Kossa staining was performed. The percentage of area mineralized was analyzed using the Image-Pro Plus system (Media Cybernetics, Silver Spring, Maryland, USA). Comparisons between mice were made using the Student *t* test.

In order to observe the effects of downregulating Nell-1, Ad*AntiNell-1* was added to fetal rat calvarial cell (FRCC) cultures as described above.

Microarray analysis. Microarrays were performed using RNA from Ad*Nell-1*– and Ad*β-Gal*–infected MC3T3 cells at 6, 9, and 12 days after infection. I. Nishimura and the University of California Los Angeles Microarrays Core Facility staff have developed bone-related microarrays. The microarrays contain over 37 genes with more than ten internal control genes. Confirmed markers include the following: bone matrix proteins (osteopontin, osteonectin, osteocalcin, bone sialoprotein); receptors (α_2-integrin, vitamin D receptor, parathyroid receptor, estrogen receptor); osteoblastic markers (alkaline phosphatase, Cbfa1); adhesive proteins (fibronectin, chondroitin sulfate proteoglycan 1, decorin, tenascin, syndecan, laminin); metalloproteinases (matrix metalloproteinases 1 and 2); growth factors (Bmp2, Bmp7); fibrillar collagens (collagens 1A1, 1A2, 3A1, 5A2, and 11A1); other collagens (collagens 4A1, 6A1, 7A1, 10A1, and 15A1); and fibril-associated collagen with interrupted triple helices (FACITs) (collagens 9A1, 9A2, 12, 14, 16, and 19).

RNA (30 μg total RNA for Cy3 and 60 μg for Cy5) was labeled with random hexamer primers and Cy3- or Cy5-dUTP. The reverse transcriptase-labeled probes were hybridized onto the arrays. Multiple laser scans were performed with a 418 Array Scanner (Affymetrix Inc., Santa Clara, California, USA) to provide mean readouts and standard deviations to verify the reproducibility of the measurements. An average of all the internal controls was calculated and used to normalize hybridization intensities using the IPLab version 3.2 MicroArray suite (Scanalytics Inc., Fairfax, Virginia, USA). The correlation of all osteoblastic markers as a group was calculated and compared between the Ad*Nell-1*–infected cells and the Ad*β-Gal*–infected control cells.

RT-PCR. DNase-treated total RNA was used. After initial verification of gene fragment expression through high-cycle PCR, another low-cycle PCR was performed to quantify relative gene expression (12). For each candidate molecule, we determined the cycle number most likely to fall within the linear amplification range by successively reducing the number of cycles (range, 15–35 cycles). Electrophoreses were performed and hybridized with sequence-specific probes labeled wit P32. A PhosphorImager (Molecular Dynamics, Sunnyvale, California, USA) was used to measure the intensities. For each sample, the densitometry value was divided by the *Gapdh* value (performed at 20 cycles) and normalized. Primer sequences were as follows. *Msx2*: forward, 5′-CCTCGGTCAAGTCGGAAAATTC-3′; reverse, 5′-TGGACAGGTACTGTTTCTGGCG-3′; probe, 5′-GAGCACCGTGGATACAGGAG-3′ (annealing temperature, 68°C). *Cbfa1*: forward, 5′-CTGTGTGGCTCCTAACAAGTGTG-3′; reverse, 5′-GGATTCTGGCAATCACAAGCTGTC-3′; probe, 5′-CCTACTCACTGTCCGGGGAGTCCTGC-3′

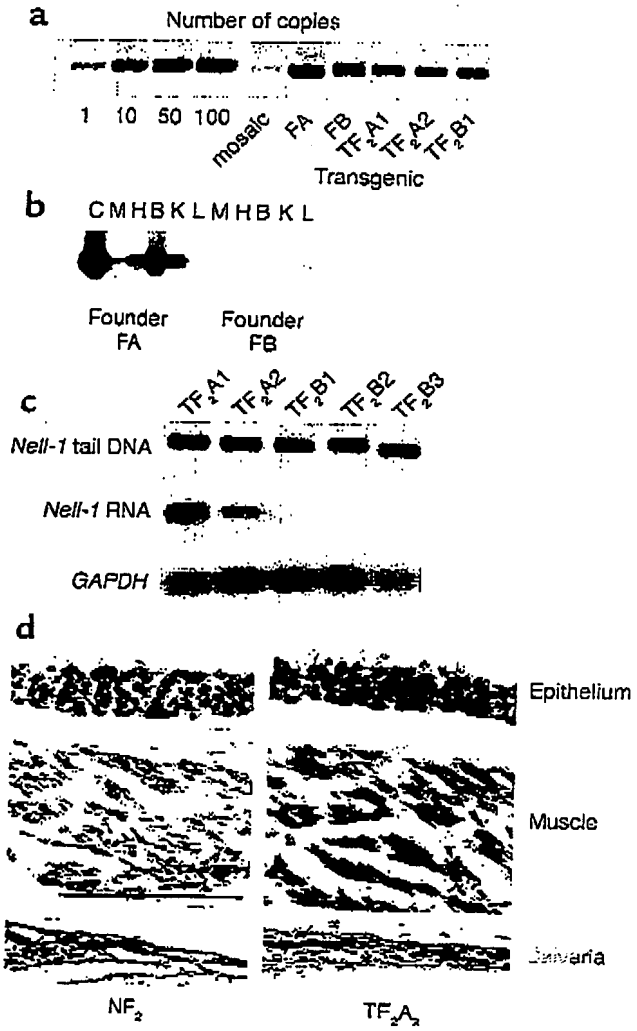

Figure 1

Nell-1 transgenic mice compared with nontransgenic littermates. (a) Transgene copy number. The founders (FA and FB) and their progeny (TF_2A1, TF_2A2, and TF_2B1) have copy numbers between 50 and 100. TF_2A1 and TF_2A2 are from the founder A line. TF_2B1, TF_2B2, and TF_2B3 are from the founder B line. (b) RT-PCR analyses of *Nell-1* RNA expression in both founders. C, control *Nell-1* plasmid; M, muscle; H, heart; B, bone; K, kidney; L, liver. (c) Whole body (without head) RNA of newborn progeny. TF_2A1 and TF_2A2 express different levels of *Nell-1*. TF_2B1 expresses *Nell-1* weakly, while TF_2B2 and TF_2B3 have no *Nell-1* expression. (d) Left panels, immunolocalization of Nell-1 protein in newborn NF_2 epithelium, muscle, and calvarial bone. There is no detectable Nell-1 expression (brown staining indicates the presence of Nell-1) except some staining in the calvarial bone. Right panels, immunolocalization of Nell-1 protein in TF_2A2 epithelium, muscle, and calvarial bone. Abundant Nell-1 expression is present throughout all soft tissue layers as well as in bone. Bar represents 50 μm.

(annealing temperature, 66°C). Osteocalcin: forward, 5′-ATGAGGACCCTCTCTCTGCTC-3′; reverse, 5′-GTGGTGCCATAGATGCGCTTG-3′; probe CATGTCAAGCAGGGAGGGCA-3′ (annealing temperature, 66°C). Osteopontin: forward, 5′-AGCAGGAATACTAACTGC-3′; reverse, 5′-GATTATAGTGACACAGAC-3′; probe 5′-GCCCTGAGCTTAGTTCGTTG-3′ (annealing temperature, 66°C). *Nell-1*: (12).

Flow cytometry analysis. Cells were seeded on 60-mm plates at 5×10^5 cells/plate. Cells were harvested at 24, 36, 48, and 72 hours after infection with Ad*Nell-1* and Ad*β-Gal*. One million cells were used for flow cytometry, and this procedure was repeated three times. Hypotonic DNA staining buffer containing propidium iodide was added to the cells for flow cytometry.

Results

Construction of CMV promoter/Nell-1 transgenic mice. To investigate the effects of generalized *Nell-1* overexpression in vivo, transgenic mice in which *Nell-1* is expressed under the control of the CMV promoter were produced. Copy number was confirmed by Southern blot and PCR (Figure 1a). RNA analysis (Figure 1b) and immunohistochemistry (data not shown) further confirmed expression of Nell-1 in founders. *Nell-1*–overexpressing founders were crossed with nontransgenic littermates, and comprehensive analyses were conducted on F_2 progeny. Because most human CS phenotypes are readily apparent in newborns, 42 newborn mice, representing six litters from two lines, were examined. The morphology of these mice was assessed for developmental anomalies, including suture closure. The mice were subsequently genotyped. Suture patency was determined by the absence (indicating suture closure) or the presence (indicating suture patency) of visible blood vessels underneath the suture. Suture closure was further confirmed under a dissecting microscope. Two of the six litters examined, representing 20 progeny, did not yield any newborns with obvious craniofacial defects and were *Nell-1* transgene negative. These litters were not examined further. Progeny with craniofacial defects were recovered in each of the four remaining litters. The progeny of these four litters (22 mice) were analyzed further. A limitation of this rapid screening method is that mild CS with only focal points of suture closure may not be detected, and therefore *Nell-1* overexpression might appear to have lower penetrance.

Thirteen (60%) of the 22 newborn progeny were transgenic, with gene copy numbers similar to the founder *Nell-1* mice (prediction is 50%). *Nell-1* RNA levels of the 13 *Nell-1* DNA–positive transgenic F_2 (TF_2) mice were examined. Eight (62%) were positive for *Nell-1* RNA expression. However, the level of expression varied (Figure 1c). The reason for low or nearly absent *Nell-1* expression in some TF_2 mice despite their high transgene copy numbers is not clear, but epigenetic effects such as heterochromatin formation around the inserts may play a significant role in the high variability of transgene expression (17). RNA levels also differed in different tissues isolated from the same litter. Liu et al. also made this observation of variegation when they overexpressed *Msx2* using a *CMV* promoter (5, 6). Therefore transgenic *Nell-1* transcription may not necessarily correlate with gene copy number, and may also vary according to cell type.

To determine whether *Nell-1* overexpression in our transgenic model was physiologically relevant, we compared *Nell-1* RNA expression levels from the whole heads of three TF_2 progeny with mild CS phenotypes to levels

in nontransgenic normal littermates (NF_2 mice). TF_2 mice displayed up to fourfold-increased *Nell-1* expression (data not shown). This was comparable to levels of *NELL-1* overexpression in human CS patients in whom two- to fourfold increases have been observed (12). This suggests that *Nell-1* overexpression levels in our model were clinically relevant rather than superphysiologic.

Phenotypic analyses of Nell-1 transgenic mice. Three of the eight *Nell-1* RNA-positive TF_2 mice demonstrated severe craniofacial anomalies and died shortly after birth (see Figure 2, a–c, and Figure 4). These mice also demonstrated detectable *Nell-1* transgene expression in their total body mRNA (Figure 1e) that was verified by Nell-1 immunostaining of skin, liver, and calvaria (Figure 1d).

Morphological examination of one of the most severely affected TF_2 mice revealed a large protuberance in the paramedial parietal area with completely closed sagittal and posterior-frontal (PF) sutures and partially closed coronal sutures (Figure 2, a–c). Clinically, this is similar to craniotelencephalic dysplasia, a form of human CS with premature sagittal, metopic, and coronal suture closure with secondary frontal bone bossing and paramedial encephalocele (Figure 2d) (1). Brain MRI of this TF_2 mouse revealed significantly reduced ventricle size and increased parenchymal edema, both of which are suggestive of increased intracranial pressures (Figure 2e). Continued brain growth in the face of premature suture closure also generates increased intracranial pressures in humans with untreated CS. Microcomputerized tomography (MCT) scan and MRI analysis also demonstrated structural abnormalities in the cranium of this TF_2 mouse (Figure 2, f and g).

Histological examination of Nell-1 phenotype-positive TF_2 mice revealed distinct differences from NF_2 littermates. As in human CS, TF_2 mice displayed prematurely closing sutures seen histologically as thickened, disorganized ridges of calvarial ridges with closing/overlapping osteogenic fronts (Figure 3, a and b). Whole-mount skeletal staining did not show any observable extracranial skeletal anomalies. Hematoxylin and eosin and tartrate-resistant acid phosphatase staining of palatal and midmandible sutures, vertebrae, and long bones did not reveal any abnormal histology or increase in osteoclast number. Therefore, the effects of Nell-1 expression appear to be confined to the calvaria. Despite pan-tissue *Nell-1* expression due to the use of the *CMV* promoter, TF_2 mice exhibited cranial-specific anomalies that primarily affected calvarial suture patency and closure. Immunohistochemistry showed increased in vivo expression of osteoblastic differentiation markers (Figure 3, c and d).

In situ BrdU analysis of prematurely closing cranial sutures in *Nell-1*–expressing TF_2 mice demonstrated significantly reduced numbers of proliferating cells within osteogenic areas along suture edges (Figure 3, e and f). These data suggest that *Nell-1* overexpression is associated with osteoblast differentiation. No statistically significant difference was observed in the total number (Figure 3g) of cells per field along the sutures of TF_2 and NF_2 mice. The observed decrease in proliferating cells may be secondary to the decreased proliferative abilities of differentiated osteoblasts or may reflect a primary defect in osteoblast proliferation.

Morphologic examination of a second severely affected TF_2 animal showed significant cranial suture

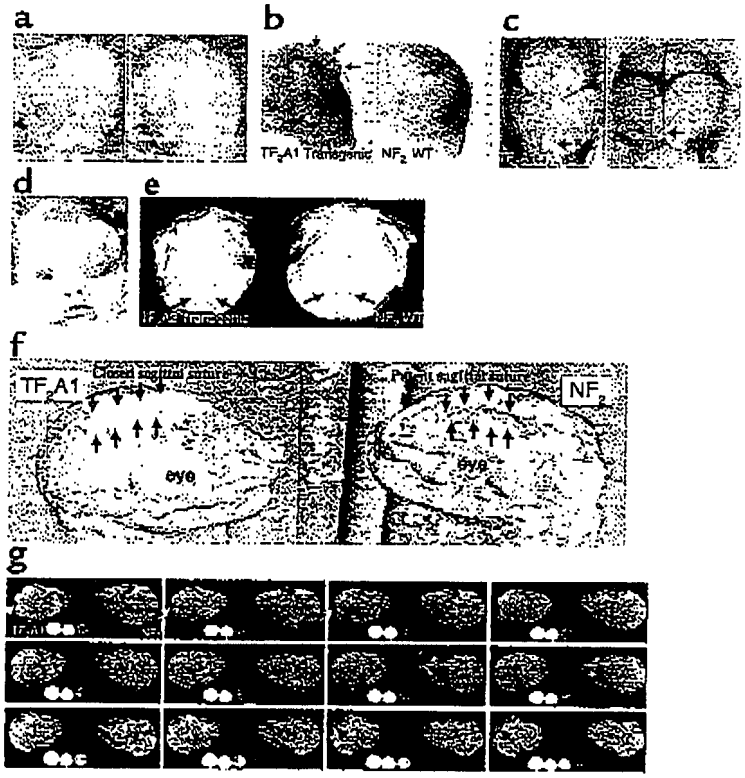

Figure 2
Phenotypic evaluation of *Nell-1* transgenic mice. (a and b) Left panels show a newborn Nell-1 phenotype–positive (TF_2A1) mouse. Note the protrusion in the frontoparietal area (arrows). Right panels show an NF_2 littermate. (c) Left panel, TF_2A2 mouse with the scalp removed. The sagittal (yellow arrow) and PF (black arrow) sutures are closed. Right panel, skull of the NF_2 littermate with patent sagittal (yellow arrows) and PF (black arrow) sutures and normal vasculature underneath the patent sutures. (d) An infant with craniotelencephalic dysplasia, a severe form of CS. (e) Brain MRI of TF_2A1 mouse (left) and NF_2 littermate (right). Note the complete absence of ventricles, suggesting elevated intracranial pressure in the TF_2A1 mouse (arrows, left) relative to its NF_2 littermate (arrows, right). (f) MCT-reconstructed three-dimensional skull views of the newborn Nell-1 phenotype-positive TF_2A1 (left) and NF_2 (right) littermates. Arrows indicate sagittal and PF suture sites. In TF_2A1 mice, the sagittal and PF sutures are largely closed and replaced with an abnormal ridge. In the NF_2 littermate, both sagittal and PF sutures are patent. Complete opacity corresponds to greater than 50 mg/cc mineralization. The vertical rods in the background are phantom reference rods corresponding to mineralization densities (from left to right) of 50, 100, 150, and 200 mg/cc. (g) Serial axial MCT sections of the TF_2A1 (left) and NF_2 littermates (right) shown in f. Yellow arrows indicate the distortion of the cranium. Green arrows indicate increased mineralization of the calvarium in the TF_2A mouse (arrow, right).

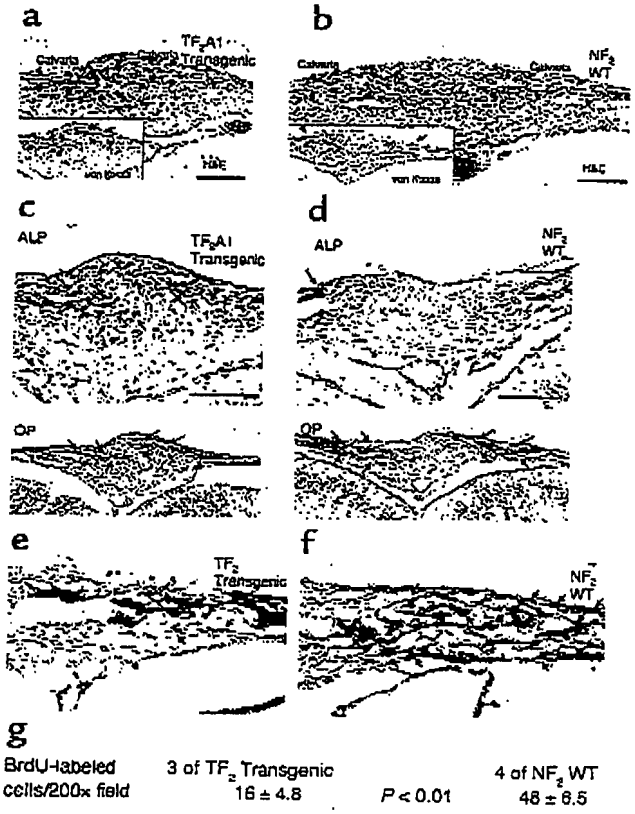

Figure 3
Histologic and immunohistologic evaluation of *Nell-1* transgenic mice. (a) Hematoxylin and eosin staining of the sagittal suture of a Nell-1 phenotype-positive TF_2A1 mouse. There is closure of the suture, shown by the overlap of calvarial edges (black arrows) and closing osteogenic fronts (red arrows). Lower left panel shows von Kossa staining. Note the close proximity of mineralized calvarial edges. (b) Hematoxylin and eosin staining of the sagittal suture from an NF_2 littermate. Note the large distance separating the two calvarial edges (black arrows) at the patent suture site, as well as the advancing osteogenic fronts (red arrows). Lower left panel shows von Kossa staining. Black color indicates mineralization. (c) Immunolocalization of alkaline phosphatase (ALP) in a TF_2A1 mouse. Brown staining indicates the presence of alkaline phosphatase (arrows). Lower panel represents the immunolocalization of osteopontin at lower magnification. (d) Upper panel shows immunolocalization of alkaline phosphatase in newborn NF_2 cranial suture. Lower panel represents the immunolocalization of osteopontin (OP) at a lower magnification. Bar represents 50 μm. (e) BrdU staining of a TF_2 sagittal suture. The nuclei of proliferating cells are stained brown (black arrows). Proliferating cells are significantly decreased relative to those shown for NF_2 in d. (f) BrdU staining of a newborn NF_2 mouse sagittal suture. Numerous brown-stained cells are proliferating along the calvarial edges (black arrows) of the patent suture, as well as along the advancing osteogenic fronts (red arrows). H&E, hematoxylin and eosin. (g) Number of proliferating cells per field.

obliteration, primarily in the midline (i.e., sagittal and posterior frontal sutures), with bulging in the occipital (posterior) area. Overall, the skull was narrow and resembled those of humans with scaphocephaly and premature sagittal synostosis. MCT scanning revealed complete PF suture and partial sagittal and coronal suture closure (Figure 4b). Histological correlation revealed marked calvarial bone overgrowth and overlap in the closed area of the sagittal suture (Figure 4b).

To examine TF_2 embryologic development during gestation, two litters of E15 TF_2 progeny were sacrificed. Nonviable littermates with exencephaly-like phenotypes were observed in two of 19 embryos. Interestingly, Liu et al. reported a similar finding of exencephaly for *Msx2*-overexpressing mice (6). The etiology for this phenotype is not clear. This result may also help to explain the observed low incidence of severely affected TF_2 progeny among newborn mice.

Overexpression of Nell-1 in vitro accelerates osteoblast differentiation. Dysregulated bone formation has been proposed as a possible mechanism for calvarial overgrowth/overlap and premature suture closure (18). Because abnormal suture site osteogenesis is the cardinal feature of *Nell-1* TF_2 mice exhibiting premature suture closure, we hypothesized that *Nell-1* overexpression may alter normal calvarial osteoblast cell cycling and differentiation pathways to promote premature osteogenesis.

To test our hypothesis, we first examined the effect of *Nell-1* on mineralization, a hallmark of osteoblast differentiation in vitro. Primary FRCC and MC3T3 (a mouse calvarial osteoblast-like cell line) cultures were infected with Ad*Nell-1* at 20 pfu/cell in the presence of ascorbic acid. Ascorbic acid is essential for the induction and terminal differentiation/mineralization of osteoblasts (19). Ad*Nell-1*–infected FRCC and MC3T3 cultures mineralized more rapidly and profusely (more than sixfold) than Ad*β-Gal*–infected controls did (Figure 5, a and b). In contrast, Ad*Nell-1* infection did not elicit any mineralization response in NIH3T3, adult, or fetal rat primary fibroblast cells (data not shown). These data suggest that *Nell-1* accelerates osteoblast mineralization and that the effects are osteoblast-specific.

Our previous in vivo BrdU results demonstrated significantly reduced cell proliferation along the osteogenic front in TF_2 mice. To determine whether *Nell-1* overexpression in vitro also affects cell cycling, Ad*Nell-1*–infected MC3T3 cells (and Ad*β-Gal* controls, with and without ascorbic acid treatment and with and without 24 hours of serum starvation) were examined by flow cytometry at 24 and 48 hours after infection. No statistically significant changes were observed in populations in different phases of the cell cycle (two-tailed Student *t* test, $P > 0.05$). The fact that MC3T3 cells did not demonstrate decreased proliferation after *Nell-1* transfection may reflect inherent differences between in vivo and in vitro osteoblast cells or the influence of the extracellular milieu and stage of cellular differentiation.

Normal in vitro osteoblast differentiation is heralded by nodule formation (osteoblast cell aggregates) followed by mineralization. This differentiation program requires ascorbic acid. Interestingly, Ad*Nell-1*–infected MC3T3 cells, when cultured *without* ascorbic acid, also formed nodules expressing alkaline phosphatase beginning on day 3 after infection; control Ad*β-Gal*–infected cells did not. *Nell-1*–induced nodules in the absence of

ascorbic acid, however, were smaller (≤ 20 cells per nodule, detectable at 100× magnification), and did not reveal mineralization with von Kossa staining (Figure 5c). Moreover, late differentiation markers such as osteopontin were not expressed in these "micronodules." The formation of micronodules by Ad*Nell-1*-infected osteoblasts in the absence of ascorbic acid suggests that *Nell-1* alone may influence cell-cell adhesion but is not sufficient to induce full osteoblast differentiation.

To prove that *Nell-1* enhances osteoblast differentiation, RNA from Ad*Nell-1*-infected MC3T3 cells, cultured under normal conditions with ascorbic acid, were subjected to microarray analyses of various bone-specific markers at 6, 9, and 12 days after infection (Figure 5, d–f). The purpose of the microarray was to determine whether Ad*Nell-1*-infected and control Ad*β-Gal*-infected cells demonstrated distinct differences in overall osteoblast differentiation marker expression patterns using regression analysis. By day 12, the expression pattern of osteoblast differentiation markers was distinctly different between Ad*Nell-1*– infected cells and Ad*β-Gal*-infected cells (r^2 = 0.334). Microarray analyses used in this experiment were not meant to quantitate the expression of individual genes. Individual gene expression patterns should be interpreted with caution, e.g., genes with two or more fold up or downregulation should then be analyzed. Results should also be confirmed with RT-PCR or RNA analyses. Late differentiation markers, such as Bmp7, osteopontin, and osteocalcin, were upregulated more than twofold in Ad*Nell-1*–infected cells, while earlier markers, such as type I collagen and osteonectin, were downregulated more than twofold (Figure 5g). This suggests that *Nell-1* promotes osteoblast differentiation. Osteocalcin and osteopontin RNA upregulation were verified by RNA electrophoresis (see Figure 6, c and d). Neither microarray nor reduced-cycle RT-PCR analyses demonstrated any significant changes in expression of *Cbfa1*, *Tgf-β1*, *-β2*, *and -β3*, or *Tgf-β types -I*, *-II*, and *-III* receptors, *Fgfr1*, or *Fgfr2* in Ad*Nell-1*–infected MC3T3 cells (data not shown). This suggests that *Nell-1* may operate downstream of these candidate genes or may affect distinctly different pathways.

Downregulation of Nell-1 in vitro delays osteoblast differentiation. To further address the physiologic function of Nell-1 in osteoblast differentiation, we tested the effect of downregulating the Nell-1 protein through adenoviral antisense *Nell-1* infection in osteoblasts. FRCC cultures were infected with AdAnti*Nell-1* at 20 pfu/cell in the presence of ascorbic acid. AdAnti*Nell-1* downregulated Nell-1 protein expression to 40% of its normal expression level (Figure 6a). FRCC cultures expressed significantly less alkaline phosphatase than did Ad*β-Gal*–infected controls or Ad*Nell-1*–infected cells (Figure 6b). Osteocalcin and osteopontin RNA expression was also downregulated in AdAnti*Nell-1* cells (Figure 6, c and d). The ratio of osteocalcin in AdAnti*Nell-1*–infected cells to osteocalcin in Ad*β-Gal* controls was less than 1:4 on day 9 and 1:2 on day 12 by Northern analysis. The ratio of osteopontin in AdAnti*Nell-1*–infected cells to that in Ad*β-Gal* controls was less than 1:5 on days 6 and 9, and less than 2:5 on day 12. Therefore, knockdown data complement the overexpression data and suggest that *Nell-1* plays an important role in osteoblast differentiation.

Discussion

NELL-1 is a relatively newly discovered molecule with unknown function. Because of the observed transient upregulation of *NELL-1* during premature suture closure in CS patients (12), we simulated *NELL-1* overexpression in a mouse model in order to investigate novel potential functions of *Nell-1* in craniofacial development and pathology. We observed early suture closure and increased osteoblast differentiation in *Nell-1* transgenic mice. Therefore, *Nell-1* is likely a candidate for the control of local suture closure, and the overexpression of *Nell-1* may play an important role in the mechanism of premature suture closure in CS. Based on our overexpression and knockdown in vitro data, *Nell-1* most likely influences osteoblast differentiation. However, the molecular mechanism is unknown.

Nell-1 may induce osteoblast differentiation by binding and then sequestering or activating ligands, as well as by triggering receptor-mediated signaling (20). Nell-1's combination of chordin-like, cysteine-rich domains,

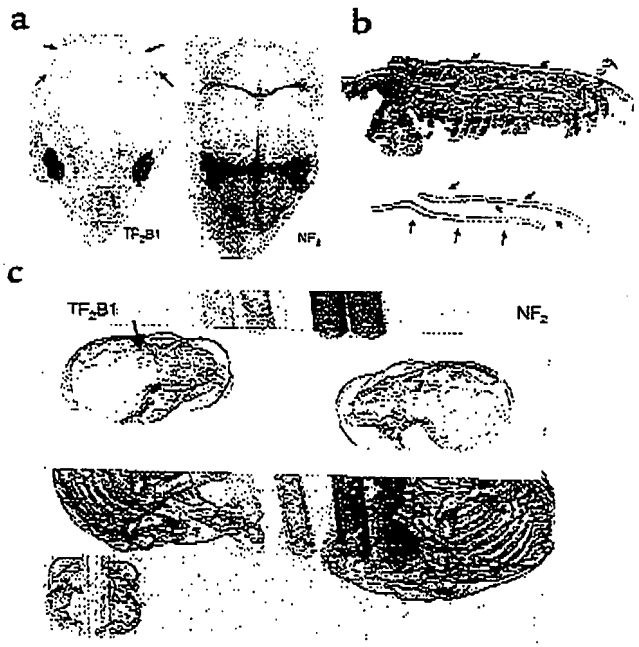

Figure 4
Nell-1 transgenic TF_2B1 mouse compared with a nontransgenic littermate. (a) Left, newborn TF_2B1 mouse with the scalp removed. Note the abnormal bulging of the occipital area and the relatively narrow width of the cranium. Right, an NF_2 littermate. In the TF_2B1 transgenic animal, the sagittal suture and several other sutures are closed. (b) Hematoxylin and eosin staining of TF_2B1 sagittal suture. Premature closure of the suture is manifest in the severe overlap of calvarial edges (red arrows). The underlying brain tissue has been removed for RNA analysis. (c) Three-dimensional MCT reconstruction of a TF_2B1 mouse (left) and its NF_2 littermate (right). Note the area of premature midline suture closure in the TF_2B1 mouse (arrow, left).

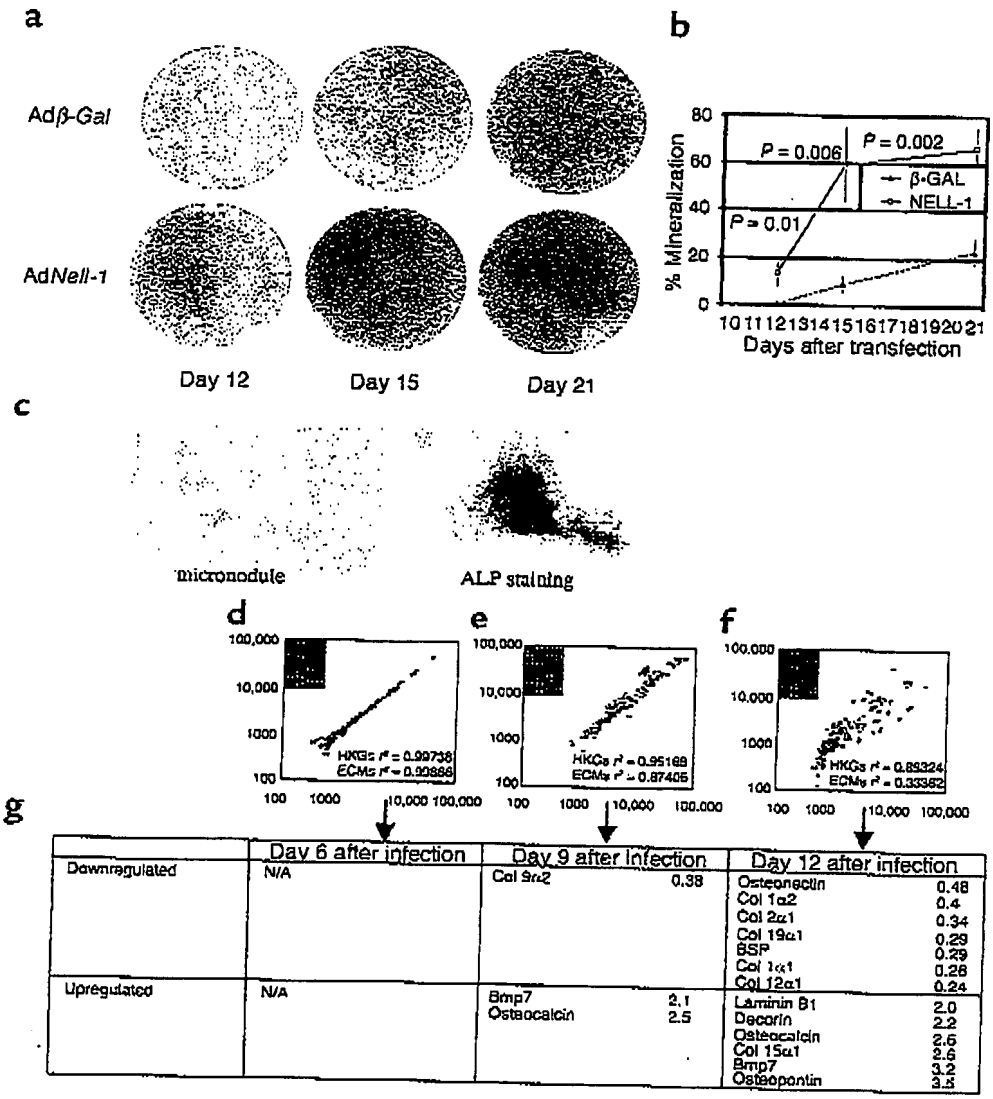

g

	Day 6 after infection	Day 9 after infection		Day 12 after infection	
Downregulated	N/A	Col 9α2	0.38	Osteonectin	0.48
				Col 1α2	0.4
				Col 2α1	0.34
				Col 19α1	0.29
				BSP	0.29
				Col 1α1	0.28
				Col 12α1	0.24
Upregulated	N/A	Bmp7	2.1	Laminin B1	2.0
		Osteocalcin	2.5	Decorin	2.2
				Osteocalcin	2.6
				Col 15α1	2.6
				Bmp7	3.2
				Osteopontin	3.5

Figure 5

Effects of *Nell-1* overexpression on mineralization and bone marker expression. (a) FRCC culture infected with 20 pfu/cell Ad*Nell-1*, stained with von Kossa stain. Control cell cultures were infected with Ad*β-Gal*. Experiments were performed in triplicate. Mineralized nodules are stained black. (b) Quantitation and statistical analysis of mineralized areas. Ad*Nell-1*–infected cultures demonstrated significantly greater mineralization than did Ad*β-Gal* controls. (c) Ad*Nell-1*–infected MC3T3 cells grown without ascorbic acid. Typical micronodule appearance is shown. Right panel represents alkaline phosphatase staining of a micronodule. (d–f) Microarrays of Ad*Nell*-infected MC3T3 cells on postinfection days 6, 9, and 12, respectively. Gene expression intensities have been normalized using standardized housekeeping genes (HKGs). Hybridization intensities of Ad*Nell-1*–infected cells are represented on the *y* axis. Hybridization intensities of Ad*β-Gal*–infected cells are represented on the *x* axis. HKGs r^2 represents the correlation of housekeeping genes (filled squares) between the two samples. ECMs r^2 represents the correlation of candidate gene expression (open squares) between the two samples. A photograph of the microarray reading is attached in the upper left corner of each diagram. A twofold or greater upregulation is represented in red, while a twofold or greater downregulation is represented in green (g) Table summarizing genes with a difference in expression that is twofold higher or lower after Ad*Nell-1* infection. The ratio is calculated as *Nell-1*/*β-Gal*. Col, collagen.

NH_2-terminal thrombospondin-like module, and EGF-like repeats make it a likely modulator of growth factor activity. We have conducted preliminary studies to test this possibility. To determine whether Nell-1 binds to known EGF-like receptors, we previously added Nell-1 to IL-3–dependent cells expressing ErbB1, -2, -3, or -4. The addition of Nell-1 failed to produce tyrosine phosphorylation of these receptors. Nell-1, therefore, is not a ligand for these receptors even though Nell-1 is a known secretory protein with EGF-like repeats (13). Instead, Nell-1 may interact with other specific receptors that may be expressed only by certain cell types. Using the yeast two-hybrid system (14), we are in the process of isolating potential Nell-1 receptors, although no such receptors have been found yet. Because Nell-1 shares many motifs with thrombospondin-1 and chordin, it may hypothetically activate or sequester members of the TGF-β superfamily and function as a thrombospondin-1–like

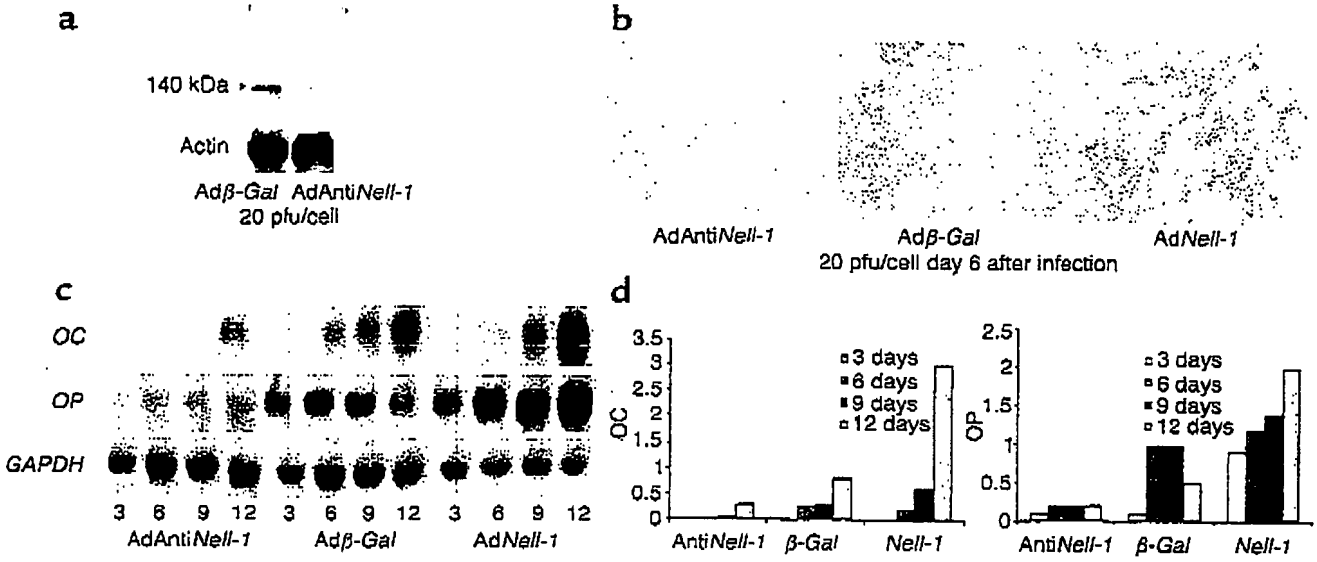

Figure 6

Effect of Nell-1 downregulation on alkaline phosphatase expression and bone marker expression. (a) Western blot analysis of Nell-1 protein expression in rat FRCCs infected with 20 pfu/cell AdAnti*Nell-1* or Ad*β-Gal* control. Downregulation of approximately 60% is observed. (b) Alkaline phosphatase staining (in red) of FRCCs. AdAnti*Nell-1*–infected cells have significantly less staining than do control and Ad*Nell-1*–infected cells. (c) Northern analyses of FRCCs on days 3, 6, 9, and 12 after infection. AdAnti*Nell-1*–infected cells have significantly less osteocalcin and osteopontin expression. (d) Expression of osteocalcin (OC) and osteopontin (OP) measured by PhosphorImager and normalized by *GAPDH*.

molecule to facilitate latent TGF-β1 activation (21). Recently, Abreu et al. suggested that Nell-1 is a member of the "chordin-like cysteine-rich domains" family, which includes chordin, kielin, crossveinless, twisted gastrulation (Tsg), and connective TGF (20). A common feature of the chordin-like cysteine-rich domains family members is that their expression is temporally and spatially specific, particularly in patterning. Another common feature is their interaction with members of the Bmp family and subsequent function as pro- or anti-Bmp's.

Specific expression and function of Nell-1 in vivo. In our previous studies, we reported the earliest detectable *Nell-1* expression in E11–E14 mice (12). *Nell-1* is preferentially expressed in the craniofacial region, both prenatally and postnatally, during growth and development. Immunohistochemistry showed that Nell-1 localizes primarily to bone-forming areas of sutures and the calvarium and ossifying membranous bone in the mandible (data not shown). Both calvarial and mandibular membranous bones are thought to be neural crest derivatives (22). Preferential *Nell-1* expression in the craniofacial region by neural crest derivatives suggests that Nell-1 may be important during skeletal craniofacial growth and development.

Surprisingly, unlike other CS models involving generalized gene overexpression, *Nell-1* transgenic mice displayed anomalies that were restricted to the calvarial bone, despite generalized, non-tissue-specific *Nell-1* overexpression. This further supports our hypothesis that Nell-1 undergoes highly specific interaction to induce osteoblast differentiation. *Nell-1* overexpression, therefore, is less likely to cause suture closure by nonspecifically perturbing the function of homologous molecules such as thrombospondin-1. This was verified by knockdown studies in vitro.

Effect of Nell-1 on osteoblast differentiation. Normal osteoblasts cultured without ascorbic acid do not differentiate. Osteoblasts overexpressing *Nell-1*, on the other hand, form micronodules and express alkaline phosphatase in the absence of ascorbic acid. This suggests that *Nell-1* alone is sufficient to induce some degree of osteoblast differentiation.

In addition, RNA microarray analyses of *Nell-1* overexpression in osteoblasts cultured under normal conditions (i.e., with ascorbic acid) demonstrated upregulation of late differentiation markers at day 12 after transfection. Ad*Nell-1*–transfected osteoblasts also exhibited increased mineralization beginning on day 12 after transfection. These data indicate that *Nell-1* may accelerate the rate of calvarial osteoblast differentiation and mineralization.

Nell-1 overexpression may not reflect the true physiological function of Nell-1, but rather the effect of *Nell-1* overexpression on other thrombospondin-like molecules. Downregulation of *Nell-1* clearly inhibited osteoblast differentiation. Nell-1 is therefore likely to

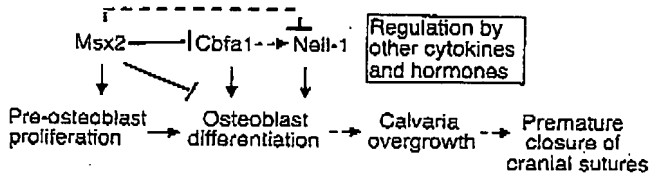

Figure 7

Hypothetical model of *Nell-1* function in premature suture closure. Dashed line represents potential modulation.

be both sufficient and required for osteoblast differentiation in vitro. However, *Nell-1* null mice need to be produced in order to justify this conclusion in vivo.

Nell-1's relation to currently known CS models. *Nell-1* overexpression produces craniofacial abnormalities similar to those resulting from *Msx2* overexpression in vivo. Both mouse models exhibit suture overgrowth and an increased incidence of exencephaly. However, the cellular functions of these two genes appear to be distinctly different; continuous *Msx2* overexpression induces proliferation and inhibits differentiation, while *Nell-1* enhances differentiation. Mice with a $Pro^{250} \rightarrow Arg$ mutation in *Fgfr1*, which induces *Cbfa1* overexpression, have distinctly different phenotypes from mice overexpressing *Nell-1* because calvarial fusion occurs much later (postnatal days 16–21) and gross suture overlap does not occur (8) in the mice with the Pro^{250} mutation. However, *Cbfa1* has a similar cellular function to *Nell-1* in vitro; both induce osteoblast differentiation with upregulation of bone marker genes. *Nell-1* expression is modulated by *Msx2* and *Cbfa1*. *Cbfa1* transfection of FRCCs upregulated *Nell-1* expression within 24 hours, while *Msx2* transfection and *Cbfa1/Msx2* cotransfection downregulated *Nell-1* expression (unpublished observations). While all these candidate genes are important to the understanding of CS, *Msx2* may be important in the earlier stages of CS (5, 6), while *Fgfr1/Cbfa1* may play a role in the later stages of suture closure. Future investigation of the *Nell-1* promoter, which contains conserved Cbfa1 and Msx binding sequences, may provide further understanding of their interactions (Figure 7). These observations underscore the complexity of the dynamic genetic and environmental interactions in craniofacial growth and development.

In conclusion, we have created an animal model of human nonsyndromic CS by overexpressing *Nell-1*. Unlike other available CS models involving mutations in *FGFRs* or homeobox genes (1, 2, 8), our animal model exhibited anomalies that were localized to the craniofacial skeleton. We hypothesize that *Nell-1* is sufficient, and probably required, to promote and accelerate calvarial osteoblast differentiation and bone formation. Mechanistically, *Nell-1* overexpression induces intramembranous bone formation in cranial sutures and may lead to calvarial overgrowth/overlap and subsequent premature suture closure.

Although *Nell-1* has not yet been identified as a cause of CS in human genetic studies, the data strongly suggest that Nell-1 is part of a complex chain of events resulting in premature suture closure (1). The resemblance of *Nell-1* transgenic mice to humans with nonsyndromic CS and *Nell-1*'s association with known CS candidate genes provides new insights for CS research. Further investigation of the regulation and mechanism of *Nell-1* in suture closure and bone formation can potentially accelerate our understanding of the cascade of events leading to premature suture closure in CS.

Acknowledgments

We thank Frank Netter, Ernie Kwong, and Hao Fu Lee for assistance with graphics. We thank Sharon Hunt and Karen Lyons for editing the manuscript. We thank Robert Maxson, M. Luisa Truela-Arispe, and E.M. DeRobertis for their input. This research is supported by the Wunderman Family Foundation, the Oral and Maxillofacial Surgery Foundation, the NIH and University of California, Los Angeles, Clinical Research Center, the National Institute of Dental and Craniofacial Research (K23DE00423), and the American Association of Orthodontists Foundation.

1. Cohen, M.M., Jr., and MacLean, R.E. 2000. *Craniosynostosis: diagnosis, evaluation and management.* 2nd edition. Oxford University Press. New York, New York, USA. 454 pp.
2. Coffin, J.D., et al. 1995. Abnormal bone growth and selective translational regulation in basic fibroblast growth factor (FGF-2) transgenic mice. *Mol. Biol. Cell.* 6:1861–1873.
3. Carlton, M.B., Colledge, W.H., and Evans, M.J. 1998. Crouzon-like craniofacial dysmorphology in the mouse is caused by an insertional mutation at the Fgf3/Fgf4 locus. *Dev. Dyn.* 212:242–249.
4. Jabs, E.W., et al. 1993. A mutation in the homeodomain of the human MSX2 gene in a family affected with autosomal dominant craniosynostosis. *Cell.* 75:443–450.
5. Liu, Y.H., et al. 1995. Premature suture closure and ectopic cranial bone in mice expressing Msx2 transgenes in the developing skull. *Proc. Natl. Acad. Sci. USA.* 92:6137–6141.
6. Liu, Y.H., et al. 1999. Msx2 gene dosage influences the number of proliferative osteogenic cells in growth centers of the developing murine skull: a possible mechanism for MSX2-mediated craniosynostosis in humans. *Dev. Biol.* 205:260–274.
7. Ma, L., Golden, S., Wu, L., and Maxson, R. 1996. The molecular basis of Boston-type craniosynostosis: the Pro148→His mutation in the N-terminal arm of the MSX2 homeodomain stabilizes DNA binding without altering nucleotide sequence preferences. *Hum. Mol. Genet.* 5:1915–1920.
8. Zhou, Y.X., et al. 2000. A Pro250Arg substitution in mouse Fgfr1 causes increased expression of Cbfa1 and premature fusion of calvarial sutures. *Hum. Mol. Genet.* 9:2001–2008.
9. Otto, F., Kanegane, H., and Mundlos, S. 2002. Mutations in the RUNX2 gene in patients with cleidocranial dysplasia. *Hum. Mutat.* 19:209–216.
10. Matsuhashi, S., et al. 1996. New gene, net, encoding a Mr 91 K protein with EGF-like repeats is strongly expressed in neural tissues of early stage chick embryos [erratum 1996, 207:233–234]. *Dev. Dyn.* 203:212–222.
11. Watanabe, T.K., et al. 1996. Cloning and characterization of two novel human cDNAs (NELL1 and NELL2) encoding proteins with six EGF-like repeats. *Genomics.* 38:273–276.
12. Ting, K., et al. 1999. Human NELL-1 expressed in unilateral coronal synostosis. *J. Bone Miner. Res.* 14:80–89.
13. Kuroda, S., and Tanizawa, K. 1999. Involvement of epidermal growth factor-like domain of NELL proteins in the novel protein-protein interaction with protein kinase C. *Biochem. Biophys. Res. Commun.* 265:752–757.
14. Kuroda, S., et al. 1999. Biochemical characterization and expression analysis of neural thrombospondin-1-like proteins NELL1 and NELL2. *Biochem. Biophys. Res. Commun.* 265:79–86.
15. Hogan, B.C., Beddington, R., Constantini, F., and Lacy, E. 1986. Manipulating the mouse embryo: a laboratory manual. Cold Springs Harbor Laboratory Press. Cold Springs Harbor, New York, USA. 332 pp.
16. Laird, P.W., et al. 1991. Simplified mammalian DNA isolation procedure. *Nucleic Acids Res.* 19:4293.
17. Palmiter, R.D., Wilkie, T.M., Chen, H.Y., and Brinster, R.L. 1984. Transmission distortion and mosaicism in an unusual transgenic mouse pedigree. *Cell.* 36:869–877.
18. Kim, H.J., Rice, D.P., Kettunen, P.J., and Thesleff, I. 1998. FGF-, BMP- and Shh-mediated signalling pathways in the regulation of cranial suture morphogenesis and calvarial bone development. *Development.* 125:1241–1251.
19. Franceschi, R.T., Iyer, B.S., and Cui, Y. 1994. Effects of ascorbic acid on collagen matrix formation and osteoblast differentiation in murine MC3T3-E1 cells. *J. Bone Miner. Res.* 9:843–854.
20. Garcia Abreu, J., Coffinier, C., Larrain, J., Oelgeschlager, M., and De Robertis, E.M. 2002. Chordin-like CR domains and the regulation of evolutionarily conserved extracellular signaling systems. *Gene.* 287:39–47.
21. Murphy-Ullrich, J.E., and Poczatek, M. 2000. Activation of latent TGF-beta by thrombospondin-1: mechanisms and physiology. *Cytokine Growth Factor Rev.* 11:59–69.
22. Hall, K.B., and Horstadius, S. 1988. *The neural crest.* Oxford University Press. Oxford, United Kingdom. 305 pp.

Human Molecular Genetics, 2006, Vol. 15, No. 8 *1329–1341*
doi:10.1093/hmg/ddl053
Advance Access published on March 14, 2006

Nell1-deficient mice have reduced expression of extracellular matrix proteins causing cranial and vertebral defects

Jayashree Desai[1], Mark E. Shannon[2], Mahlon D. Johnson[3], David W. Ruff[2], Lori A. Hughes[4], Marilyn K. Kerley[4], Donald A. Carpenter[4], Dabney K. Johnson[4], Eugene M. Rinchik[4,5,†] and Cymbeline T. Culiat[4,*]

[1]Graduate School for Genome Science and Technology, University of Tennessee-Oak Ridge National Laboratory, 1060 Commerce Park, Oak Ridge, TN 37831, USA, [2]Applied Biosystems, 850 Lincoln Centre Drive, Foster City, CA 94404, USA, [3]The University of Tennessee Graduate School of Medicine, 1924 Alcoa Highway, Knoxville, TN 37920-6999, USA, [4]Life Sciences Division, Oak Ridge National Laboratory, PO Box 2008, Bethel Valley Road, Oak Ridge, TN 37831-6445, USA and [5]Department of Biochemistry, Cellular and Molecular Biology, The University of Tennessee, Knoxville, TN 37996, USA

Received January 4, 2006; Revised and Accepted March 7, 2006 GenBank accession no. AY622226.

The mammalian *Nell1* gene encodes a protein kinase C-β1 (PKC-β1) binding protein that belongs to a new class of cell-signaling molecules controlling cell growth and differentiation. Over-expression of *Nell1* in the developing cranial sutures in both human and mouse induces craniosynostosis, the premature fusion of the growing cranial bone fronts. Here, we report the generation, positional cloning and characterization of *Nell1*^{6R}, a recessive, neonatal–lethal point mutation in the mouse *Nell1* gene, induced by *N*-ethyl-*N*-nitrosourea. *Nell1*^{6R} has a T→A base change that converts a codon for cysteine into a premature stop codon [Cys(502)Ter], resulting in severe truncation of the predicted protein product and marked reduction in steady-state levels of the transcript. In addition to the expected alteration of cranial morphology, *Nell1*^{6R} mutants manifest skeletal defects in the vertebral column and ribcage, revealing a hitherto undefined role for *Nell1* in signal transduction in endochondral ossification. Real-time quantitative reverse transcription-PCR assays of 219 genes showed an association between the loss of *Nell1* function and reduced expression of genes for extracellular matrix (ECM) proteins critical for chondrogenesis and osteogenesis. Several affected genes are involved in the human cartilage disorder Ehlers-Danlos Syndrome and other disorders associated with spinal curvature anomalies. *Nell1*^{6R} mutant mice are a new tool for elucidating basic mechanisms in osteoblast and chrondrocyte differentiation in the developing skull and vertebral column and understanding how perturbations in the production of ECM proteins can lead to anomalies in these structures.

INTRODUCTION

Bone and cartilage are specialized connective tissues that provide structural support for the vertebrate organism and participate in key metabolic processes (e.g. calcium homeostasis). The formation of bone (osteogenesis) and cartilage (chondrogenesis) are complex processes governed by numerous genes acting in several stages: (a) commitment of the precursor cells; (b) the proliferation of the osteoprogenitor/chondroprogenitor cells; (c) differentiation of osteoblasts and chondrocytes; and (d) formation of cartilage or a calcified bone matrix (1). In the developing skull, calvarial bones are formed by intramembranous ossification, wherein mesenchymal cells differentiate into osteoblasts and the production of

*To whom correspondence should be addressed. Tel: +1 8652410672; Fax: +1 8655745345; Email: culiatct@ornl.gov
†Present address: Taconic, One Hudson City Centre, Hudson, New York 12534, USA.

bone matrix occurs directly without previous cartilage formation. Other bones in the body are formed by endochondral ossification, wherein mesenchymal cells aggregate, differentiate into chondrocytes and form cartilaginous tissue that is ultimately replaced by mineralized bone (1,2). Normal bone formation requires a delicate balance between proliferation, differentiation and apoptosis in osteoblasts and chondrocytes.

Craniosynostosis (CS) is among the numerous abnormalities resulting from perturbations in intramembranous ossification in the developing skull. CS is a significant medical condition because of its high incidence (1/3000 births) and the fact that cessation of skull growth at the prematurely fused suture sites can severely constrain the growth of the underlying brain, leading to increased intracranial pressure, impaired cerebral blood flow and airway obstruction (3,4). Moreover, certain types of CS are associated with defects in limb and spine development (5,6). Several genes controlling the establishment, maintenance and closure of cranial sutures have been identified (e.g. *MSX2*, *FGFR1*, *2*, *3*, *TWIST*) and the underlying molecular mechanisms elucidated by examining the consequences of mutations in mice (3,4,7–10). The importance of the *NELL1* gene in cranial development was first postulated with the discovery that it was dramatically up-regulated in prematurely fusing and fused sutures of patients with unilateral coronal synostosis (11). Transgenic mice over-expressing the rat *Nell1* gene displayed CS at birth, thereby confirming the earlier report that *Nell1* has a key role in human cranial development and suggesting that the underlying mechanisms can be investigated accurately using mouse models (12). The over-expressing transgenic mice have abnormalities specific to calvarial development and are viable. Further *in vivo* and *in vitro* studies showed that *Nell1* over-expression triggers premature fusion of growing skull bones by increasing osteoblast differentiation, apoptosis and mineralization (12,13).

The *NELL1* gene encodes a polypeptide (810 amino acids) that is glycosylated and processed in the cytoplasm and then secreted as a 400 kDa trimer. The protein contains thrombospondin-like, laminin G, von Willebrand factor-like repeats and epidermal growth factor (EGF)-like domains (14,15). The NELL1 protein binds to and is phosphorylated by PKC-β1 via the EGF-like domains, suggesting that *Nell1* represents a novel class of cell-signaling ligand molecules critical for growth and development (15).

While investigating the molecular basis for phenotypes of *N*-ethyl-*N*-nitrosourea (ENU)-induced lethal mutations mapping to a small segment of mouse chromosome 7, we previously defined mutations in the *l7R6* locus as late gestation/neonatal lethals (16). In this report, we present a new allele, designated *l7R6*^{6R}, which is a point mutation in *Nell1* resulting in severe loss of expression. The loss of *Nell1* function leads to skeletal defects in the cranial vault, vertebral column and ribcage. Gene expression assays reveal that these aberrant phenotypes are because of the downregulation of extracellular matrix (ECM), cell adhesion and cell communication proteins that are necessary in osteogenesis and chondrogenesis. This report is the first demonstration of the significance of *Nell1*-mediated pathways in cartilage development and the consequences of loss-of-function of *Nell1 in vivo*.

RESULTS

l7R6^{6R} mice die during birth, exhibit enlarged heads and abnormal body curvature

l7R6^{6R} hemi- and homozygotes develop to late gestation (E19 days) but do not survive the physical trauma of birth. Observations on females during delivery showed that all *l7R6*^{6R} mutant neonates were born dead, whereas remaining undelivered mutants were alive when recovered by caesarean section. However, rescued mutant mice quickly succumbed because they were unable to breathe and foster mothers usually cannibalized them. Mutant fetuses are easily distinguished from normal littermates by their pronounced curled position, enlarged head region (Fig. 1A), inability to open their mouths and very weak reflexes in extremities when stimulated by touching. Heterozygotes survive to adulthood and breed normally, with no readily visible phenotypic differences when compared with wild-type mice.

Gross anatomical observations indicated that compared with their wild-type littermates, homozygous mutant fetuses manifested a decreased body length because of the pronounced altered curvature of the spine and an enlarged altered head shape brought about by increased head length (Table 1). No significant changes in head height and width were detected.

l7R6^{6R} is a point mutation in the *Nell1* gene resulting in a Cys → Ter codon substitution and severe reduction in transcript levels

Trans-complementation analysis with a number of *P*-deletions localized *l7R6*^{6R} to the same <1 cM segment of chromosome 7 (Fig. 1B, Materials and Methods) as other *l7R6* alleles, with homology to a region of human 11p15. Gene content analysis of the human chromosomal region suggested at least six candidate genes for *l7R6* (http://genome.ucsc.edu), including *NELL1*, which was particularly provocative because of its over-expression in the prematurely fused sutures of patients manifesting unilateral coronal synostosis. The pronounced enlarged head phenotype, along with the deletion-map position, suggested that recessive *l7R6*^{6R} mutation may be a loss-of-function allele in the *Nell1* gene. To test this hypothesis, *Nell1* gene expression in wild-type and mutant embryos and in wild-type adult tissues was assayed by Northern blot analysis. The cDNA probe detected a 3.5 kb message in polyA$^+$ RNA extracted from wild-type embryos from E10–18 days of gestation (Fig. 2B). During gestation, expression was first detected at E10 and steadily increased in the head region and decreased in the body. In adult tissues, normal expression was observed primarily in adult brain (Fig. 2A). In contrast, northern blot assays of RNA samples isolated from E15 fetuses showed little detectable expression of *Nell1* in *l7R6*^{6R} mutants (Fig. 2B).

To identify the presumed *Nell1*^{6R} (*l7R6*^{6R}) mutation, each exon along with flanking intron sequences was amplified from genomic DNA and analyzed for single base pair changes by heteroduplex analysis using temperature gradient capillary electrophoresis (17). Heteroduplexes were detected in exon 14 (not shown), hence the samples were sequenced in mutant animals and compared with the sequence in the wild-type controls. Sequence analysis showed a single base

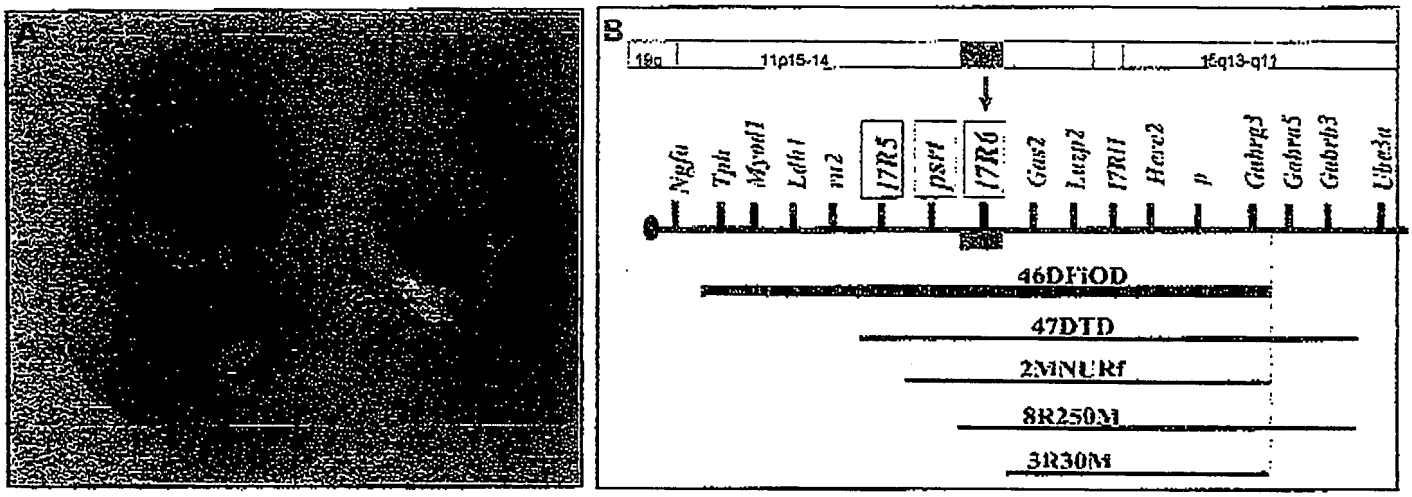

Figure 1. (A) Phenotype of *17R6*^{6R} homozygote mutants at 19 days of gestation. On the right is a fetus homozygous for the *17R6*^{6R} allele (stock 102DSJ) showing a very curled position and enlarged head size compared with the control littermate (left). *17R6*^{6R} mouse fetuses are recovered alive by caesarean rescue because they do not survive delivery through the birth canal, perhaps owing to the physical trauma in the neck and spine region brought about by the abnormal spinal curvature. (B) Complementation analysis showing the mapping of the *17R6* locus into an interval in mouse chromosome 7 (red box) that is homologous to a segment of human chromosome 11p15 (red box) where the *Nell1* gene is located. Mouse chromosome 7 is represented by the line with a filled circle at the left (indicating the centromere) and relative positions of genes and markers are indicated above the line. Five mutant mouse lines carrying deletions of varying lengths and surrounding the pink-eyed dilution gene (p) are shown as 46DFiOD, 47DTD, 2MNURf, 8R250M and 3R30M. Among these mutations, only the 3R30M deletion can complement the ENU-induced mutations at *17R6* indicating that this deletion does not extend to the position where the *17R6* gene is located. The interval is therefore defined by the proximal deletion breakpoints of the 8R250M and 3R30M mutant mouse lines.

Table 1. Quantitative analysis of changes in body length and head size of *Nell1*^{6R} homozygous mutants compared with wild-type littermates, measured (in mm) at E18.5 days of gestation

Litter no.	Genotype	No. of embryos per litter	Body length	±SEM	Head length	±SEM	Head height	±SEM	Head width	±SEM
1	Wild-type	2	21.49	±0.28	10.23	±0.17	5.95	±0.01	6.37	±0.35
	Mutant	2	19.28	±0.05	11.5	±0.70	6.96	±0.41	6.88	±0.54
2	Wild-type	2	17.15	±0.06	9.72	±0.20	9.06	±0.69	6.42	±0.78
	Mutant	4	16.90	±0.50	10.37	±0.75	8.50	±0.54	6.14	±0.33
3	Wild-type	1	21.3	±0.0	10.1	±0.0	8.0	±0.0	6.4	±0.0
	Mutant	1	18.5	±0.0	11.0	±0.0	8.7	±0.0	6.8	±0.0
4	Wild-type	1	19.9	±0.0	11.0	±0.0	8.1	±0.0	6.5	±0.0
	Mutant	2	17.8	±0.4	11.2	±0.4	8.65	±0.3	6.95	±0.5
5	Wild-type	1	23.24	±0.0	9.77	±0.0	6.01	±0.0	6.49	±0.0
	Mutant	1	20.30	±0.0	11.15	±0.0	5.53	±0.0	6.19	±0.0
6	Wild-type	4	22.69	±1.64	10.32	±0.93	5.17	±0.41	6.42	±0.37
	Mutant	2	18.50	±0.37	11.44	±0.32	4.55	±0.14	6.75	±0.21
7	Wild-type	2	23.86	±0.37	10.71	±0.43	5.44	±0.52	6.66	±0.61
	Mutant	3	19.11	±0.63	11.2	±1.45	5.39	±0.68	6.67	±0.06
8	Wild-type	1	22.77	±0.0	9.47	±0.0	5.31	±0.0	6.53	±0.0
	Mutant	2	18.33	±0.65	9.94	±0.88	6.28	±0.39	6.85	±0.3
9	Wild-type	2	22.32	±1.4	10.22	±0.88	5.66	±0.46	6.86	±0.6
	Mutant	2	17.98	±0.55	10.45	±1.32	7.19	±0.41	6.91	±0.14
Total	Wild-type	16	21.72		10.21		6.27		6.51	
	Mutant	19	18.25		10.86		6.28		6.64	
	P-value		4.2×10^{-6}		0.003		0.172		0.266	

The body length of mutant fetuses were significantly decreased and the head length increased in comparison with the wild-type mice.

pair substitution of T→A that converts a codon for cysteine into a premature stop codon [TGT→TGA; Cys(502)Ter] that truncates the 810 amino acid polypeptide at residue no. 502 and eliminates the EGF-like domains that bind PKC-β1 protein (Fig. 3). As transcripts bearing premature stop codons in positions such as the one present in the *Nell1*^{6R} transcript are subject to nonsense-mediated decay (18,19), the mutation scanning data are consistent with the

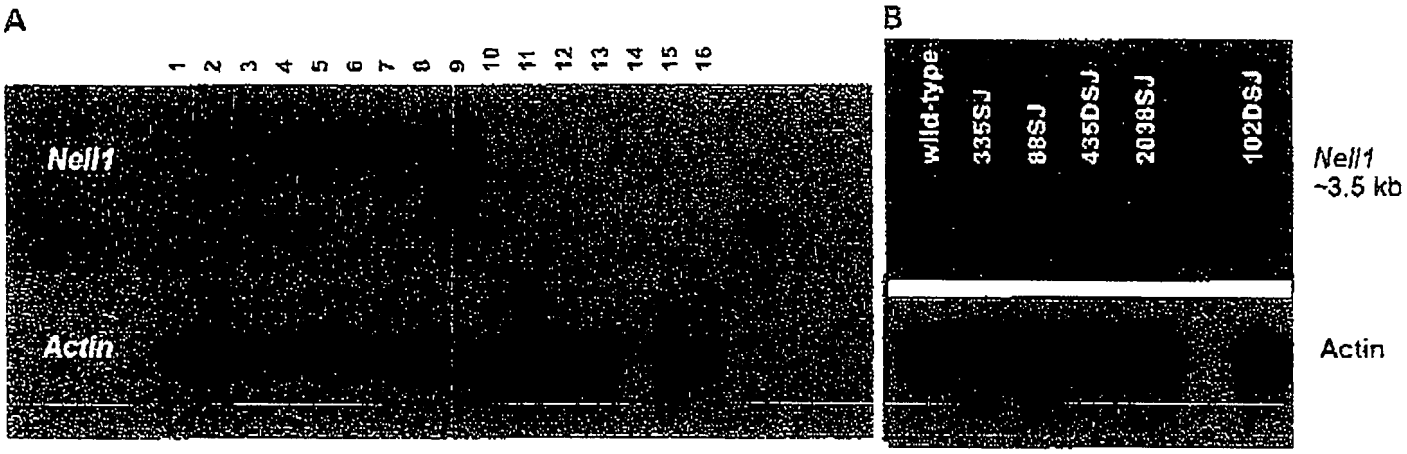

Figure 2. Expression of the mouse *Nell1* gene. (A) Northern blot analysis on polyA$^+$ RNAs from heads (H) and bodies (B) of wild-type embryos/fetuses (samples 1–8) and adult mouse tissues (samples 9–16). The lane positions, developmental stages and adult tissues are: 1, E10; 2, E12; 3, E14 H; 4, E14 B; 5, E16 H; 6, E16 B; 7, E18 H; 8, E18 B; 9, brain; 10, liver; 11, spleen; 12, kidney; 13, thymus; 14, heart; 15, lung; 16, muscle. The *Nell1* cDNA probe detects a 3.5 kb transcript as early as E10 days. From E14 to E18 days, the *Nell1* message is abundant in both fetal heads and bodies, increasing markedly in the head as development proceeds. Hybridization of the blot with an actin probe serve as control to compare levels of samples loaded in each lane. (B) Northern blot analysis on polyA$^+$ RNAs extracted from the heads of hemizygous E15 *l7R6* fetuses, shows a severely reduced expression of the *Nell1* gene in the *l7R6*^{6R} (102DSJ) allele compared with normal levels of expression detected in mice with the following genotypes: wild-type, mutant hemizygotes for four other alleles at the *l7R6* locus (335SJ, 88SJ, 45DSJ, 2038SJ).

observation of severely decreased *Nell1* mRNA levels in mutants (Fig. 2B).

Nell1^{6R} mutant mice have skeletal defects in the skull and vertebral column

Because of prior reports on the role of *Nell1* in cranial development and osteoblast differentiation, we performed a detailed analysis of skull and skeletal defects in the *Nell1*^{6R} mutants (E18.5 days) using Alizarin Red–Alcian Blue staining. Skeletal analysis showed compression of intervertebral spaces and alteration of spinal curvature, and anomalies in the shape and volume of the ribcage (Fig. 4A and B). The cervical region of the vertebral column displayed the most dramatic reduction in the intervertebral disc matrix and a pronounced change in spinal curvature is observed at the juncture of the cervical and thoracic vertebral bones (Fig. 4A and B). Enlargement and thinning of the parietal, frontal and interparietal bones in the skull were readily apparent (Fig. 4C–F). The nasal bones were also enlarged but thinning was not clearly observed in these structures. The consistently decreased staining by Alizarin Red in the *Nell1*^{6R} calvarial bones indicated decreased ossification in the mutant. These *Nell1*^{6R} skeletal defects were confirmed by microcomputerized tomography scanning (Fig. 4G and H). Radiographs showed the sharp curvature change between the cervical and thoracic vertebrae (Fig. 4G). Moreover, the microCat scanning data suggested lesser bone density (Fig. 4G) and areas of ossification (Fig. 4H) in the *Nell1*^{6R} mutant homozygotes. Although the effect of *Nell1*^{6R} mutation in the head region was expected, its profound impact on the development of the vertebral and thoracic skeleton was not anticipated as the deleterious effects of *Nell1* over-expression were confined to the growth and differentiation of the calvarial bones (12).

Loss of *Nell1* function reduces expression of genes coding for ECM, cell adhesion and communication proteins

Nell1 is a novel gene, thus the molecular and cellular mechanisms of its role in mammalian development are unknown. In order to define the genes and pathways that were perturbed by the *Nell1*^{6R} mutation, we screened hundreds of potential 'downstream' genes for differences in expression levels between wild-type and mutant *Nell1*^{6R} fetuses. Real-time quantitative RT-PCR analysis of 219 experimental and six control genes was carried out in RNA samples extracted from individual heads and bodies of four *Nell1*^{6R} mutants and four wild-type E18 fetuses. These assays on whole tissues enabled a rapid and efficient assessment of the impact of the *Nell1*^{6R} mutation on a wide range of genes. Changes in 'expression levels' of these genes may either be direct (e.g. transcriptional changes) or indirect (e.g. expansion or reduction of specific cell populations). The 219 genes were carefully selected based on the observed mutant phenotype and the putative domains and functions of the *Nell1* gene. Genes associated with CS (e.g. *Runx2*, *Msx2*, *Fgfr3*), bone and cartilage development, cell growth and differentiation, neural development and signal transduction pathways were also included. The complete list of genes assayed by qRT-PCR is presented in Supplementary Material, Table S1 online.

Gene expression analyses revealed reduced expression of 13 genes in the head and 28 genes in the body because of the *Nell1*^{6R} mutation (Fig. 5). Expression levels of the following nine genes were affected in both heads and bodies: collagen 5 alpha 3 subunit (*Col5a3*), tenascin (*Tnxb*), procollagen type XV alpha 1 (*Col15a1*), procollagen type V alpha 1 (*Col5a1*), thrombospondin 3 (*Thbs3*), matrilin 2 (*Matn2*), tumor necrosis factor receptor superfamily member 11b (*Tnfrsf11b*), osteoblast-specific factor (*Osf2*) and chondroadherin (*Chad*). Further analysis using publicly available

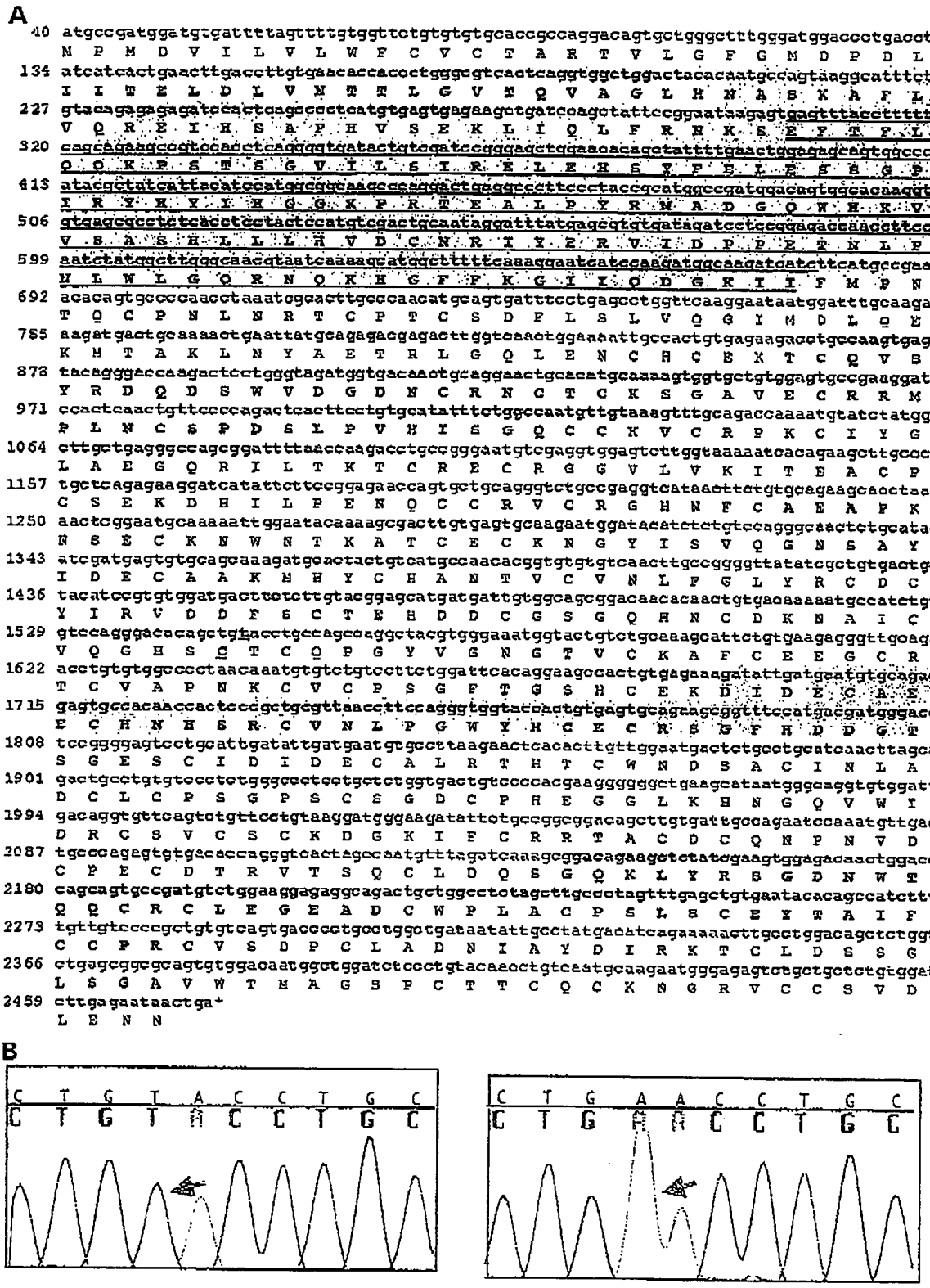

Figure 3. Identification of the *Nell1*^{6R} mutation. (A) Mouse *Nell1* cDNA sequence (GenBank accession no. AY622226) and position of predicted protein domains [Thrombospondin (gray); Laminin G (underlined); von Willebrand factor type C (yellow); calcium-binding EGF-like (blue)]. The locations of the ENU-induced mutation at base pair no. 1546 in the cysteine codon and the change in amino acid no. 502 are both highlighted in red text. The premature termination codon introduced at this site will truncate the protein and remove the EGF-like domains that are essential for the binding to PKC-βI. One von Willebrand factor type C domain will also be missing from the putative mutant protein product. (B) Sequence electropherograms showing the T to A base change (red arrows) in the wild-type (left) and the mutant sequence (right) of the *Nell1* gene.

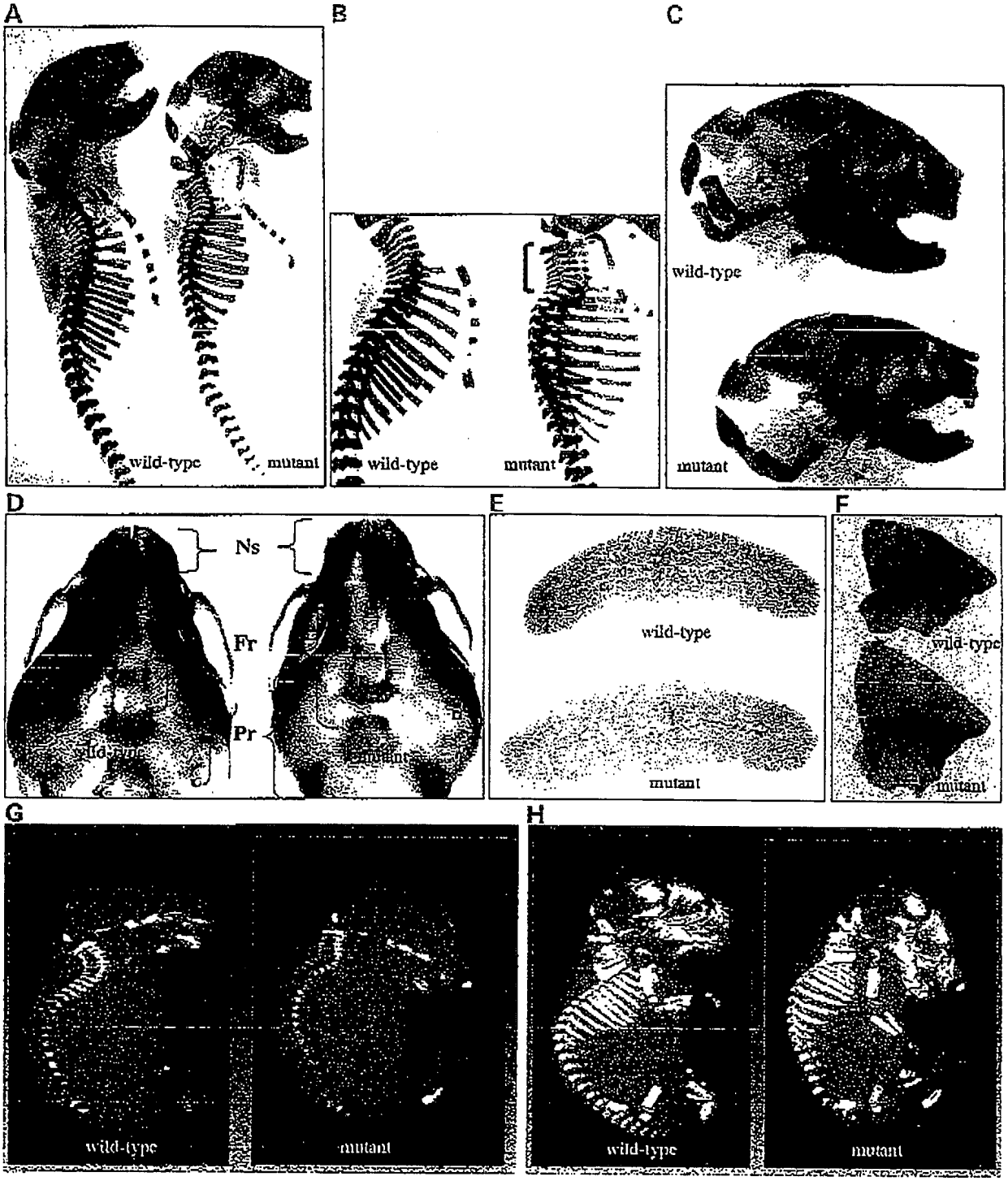

Figure 4. Skeletal defects in *Nell1*^{6R} homozygote mutant fetuses at 18.5 days of gestation. (A) Alizarin Red and Alcian Blue staining showed that mutant homozygotes have altered spinal curvature, decreased intervertebral disc spaces, reduced thoracic cavity, protruding sternum and a slight enlargement of the skull. (B) Close-up of the cervical region where the most pronounced vertebral compression was observed. The skeletal specimens in (B) are a different pair of littermates from those in (A). (C) Side view of the cranial vault showing enlargement of parietal bones (Pr) in mutant fetal heads. (D) Top view of the skull showing the increased size of the nasal (Ns), frontal (Fr) and parietal (Pr) bones in the *Nell1*^{6R} mutant mice. (E) Enlargement of the interparietal and (F) frontal bones. (D–F) The calvarial bones of the *Nell1*^{6R} mutant mice are thinner than those of the wild-type and consistently have less Alizarin Red staining, suggesting a lesser degree of ossification. (G) Radiographs of a wild-type fetus compared to a *Nell1*^{6R} mutant littermate. A pronounced alteration in spine curvature occurs at the cervical vertebrae in the mutant fetuses (arrow). The lesser intensity of signals in the craniofacial and vertebral skeletons of the mutant suggests lesser bone density. (H) Images from 3D re-construction of microCat scans for wild-type and mutant fetuses show lesser areas of ossification in the mutant fetal head (arrow). The observation in earlier skeletal analysis that the mutant calvarial bones are thinner is consistent with microCat data showing larger areas of dense bone in the wild-type fetus (arrows).

E18 HEADS

Gene symbol	Gene name	NM number	Gi number	qRT-PCR data summary							Annotation			
				P-value	AVG ΔC_T (wt)	SD (wt)	AVG ΔC_T (mt)	SD(mt)	$\Delta\Delta C_T$	FOLD	ECM	Adhn	Comm.	Others
Tnxb	tenascin	NM 031176	13928671	0.00000007	1.76	0.15	3.34	0.39	-1.58	2.99				
Col5a3	collagen 5 alpha 3 subunit	NM 016919	8393172	0.0000006	0.58	0.16	1.61	0.22	-1.03	2.04				
Thbs4	thrombospondin 4	NM 011582	6755780	0.0045330	1.37	0.16	1.93	0.36	-0.56	1.47				
Col12a1	procollagen type XII, alpha 1	NM 009928	24475606	0.0010000	0.69	0.16	0.63	0.23	-0.54	1.46				
Chad	chondroadherin	NM 007689	31982462	0.0049249	1.32	0.26	1.8	0.26	-0.49	1.4				
Adamts5	metalloproteinase	NM 013906	7304856	0.0014971	3.98	0.26	4.45	0.15	-0.47	1.39				
Col5a1	procollagen type V, alpha 1	NM 015734	7656986	0.0605688	-2.25	0.11	-1.79	0.22	-0.47	1.38				
Tnfsf11	tumor necrosis factor (ligand)	NM 009784	31543881	0.0020684	4.3	0.12	4.75	0.26	-0.45	1.37				
Col10a1	procollagen type X, alpha 1	NM 009925	6753479	0.0030265	0.25	0.22	0.71	0.24	-0.45	1.37				
Thbs3	thrombospondin 3	NM 013691	8567413	0.0608943	1.55	0.13	1.98	0.21	-0.43	1.35				
Osf2 paralog	osteoblast specific factor 2	NM 015784	7657428	0.0023714	-3.98	0.2	-3.61	0.14	-0.34	1.27				
Col18a1	procollagen type XVIII, alpha 1	NM 009929	40789281	0.0039774	-0.85	0.09	-0.51	0.22	-0.34	1.27				
Matn2	matrilin 2, cartilage matrix protein 2	NM 016762	7949075	0.0020528	0.14	0.1	0.45	0.17	-0.31	1.24				
									No. of genes		10	8	6	1
									Percentage		77%	62%	76%	8%

E18 BODIES

Gene symbol	Gene name	NM number	Gi number	qRT-PCR data summary							Annotation			
				P-value	AVG (wt)	SD (wt)	AVG(mt)	SD(mt)	ΔΔct	FOLD	ECM	Adhn	Comm.	Others
Tnxb	tenascin	NM 031176	13928671	0.000000002	0.52	0.16	2.24	0.17	-1.71	3.28				
Prg4	proteoglycan 4	NM 021480	7209718	0.000000685	3.5	0.12	4.74	0.25	-1.23989	2.35				
Thbs3	thrombospondin 3	NM 013691	8567413	0.000261732	1.3	0.18	2.31	0.4	-1.01	2.02				
Col5a3	collagen 5 alpha 3 subunit	NM 016919	8393172	0.000081796	-0.05	0.14	0.92	0.21	-0.98	1.97				
Neurog2	neurogenin 2	NM 009718	34328159	0.002524664	9.34	0.47	10.29	0.41	-0.96	1.94				
Col5a1	procollagen type V, alpha 1	NM 015734	7656986	0.000348035	-2.49	0.27	-1.78	0.23	-0.71	1.63				
Col6a1	procollagen Type VI, alpha 1	NM 009933	6753483	0.000073349	-3.54	0.23	-2.89	0.16	-0.65	1.57				
Col12a1	procollagen type XII, alpha 1	NM 009928	24475606	0.001447092	-0.78	0.16	-0.17	0.29	-0.61	1.53				
Pacsin3	PKC and casein kinase substrate in neurons 3	NM 030880	13559451	0.000000251	0.03	0.16	0.63	0.16	-0.6	1.51				
Tnc	tenascin c	NM 011607	7106434	0.099884612	-1.7	0.3	-0.62	0.17	-0.58	1.5				
Col12a1	procollagen type XII, alpha 1	NM 007730	66809599	0.000187290	-2.25	0.12	-1.69	0.19	-0.57	1.48				
Chad	chondroadherin	NM 007689	31982462	0.002787124	0.09	0.13	-0.66	0.31	-0.56	1.48				
Osf2 paralog	osteoblast specific factor 2	NM 015784	7657428	0.000123764	-4.46	0.14	-3.9	0.18	-0.56	1.47				
Col17a1	procollagen type XVII alpha 1	NM 007732	6680953	0.001828273	0.85	0.09	1.37	0.27	-0.52032	1.43				
Prkce	protein kinase C	NM 011102	31982442	0.000930065	5.49	0.14	5.95	0.2	-0.46006	1.38				
Pitch	protein kinase C, eta symbol	NM 008856	31543510	0.000020264	1.62	0.05	1.47	0.13	-0.45	1.36				
Bt-penning	brain and kidney protein	NM 139649	20149721	0.008117374	4.92	0.08	5.36	0.15	-0.44	1.35				
Ptk9l	PTK9L protein tyrosine kinase 9-like	NM 011876	31981351	0.004420696	1.4	0.09	1.82	0.25	-0.42	1.34				
Hpde1	neural proliferation, differentiation and control gene	NM 008721	31982835	0.000036598	0.05	0.07	0.46	0.12	-0.41	1.33				
Bmpr1a	bone morphogenetic protein receptor type 1a	NM 009758	46519167	0.003042146	0.1	0.13	0.52	0.22	-0.42	1.33				
Pkd1	polycystic kidney disease 1 homolog	NM 013630	7305388	0.000077257	0.19	0.09	0.58	0.12	-0.39	1.31				
Tnfsf11b	tumor necrosis factor (ligand)	NM 008764	31543881	0.000525056	3.65	0.15	4.03	0.13	-0.38	1.3				
Mfge8	milk fat globule-EGF factor 8 protein	NM 008594	6678869	0.001210853	-1.69	0.14	-1.35	0.14	-0.35	1.27				
Matn3	matrilin 3, cartilage matrix protein	NM 010770	48976188	0.003725834	0.62	0.13	0.97	0.18	-0.35	1.27				
Bmp7	bone morphogenetic protein type 7	NM 007557	31982456	0.034147469	1.58	0.15	1.93	0.18	-0.35	1.27				
Matn2	matrilin 2, cartilage matrix protein 2	NM 016762	7949075	0.000021505	-0.29	0.06	0.03	0.09	-0.32	1.25				
Ptger4	prostaglandin E receptor 4	NM 008965	6679530	0.000059844	3.8	0.11	3.91	0.06	-0.3	1.23				
Notch3	notch gene homolog 3	NM 008716	6679985	0.000765294	0.25	0.09	0.54	0.12	-0.28	1.22				
									No. of genes		12	11	20	4
									Percentage		43%	39%	71%	14%

Figure 5. Gene expression profile of *Nell1*^{6R} mutants compared with wild-type fetuses (E18). Genes with significantly reduced expression in mutant mice are listed from highest to lowest fold change. Nine genes (in red text) are affected in both heads and bodies. Majority of the genes that are affected by the *Nell1*^{6R} mutation encode proteins for the ECM, cell adhesion (Adhn) and cell communication (Comm) during bone and cartilage development.

tools such as DAVID (Database for Annotation, Visualization and Integrated Discovery) (20). GeneCards®, UCSC genome browser and extensive PubMed literature searches showed that the majority of the genes with reduced expression encode ECM proteins such as specific collagens, thrombospondins, tenascins and matrilins. These proteins provide cell adhesion and communication, and impart strength and flexibility to tissues. The most severely affected genes (2–3-fold) in the fetal head were *Tnxb* and *Col5a3*, whereas in the body they were: *Tnxb*, proteoglycan 4 (*Prg4*), *Thbs3* and *Col5a3*.

Eight out of 21 collagen genes assayed showed significant changes in expression indicating that the loss of *Nell1* influences only a specific set of collagen subunits. Another striking result is that mutations in the human counterparts of two dramatically affected genes, *Tnxb* and *Col5a1*, cause Ehlers-Danlos Syndrome (EDS), a severe cartilage defect (1/5000 individuals) characterized by hyperextensibility of the skin and extreme flexibility of joints (21,22). EDS patients do not have the ability to make certain components of the connective tissue, particularly fibrillar collagens, or they have defective regulation of collagen synthesis and deposition (22,23). Because of the importance of collagen V in EDS, it is predicted that mutations in *Col5a3*, another gene whose expression is globally reduced (2-fold) in *Nell1*-deficient mice, will generate certain forms of EDS (22,24). Of the six distinct EDS clinical syndromes, EDS-type VI is an autosomal recessive form characterized by abnormal curvature of the spine, hypotonia, joint laxity and ocular fragility (22). Other genes expressed in the fetal body that are affected by *Nell1* (e.g. *Tnc*, *Tnx*, *Matn3*, *Chad*, *Tnrsf11b* and *Bmpr1a*) are already known to be critical in the development of the vertebral column in human and/or mouse (25–27).

Nell1^{6R} mutant mice have reduced ECM and decreased bone mineralization

The gene expression profile resulting from the *Nell1*^{6R} mutation is further supported by standard histological analysis using haematoxylin and eosin, periodic Acid Schiff and Masson staining (Fig. 6). *Nell1*^{6R} mutant mice display considerable reduction in the amount of extracellular material surrounding cells in the developing vertebral bone and intervertebral discs, compared with the wild-type controls (Fig. 6A–D). In addition, histology data suggested lesser degree of bone and cartilage development in mutant animals (Fig. 6C and D). Results from von Kossa staining of sagittal sections through the vertebral column and parietal bones (Fig. 6E–H) showed decreased bone mineralization in *Nell1*^{6R}. The cranial and vertebral bones of mutant homozygotes have a lesser number of mineralized areas and exhibit a highly irregular pattern when compared with wild-type specimens. The frontal bones display the same defects in bone mineralization as the parietal bones (data not shown).

DISCUSSION

We have characterized the phenotypic and molecular consequences of *Nell1*^{6R}, an ENU-induced point mutation in the *Nell1* gene that converts a cysteine codon to a premature termination codon, thereby truncating an 810 amino-acid polypeptide at residue no. 502. The severe reduction of *Nell1* transcripts in *Nell1*^{6R} homozyotes (presumably because of nonsense-mediated decay) results in neonatal lethality, an enlarged skull with thinning at the calvarial bone edges, reduced intervertebral disc spaces, alteration in the vertebral column curvature, abnormal shape and size of the ribcage. The range of skeletal anomalies manifested by *Nell1*^{6R} mutants indicate that the *Nell1* gene plays a key role in both intramembranous and endochondral ossification during early mammalian development.

The impact of the loss of *Nell1* function in the cranial phenotype and the characteristic gene expression profile in the fetal heads of *Nell1*^{6R} mutant mice are consistent with the role of *Nell1* in osteoblast differentiation and the known mechanisms of suture development and closure. Developing sutures contain undifferentiated proliferating osteogenic stem cells, a proportion of which differentiate into osteoblasts at the edges of the calvarial bones. Mature osteoblasts secrete a collagen–proteoglycan matrix that binds calcium salts, mineralizes and generates new bone from the osteoid matrix. A delicate balance between stem-cell proliferation and differentiation into bone is required so that the stem-cell population is maintained until skull growth is complete (28). Signals from the dura mater directly underneath the skull maintain sutural patency by regulating cell proliferation and collagen production (29). CS involves excessive growth of the calvarial bones so that two opposing growing bone fronts become very close or overlap and the subsequent fusion of juxtaposed bone fronts (12). Over-expression experiments (*in vivo* and *in vitro*) have clearly shown that *Nell1* promotes osteoblast differentiation at the growing calvarial bones (11–13). In contrast, downregulation of *Nell1* using *in vitro* approaches demonstrated decreased cell differentiation and predicted that reduced levels of *Nell1* protein will promote cell proliferation at the suture (12). The enlargement and immature bone development of the cranial vault and the decreased levels of ECM proteins secreted by mature osteoblasts in *Nell1*^{6R} mice support these earlier observations.

The processes that regulate the ossification and fusion of cranial sutures depend on specific ECM patterns. Mutation in genes that cause CS by over-stimulating osteoblast differentiation alter ECM turnover and can increase collagen, glycosaminoglycans and fibronectin in CS-derived fibroblasts (30). The decreased bone mineralization resulting from the loss-of-function of *Nell1* gene, is also consistent with reduced levels of ECM detected in these mutant mice.

Although transgenic mice over-expressing *Nell1* confirmed its role in craniofacial development, the broader role of *Nell1* in skeletal development is revealed by the new loss-of-function allele, *Nell1*^{6R}. In particular, the alteration of spinal curvature and reduction of intervertebral disc spaces in these mutants indicate involvement of *Nell1* in signal transduction in the developing spine. The finding that *Nell1* directly or indirectly affects expression of at least eight genes (*Tnxb*, *Tnc*, *Col12a1*, *Col6a1*, *Matn3*, *Bmpr1a*, *Thbs3*) that are necessary for the development of and/or are specific constituents of the intervertebral disc matrix (25,31–35) provides additional support for a role for *Nell1* in early vertebral column development. As the expression of EDS-associated genes, *Tnxb*, *Col5a1* and *Col5a3* are severely reduced by the *Nell1*^{6R} mutation, the role of *Nell1* in the etiology of EDS (types VI, VIIa,b) or EDS-like disorders manifesting spinal curvature defects needs further investigation. Moreover, immunohistochemical studies of the proteins coded by the genes affected by the *Nell1*^{6R} mutation (based on qRT-PCR assays), especially during key stages of bone and cartilage development in the wild-type and *Nell1*^{6R} mutant mouse model, will further characterize the functions of the *Nell1* gene during early skeletal development.

Our discovery of the involvement of *Nell1* in the vertebral column development is consistent with the fact that PKC-β1

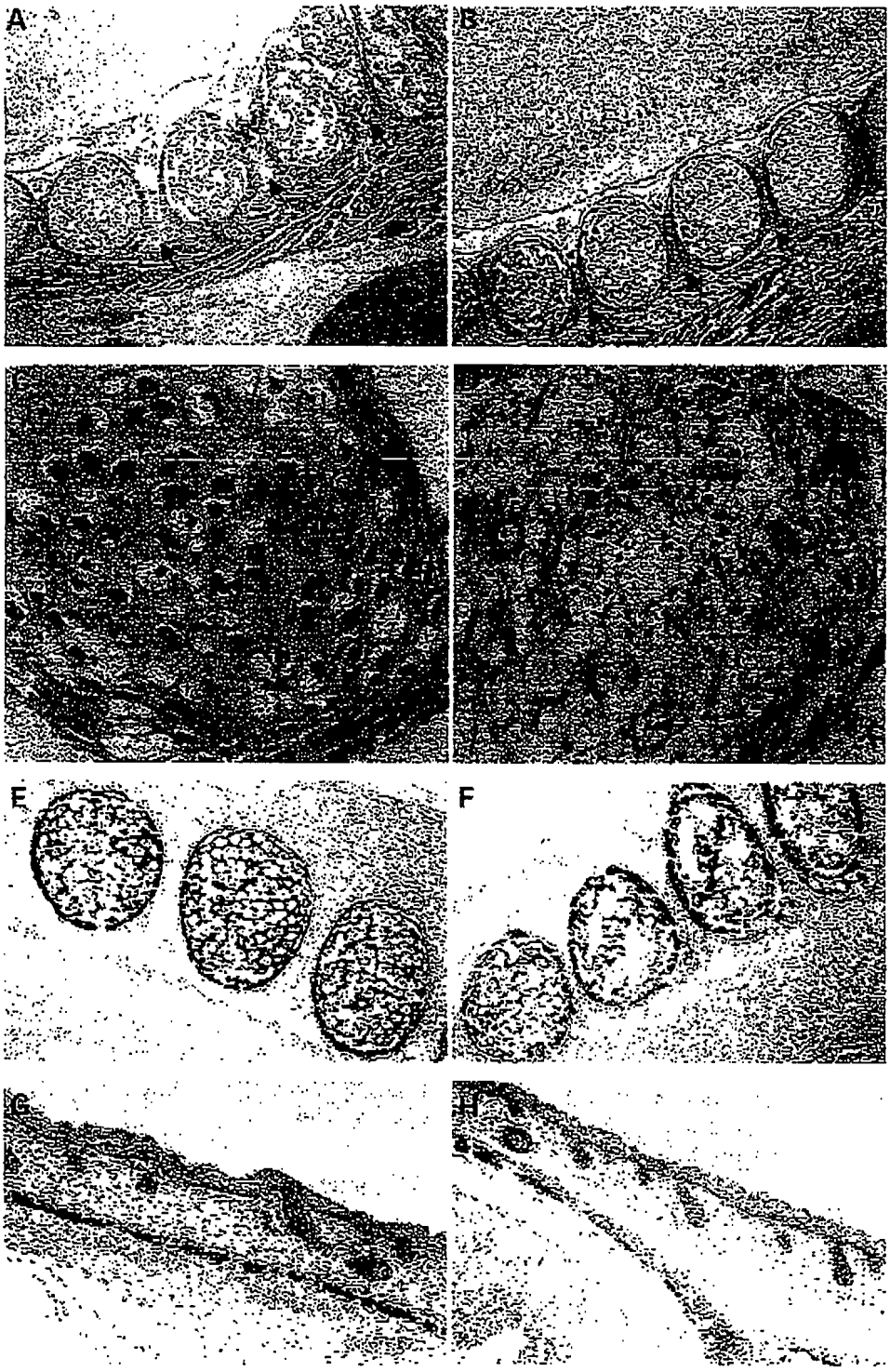

Figure 6. Histopathology indicating loss of extracellular material and disrupted bone development in the *Nell1*^{GR} mutant vertebral column and calvarial bones. (**A**) The normal architecture of the cervical vertebral column in a wild-type mouse (sagittal section; Masson Stain) compared with the mutant *Nell*^{GR} homozygote (**B**), showing the decrease of intervertebral disk matrix/space between the vertebral bodies (arrows). Higher magnification view of sagittal sections of the vertebral bodies in wild-type (**C**) and mutant (**D**) animals (haematoxylin and eosin staining) indicating lesser amount of ECM and cellular development of chondrocytes in the mutants. Von Kossa staining of sagittal sections through the vertebral columns of wild-type (**E**) and mutant E18 fetuses (**F**) showing decreased bone mineralization in the vertebral bodies of *Nell1*^{GR} homozygotes. The intensity and the distribution of stained areas (black spots) are lesser and exhibit an irregular pattern in the mutant fetuses. Von Kossa analysis of sagittal sections through the parietal bones of wild-type (**G**) and mutant (**H**) fetuses also revealed decreased mineralization. In mutant parietal (H) and frontal bones (data not shown), the intensity of von Kossa staining is less and in contrast to the wild-type *Nell1*^{GR} calvarial bones, have thinner and more 'patchy' pattern of mineralization. There are larger and more frequent gaps between mineralized regions, similar to the pattern seen in the vertebral bodies (*F*).

isozyme localizes in the vertebral bodies and intervertebral disc spaces of human fetuses during the 8th week of development, a critical developmental period when chondrogenetic and osteogenetic processes are initiated in the vertebral column (36). PKC activity has also been observed in the fetal mouse vertebral column and is abundant in the more mature cells close to the ossification center and the intervertebral disc spaces. Over-expression of the *Nell1* gene does not appear to disrupt vertebral development, but it is clearly altered by a reduction or malfunctioning of *Nell1* protein. Our data demonstrate that, in addition to its role in intramembranous bone differentiation, *Nell1* has a critical function in endochondral ossification and normal chrondrogenesis in the spine. The high degree of conservation in structure and function of the *Nell1* gene itself suggests that the spinal phenotype could also be a consequence of human *NELL1* loss-of-function mutations. Therefore, we suggest that linkage studies and mutation scanning in families segregating both cranial defects and spinal anomalies should focus on the *NELL1* gene in chromosome 11p15.

MATERIALS AND METHODS

Mouse breeding and maintenance

All animals were bred at the Mammalian Genetics Research Facility at Oak Ridge National Laboratory (ORNL) (Oak Ridge, TN, USA) using protocols approved under the ORNL Institutional Animal Care and Use Committee. The identification and fine-structure mapping of the *l7R6* locus in mouse Chr 7 are described elsewhere (16). The 102DSJ mutation was recovered in a manner similar to that described previously for the 88SJ ($l7R6^{1R}$), 335SJ ($l7R6^{2R}$) and 2038SJ ($l7R6^{3R}$) alleles at the *l7R6* locus (16). Mutagenized chromosomes marked with the *P*-mutation were recovered in G1 females from ENU-treated 21A G0 males. The 102DSJ lethal mutation was recognized when G1 female no. 102 failed to yield any pink-eyed-dilute G2 progeny when she was crossed to a $+^{P7R}$/Del($Hps5^{ru2P}$)^{46DF1OD} G1 male. Deletion mapping also similar to that performed previously (16) revealed that the 102DSJ lethal mapped to the same deletion interval as did the previously ascertained *l7R6* alleles (data not shown). Allelism was confirmed (i.e. 102DSJ = $l7R6^{6R}$) when no pink-eyed dilute progeny were found in greater than 30 progeny of a cross of 88SJ ($Hps5^{ru2}$ $l7R6^{1R}p$/$Hps5^{ru2}$++) and 102DSJ (+*102DSJP*/++p^{7R}) heterozygotes, when 25% were expected ($P < 0.001$). To generate fetuses hemizygous for 102DSJ progeny-tested males $+^{P7R}/l7R6^{6R}$ were mated with $+^{P7R}$/Del($Hps5^{ru2P}$)^{46DF1OD} females. Mice homozygous for the $l7R6^{6R}$ mutation were obtained by breeding heterozygote carriers ($l7R6^{6R}P/+P^{7R}$), which generated pink-eyed homozygotes ($l7R6^{6R}P/l7R6^{6R}P$) and dark-eyed wild-type mice ($+P^{7R}/+P^{7R}$). Matings were done for 1 h early in the morning, and females were examined for the presence of vaginal plugs (gestation day 0). Fetuses were collected at 15, 18 and 19 days of gestation.

Body and head measurements

Fetuses (E18.5) were recovered by caesarean section from nine pregnant females and a total of 16 wild-type and 19 homozygous $l7R6^{6R}$ mutant mice were measured for body length, head height, head length and head width. Measurements were obtained using a Fisher Scientific Digital Caliper. Statistically significant differences between mutant and wild-type fetuses were determined using a two-tailed *T*-test, not assuming equal variances and with a *P*-value cutoff of 0.005.

Skeletal analysis

Skeletal defects were evaluated using standard protocols for Alizarin Red–Alcian Blue staining of intact fetuses (37) and small animal microcomputerized tomography scanning (microCat) (38). Thirteen wild-type and 13 homozygous mutant fetuses were recovered by caesarean at E18.5 days of gestation from seven pregnant females. Fetuses were briefly soaked in 70°C water and the skin and internal organs were removed. Specimens were fixed in 95% ethanol, stained in Alcian Blue for 1–2 days and rinsed in 95% ethanol. They were then cleared in 1% KOH (2–6 h), subsequently, stained for 3 h in Alizarin Red solution and cleared further by placing in 2% KOH overnight. Clearing was completed by processing through the following series of solutions of 2% KOH/glycerol: (80:20), (60:40), (40:60) and (20:80) with storage indefinitely in the final solution. Three $Nell1^{6R}$ mutant and three wild-type E18.5 fetuses were analyzed using the small animal microCat system developed at Oak Ridge National Laboratory (38).

Histology

Histology was conducted on formalin-fixed, paraffin-embedded specimens of E18.5 fetuses (seven mutant and six wild-type specimens) recovered by caesarean section. Standard techniques were used for Haematoxylin and Eosin, Masson, periodic Acid Schiff (PAS) and von Kossa staining (39). Masson staining shows cytoplasm, keratin and muscle fibers as red, whereas collagens and mucus are stained blue. The PAS stains glycogen, mucopolysaccarides, glycoproteins and glycolipids purple. The presence and distribution of bone mineralization was determined by von Kossa staining, which shows deposits of calcium or calcium salts as black.

RNA analysis

Total RNAs were extracted from fetuses and adult tissues using standard guanidine isothiocyanate procedures (40). Phase Lock Gels™ (Eppendorf) were used for subsequent phenol–chloroform purifications. RNAs were precipitated with isopropanol and after centrifugation, pellets were re-suspended in nuclease-free water. About 700 μg to 1 mg total RNA per sample was used for purifying polyA$^+$ RNA using Mini-Oligo(dt) Cellulose spin columns (5′–3′ Inc.). One to two micrograms of polyA$^+$ RNAs were used for northern blots using standard electrophoresis and blotting protocols (41). Blots were hybridized with the CTC55 + 59 probe, which was generated by RT-PCR using primers designed from mouse EST sequences matching the 5′ and 3′ ends of human *NELL1* (1920 bp; ctc55-TGCAGCAGAAGCCGTCCA; ctc59-CAAACTAGGGCAAGCTAGAG).

DNA analysis and sequencing

The *Nell1*^{6R} mutation was identified by sequencing genomic DNAs extracted from the clipped tails of mutant and wild-type mice. cDNA sequencing was performed on reverse transcribed PCR-amplified segments. First-strand cDNA templates were generated from polyA$^+$ RNAs extracted from E15 fetal heads using the RETROscript Kit (Ambion). Two overlapping cDNA segments covering the entire coding region plus the 5′ and 3′-untranslated region were generated using the following primer pairs: ctc138/ctc149 and ctc150/ctc59. Ctc138/ctc149 generates a 556 bp fragment corresponding to the 5′ end of *Nell1* and was generated by standard PCR techniques. Ctc150/ctc59 amplifies a 1465 bp segment spanning the middle to 3′ end of the coding region and was generated by long-range PCR (Expand Long Template CR, Roche Diagnostic Group). The primer sequences are as follows: ctc59:CAAACTAGGGCAAGCTAGAG; ctc150:GCAGAGA CGAGACTTGGTCAACTGG; ctc138:CTGAAGCATTGGT TTCTTGC and ctc149:TCGACATGGAGTAGGAGGTGAG AGG. PCR products were sequenced using the primers that generated the products, and primers were designed using the acquired sequence data of preceding segments. Primers used for sequencing are available upon request. The mouse *Nell1* full-length cDNA sequence was submitted to GenBank as accession no. AY622226.

Mutation scanning

Twenty primer sets were designed to amplify each exon of *Nell1* from flanking intron sequences and two additional primer sets amplified conserved upstream elements. Each amplicon was amplified from genomic DNAs extracted from *Nell1*^{6R} hemizygous mutant mice, and the control strains (BJR and 21A). Corresponding PCR products were mixed in equal volumes, heteroduplexed and scanned for point mutations using TGCE (17). Three overlapping temperature gradients were used: 50–60°C, 55–62°C and 60–68°C. The 421 bp amplicon containing the mutation in the *17R6*^{6R} allele was amplified by PCR using the following primer pairs designed from the intron sequences flanking the 131 bp exon 14 of *Nell1*; NellExon14(F): ATAGACCAGGGGCA GAAACC and NellExon14R: TTGCCTCAACCTCAATATCC.

High-throughput real-time qRT-PCR assays

RNAs from the heads and bodies of four *Nell*^{6R} mutant and four wild-type E18 fetuses were extracted individually (16 RNA samples) according to the extraction method described earlier. DNaseI-treated RNAs were ethanol precipitated and re-suspended in nuclease-free water. Total RNAs (2.5 μg) were reverse transcribed to cDNA using the random-priming High-Capacity cDNA Archive Kit (Applied Biosystems).

Multiplex pre-amplification of cDNA targets. To enable maximum sensitivity and detection of hundreds of gene expression targets from a small amount of cDNA, a novel multiplex PCR pre-amplification strategy was used prior to conventional quantitative PCR. Two hundred and twenty-five (219 experimental and six endogenous control genes) Taqman Gene Expression Assays (PCR primer/FAM-probe stock solutions) were pooled together and used in a single PCR to amplify all targets equally from the same cDNA template. The FAM-probe is a component of the final configuration of the manufactured TaqMan® gene expression assays and does not interfere with the pre-amplification process. To prepare the multiplex pre-amplification primer pool, equal volumes of the 225 TaqMan® gene expression assays were mixed together, dried under vacuum and re-suspended with water to generate a multiplex-pooled primer set with a concentration of 180 nM for each primer. The pre-amplification reaction was set up as follows: a 250 μl volume of 500 ng of cDNA was combined with 250 μl of the multiplex-pooled primers. Then, 500 μl of 2X Multiplex pre-amplification Master Mix was added to generate the final 1000 μl reaction volume (Applied Biosystems). The reaction mix was divided into 50 μl aliquots in a 96-well PCR tray and cycled on an ABI 9700 thermal cycler under the following conditions: 95°C for 10 min; then 10 cycles at 95°C for 15 s; and 60°C anneal/extension for 4 min.

Real-time PCR reactions. Pre-amplification products were recombined into one tube and diluted 1:5 with water. Individual singleplex TaqMan® Gene Expression Assays for each of the 225 pre-amplified markers, along with 18S rRNA (which was not included in the pre-amplification reaction because of its high level of expression) were prepared as follows: 5.0 μl of 2X TaqMan® Universal PCR Master Mix, 0.5 μl of TaqMan® Gene Expression Assay 20X primer/FAM-probe solution and 2.0 μl of water and 2.5 μl of pre-amplified cDNA product. For all samples, each assay was carried out in quadruplicate wells of 384-well plates and run in the ABI PRISM® 7900HT Sequence Detection System under two-temperature cycling: 95°C for 10 min, then 40 cycles of 95°C for 15 sec and 60°C for 1 min. C_T (threshold cycle) values, the cycle number at which the PCR amplification fluorescence signal crosses a fluorescence threshold, were generated using the FAM dye layer setting at a threshold of 0.2 and a baseline of 3–13.

Data analysis. The relative levels of transcripts for each gene in wild-type and mutant samples were compared following normalization to endogenous control targets. GeNORM software (42) was used to select the two best targets with the least variation across samples from a collection of six potential endogenous controls (*Hprt*, *Tfrc*, *Tbp*, *Gus*, *gkl* and *18s* rRNA). *Gus* and *Hprt* were selected for heads, whereas *Gus* and *gkl* were selected for bodies. The geometric mean of the selected targets was then used as the reference for determining ΔC_T values. For each sample, ΔC_T values were determined by the following equation: $\Delta C_{T\ \text{Marker}} = C_{T\ \text{Marker}} - C_{T\ \text{Reference}}$. Statistically significant differences between ΔC_T values of wild-type and mutant groups were determined by a two-tailed *t*-test without assuming equal variances and with a *P*-value cutoff of 0.005. $\Delta\Delta C_T$s were also calculated between wild-type and mutant groups based upon average ΔC_T values for each group, and relative fold differences between them were determined by $2^{\wedge -\Delta C_T}$ (43).

SUPPLEMENTARY MATERIAL

Supplementary Material is available at HMG Online.

ACKNOWLEDGEMENTS

We thank Brynn Voy and Yie Liu for their constructive comments on this manuscript. Jennifer Millsaps generated the initial probe for the Northern Blots and Gurusahai-Khalsa Moyers assisted in the selection of gene expression assays. Mike Paulus provided training in microCat scanning and data analysis. The Office of Biological and Environmental Research, in the Department of Energy, funded this work under the contract DE-AC05-00OR22725.

Conflict of Interest statement. None.

REFERENCES

1. Bilezikian, J., Raisz, L. and Rodan, G. (2002) *Principles of Bone Biology*, 2nd ed. Academic Press, San Diego, CA, USA.
2. Shum, L., Coleman, C.M., Hatakeyama, Y. and Tuan, R.S. (2003) Morphogenesis and dysmorphogenesis of the appendicular skeleton. *Birth Defects Res. Part C. Embryo Today*, 69, 102–122.
3. Cohen, M.M. and Maclean, R.E. (2000) *Craniosynostosis: Diagnosis, Evaluation, and Management*. Oxford University Press, New York.
4. Wilkie, A.O. (1997) Craniosynostosis: genes and mechanisms. *Hum. Mol. Genet.*, 6, 1647–1656.
5. Anderson, P.J., Hall, C.M., Evans, R.D., Jones, B.M., Harkness, W. and Hayward, R.D. (1996) Cervical spine in Pfeiffer's syndrome. *J. Craniofac. Surg.*, 7, 275–279.
6. Anderson, P.J., Hall, C.M., Evans, R.D., Hayward, R.D., Harkness, W.J. and Jones, B.M. (1997) The cervical spine in Saethre-Chotzen syndrome. *Cleft Palate Craniofac. J.*, 34, 79–82.
7. Liu, Y.H., Tang, Z., Kundu, R.K., Wu, L., Luo, W., Zhu, D., Sangiorgi, F., Snead, M.L. and Maxson, R.E. (1999) *Msx2* gene dosage influences the number of proliferative osteogenic cells in growth centers of the developing murine skull: a possible mechanism for MSX2-mediated craniosynostosis in humans. *Dev. Biol.*, 205, 260–274.
8. Satokata, I., Ma, L., Ohshima, H., Bei, M., Woo, I., Nishizawa, K., Maeda, T., Takano, Y., Uchiyama, M., Heaney, S. *et al.* (2000) Msx2 deficiency in mice causes pleiotropic defects in bone growth and ectodermal organ formation. *Nat. Genet.*, 24, 391–395.
9. Zhou, Y.X., Xu, X., Chen, L., Li, C., Brodie, S.G. and Deng, C.X. (2000) A Pro250Arg substitution in mouse Fgfr1 causes increased expression of Cbfa1 and premature fusion of calvarial sutures. *Hum. Mol. Genet.*, 9, 2001–2008.
10. Carver, E.A., Oram, K.F. and Gridley, T. (2002) Craniosynostosis in Twist heterozygous mice: a model for Saethre-Chotzen syndrome. *Anat. Rec.*, 268, 90–92.
11. Ting, K., Vastardis, H., Mulliken, J.B., Soo, C., Tieu, A., Do, H., Kwong, E., Bertolami, C.N., Kawamoto, H., Kuroda, S. *et al.* (1999) Human NELL-1 expressed in unilateral coronal synostosis. *J. Bone Miner. Res.*, 14, 80–89.
12. Zhang, X., Kuroda, S., Carpenter, D., Nishimura, I., Soo, C., Moats, R., Iida, K., Wisner, E., Hu, F.Y., Miao, S. *et al.* (2002) Craniosynostosis in transgenic mice overexpressing Nell-1. *J. Clin. Invest.*, 110, 861–870.
13. Zhang, X., Carpenter, D., Bokui, N., Soo, C., Miao, S., Truong, T., Wu, B., Chen, L., Vastardis, H., Tanizawa, K. *et al.* (2003) Overexpression of *Nell-1*, a craniosynostosis-associated gene, induces apoptosis in osteoblasts during craniofacial development. *J. Bone Miner. Res.*, 18, 2126–2134.
14. Kuroda, S., Oyasu, M., Kawakami, M., Kanayama, N., Tanizawa, K., Saito, N., Abe, T., Matsuhashi, S. and Ting, K. (1999) Biochemical characterization and expression analysis of neural thrombospondin-1-like proteins NELL1 and NELL2. *Biochem. Biophys. Res. Commun.*, 265, 79–86.
15. Kuroda, S. and Tanizawa, K. (1999) Involvement of epidermal growth factor-like domain of NELL proteins in the novel protein–protein interaction with protein kinase C. *Biochem. Biophys. Res. Commun.*, 265, 752–757.
16. Rinchik, E.M., Carpenter, D.A. and Johnson, D.K. (2002) Functional annotation of mammalian genomic DNA sequence by chemical mutagenesis: a fine-structure genetic mutation map of a 1- to 2-cM segment of mouse chromosome 7 corresponding to human chromosome 11p14-p15. *Proc. Natl Acad. Sci. USA*, 99, 844–849.
17. Li, Q., Liu, Z., Monroe, H. and Culiat, C.T. (2002) Integrated platform for detection of DNA sequence variants using capillary array electrophoresis. *Electrophoresis*, 23, 1499–1511.
18. Hillman, R.T., Green, R.E. and Brenner, S.E. (2004) An unappreciated role for RNA surveillance. *Genome Biol.*, 5, R8.
19. Nagy, E. and Maquat, L.E. (1998) A rule for termination-codon position within intron-containing genes: when nonsense affects RNA abundance. *Trends Biochem. Sci.*, 23, 198–199.
20. Dennis, G., Jr., Sherman, B.T., Hosack, D.A., Yang, J., Gao, W., Lane, H.C. and Lempicki, R.A. (2003) DAVID: database for annotation, visualization, and integrated discovery. *Genome Biol.*, 4, 3.
21. Steinmann, B., Royce, P. and Superti-Furga, A. (1993) *The Ehlers-Danlos Syndrome. In Connective Tissue and its Heritable Disorders*. Wiley-Liss, New York, NY, USA.
22. Mao, J.R. and Bristow, J. (2001) The Ehlers-Danlos syndrome: on beyond collagens. *J. Clin. Invest.*, 107, 1063–1069.
23. Mao, J.R., Taylor, G., Dean, W.B., Wagner, D.R., Afzal, V., Lotz, J.C., Rubin, E.M. and Bristow, J. (2002) Tenascin-X deficiency mimics Ehlers-Danlos syndrome in mice through alteration of collagen deposition. *Nat. Genet.*, 30, 421–425.
24. Imamura, Y., Scott, I.C. and Greenspan, D.S. (2000) The pro-alpha3(V) collagen chain. Complete primary structure, expression domains in adult and developing tissues, and comparison to the structures and expression domains of the other types V and XI procollagen chains. *J. Biol. Chem.*, 275, 8749–8759.
25. Yoon, B.S., Ovchinnikov, D.A., Yoshii, I., Mishina, Y., Behringer, R.R. and Lyons, K.M. (2005) Bmpr1a and Bmpr1b have overlapping functions and are essential for chondrogenesis *in vivo*. *Proc. Natl. Acad. Sci. USA*, 102, 5062–5067.
26. Cundy, T., Hegde, M., Naot, D., Chong, B., King, A., Wallace, R., Mulley, J., Love, D.R., Seidel, J., Fawkner, M. *et al.* (2002) A mutation in the gene TNFRSF11B encoding osteoprotegerin causes an idiopathic hyperphosphatasia phenotype. *Hum. Mol. Genet.*, 11, 2119–2127.
27. Jackson, G.C., Barker, F.S., Jakkula, E., Czarny-Ratajczak, M., Makitie, O., Cole, W.G., Wright, M.J., Smithson, S.F., Suri, M., Rogala, P. *et al.* (2005) Missense mutations in the B strands of the single A-domain of matrilin-3 result in multiple epiphyseal dysplasia. *J. Med. Genet.*, 41, 52–59.
28. Johnson, D., Iseki, S., Wilkie, A.O. and Morriss-Kay, G.M. (2000) Expression patterns of Twist and Fgfr1, -2 and -3 in the developing mouse coronal suture suggest a key role for twist in suture initiation and biogenesis. *Mech. Dev.*, 91, 341–345.
29. Opperman, L.A., Chhabra, A., Nolen, A.A., Bao, Y. and Ogle, R.C. (1998) Dura mater maintains rat cranial sutures *in vitro* by regulating suture cell proliferation and collagen production. *J. Craniofac. Genet. Dev. Biol.*, 18, 150–158.
30. Carinci, F., Bodo, M., Tosi, L., Francioso, F., Evangelisti, R., Pezzetti, F., Scapoli, L., Martinelli, M., Baroni, T., Stabellini, G. *et al.* (2002) Expression profiles of craniosynostosis-derived fibroblasts. *Mol. Med.*, 8, 638–644.
31. Gruber, H.E., Ingram, J.A. and Hanley, E.N.J. (2002) Tenascin in the human intervertebral disc: alterations with aging and disc degeneration. *Biotech. Histochem.*, 77, 37–41.
32. Nerlich, A.G., Boos, N., Wiest, I. and Aebi, M. (1998) Immunolocalization of major interstitial collagen types in human lumbar intervertebral discs of various ages. *Virchows Arch.*, 432, 67–76.
33. Roberts, S., Ayad, S. and Menage, P.J. (1991) Immunolocalisation of type VI collagen in the intervertebral disc. *Ann. Rheum. Dis.*, 50, 787–791.
34. Jackson, G.C., Barker, F.S., Jakkula, E., Czarny-Ratajczak, M., Makitie, O., Cole, W.G., Wright, M.J., Smithson, S.F., Suri, M., Rogala, P. *et al.* (2004) Missense mutations in the beta strands of the single A-domain of matrilin-3 result in multiple epiphyseal dysplasia. *J. Med. Genet.*, 41, 52–59.
35. Miller, R.R. and McDevitt, C.A. (1991) Thrombospondin in ligament, meniscus and intervertebral disc. *Biochim. Biophys. Acta*, 1115, 85–88.
36. Bareggi, R., Martelli, A.M., Grill, V., Sandrucci, M.A., Zweyer, M. and Narducci, P. (1995) Protein kinase C (PKC) isozymes exhibit specific expression in the vertebral column of human fetuses. *J. Biol. Res.*, 121, 83–90.

37. Hogan, B., Beddington, R., Constantini, F. and Lacy, E. (1994) *Manipulating the Mouse Embryo: A Laboratory Manual*. Cold Spring Harbor Laboratory Press, New York.
38. Paulus, M.J. (1999) A new X-ray computed tomography system for laboratory mouse imaging. *IEEE Trans. Nucl. Sci.*, 46, 558–564.
39. Carson, F.L. (1990) *Histotechnology*. American Society of Clinical Pathologists Press, Chicago, USA.
40. Ausubel, F.M., Brent, R., Kingston, R.E., Moore, D.D., Seidman, J.G., Smith, J.A. and Struhl, K. (1997) *Current Protocols in Molecular Biology*. John Wiley and Sons, New York.
41. Sambrook, J., Fritsch, E.F. and Maniatis, T. (1989) *Molecular Cloning: A Laboratory Manual*. 2nd ed. Cold Spring Harbor Laboratory Press, New York, USA.
42. Vandesompele, J., De Preter, K., Pattyn, F., Poppe, B., Van Roy, N., De Paepe, A. and Speleman, F. (2002) Accurate normalization of real-time quantitative RT-PCR data by geometric averaging of multiple internal control genes. *Genome Biol.*, 3, RESEARCH0034.
43. Applied, B. (2001) Relative quantitation of gene expresssion. User Bulletin 2.